AECL-10542

ATOMIC ENERGY OF CANADA LIMITED

ÉNERGIE ATOMIQUE DU CANADA LIMITÉE

A GAS MIGRATION TEST IN SATURATED, FRACTURED ROCK

ESSAI DE MIGRATION DE GAZ DANS LA ROCHE FRACTURÉE SATURÉE

M. Gascoyne, D. M. Wuschke, A. Brown, J. G. Hayles,
E. T. Kozak, G. S. Lodha, G. A. Thorne

Whiteshell Laboratories
Pinawa, Manitoba R0E 1L0
December 1991 décembre

Laboratoires de Whiteshell

AECL RESEARCH

A GAS MIGRATION TEST IN SATURATED, FRACTURED ROCK

Final Report for the Joint UKDOE/AECL Project, Phase 2

by

M. Gascoyne, D.M. Wuschke, A. Brown, J.G. Hayles
E.T. Kozak, G.S. Lodha and G.A. Thorne

Whiteshell Laboratories
Pinawa, Manitoba ROE 1LO
1991

AECL-10542

ESSAI DE MIGRATION DE GAZ DANS LA ROCHE FRACTURÉE SATURÉE

Rapport final pour la Phase 2 du Projet commun UKDOE/EACL

par

M. Gascoyne, D.M. Wuschke, A. Brown, J.G. Hayles,
E.T. Kozak, G.S. Lodha and G.A. Thorne

RÉSUMÉ

On a injecté de l'hélium à une pression constante dans une zone de fractures inclinée, par un trou de forage d'accès, à une profondeur d'environ 40 m; on a effectué le forage dans la formation granitique de Lac du Bonnet située au sud-est du Manitoba. On a mesuré la vitesse d'écoulement, le temps d'arrivée et le régime de distribution du gaz à la surface à l'aide d'analyses de gaz provenant du sol. On a comparé les résultats des travaux sur le terrain avec les résultats prédits par un modèle analytique simple tiré du modèle présenté dans le rapport de Thunvik et Braester (1987). On a constaté un bon accord lorsqu'on a incorporé au modèle l'influence de la fracturation verticale de la roche de fond et des morts-terrains de faible perméabilité. On s'est ensuite servi du modèle pour déterminer la conductivité hydraulique des voies individuelles d'écoulement de gaz dans la roche fracturée.

EACL Recherche
Laboratoires de Whiteshell
Pinawa, Manitoba ROE 1LO
1991

AECL-10542

A GAS MIGRATION TEST IN SATURATED, FRACTURED ROCK

Final Report for the Joint UKDOE/AECL Project, Phase 2

by

M. Gascoyne, D.M. Wuschke, A. Brown, J.G. Hayles,
E.T. Kozak, G.S. Lodha and G.A. Thorne

ABSTRACT

Helium gas was injected at constant pressure into an inclined fracture zone through an access borehole at a depth of about 40 m, in the Lac du Bonnet granite, southeastern Manitoba. The gas flow rate, arrival time and pattern of distribution of gas at the surface were monitored by soil gas surveys. The field results were compared with predictions of a simple analytical model derived from Thunvik and Braester (1987). Good agreement was found when the influence of vertical fracturing in the bedrock and a low-permeability overburden were included in the model. The model was then used to determine the hydraulic conductivity of individual gas flow paths in the fractured rock.

AECL Research
Whiteshell Laboratories
Pinawa, Manitoba ROE 1LO
1991

AECL-10542

CONTENTS

continued...

CONTENTS (concluded)

EXECUTIVE SUMMARY

Anomalies in helium (He) concentrations of soil gases, in an area near the Underground Research Laboratory, near Lac du Bonnet, southeastern Manitoba, have been reported in previous work done as part of a joint UKDOE-AECL program of research (Gascoyne and Wuschke 1990). The anomalies were interpreted in terms of discharge of groundwater from a subsurface fracture zone in granitic rock. An analytical model of two-phase flow was developed as part of this research to describe the migration of an injected gas phase through the fracture zone to the surface.

This report describes the results of testing the model by injecting He gas into a borehole that intersects an inclined fracture zone at a depth of about 40 m, monitoring gas inflow rate and determining its arrival and concentration distribution at the surface. Various characteristics of the location were studied in detail to determine factors that might influence gas migration, including the geology and hydrogeology of the area. Geophysical techniques were used to estimate thickness of the overburden and the topography of the underlying bedrock and piezometers were installed to monitor groundwater levels and the response to gas injection.

Helium was injected into an isolated section of a borehole for a 11-day period in 1989 October. Gas flow rate increased over this period from 5 $L \cdot min^{-1}$ to about 20 $L \cdot min^{-1}$ for a constant injection pressure. Breakthrough of gas at the surface was detected near the borehole within 2 days and by the end of the test most soil gas monitoring sites were showing elevated He levels. High He concentrations (up to 4% of total soil gas) were found at two sites within 40 m of the borehole and these appear to lie on strike with steep fractures observed in the upper parts of the borehole and on adjacent outcrop. This indicates that the preferential pathway for the gas was along steep fractures that intersect the fracture zone and transport was limited largely by the time required for the gas phase to migrate through the low-permeability overburden. Lower He concentrations in soil gases in the area of subcrop of the fracture zone indicate that some of the gas also migrated along the fracture zone but was well dispersed before arriving at the surface.

Comparison of the test results with predictions of the model shows good agreement, especially if actual transport distances and hydraulic head characteristics are used. The model was then used to calculate hydraulic conductivities of individual pathways for each sampling site where the gas breakthrough time was fairly well known. The hydraulic conductivities were found to range between 10^{-5} to 10^{-8} $m \cdot s^{-1}$, values comparable to those measured by hydraulic testing. This work has demonstrated the usefulness of soil gas analyses and gas injection testing in determining the hydrogeological characteristics of fractured rock.

1. INTRODUCTION

Localized high concentrations of helium (He) and radon-222 (Rn) in soil gases and surface waters have been interpreted in terms of groundwater discharge through subsurface fractures in the bedrock (Larocque and Gascoyne 1986, Gregory and Durrance 1987, Banwell and Parizek 1988, Malmqvist et al. 1989). Phase 1 of a joint AECL/UKDOE program involved measurement of He and Rn in soil gases on and near the Underground Research Laboratory (URL) lease area, near Lac du Bonnet, southeastern Manitoba, (Gascoyne and Wuschke 1990) where groundwater flow conditions were well known from other studies (Davison 1984, Davison and Kozak 1988, Thorne 1990). Results of the He gas analyses for the groundwater discharge area indicated that channelling of groundwater flow within the subsurface fractures was probably the cause for the discrete areas of high He concentrations. Variations in the Rn content of soil gas were thought to be caused by enrichments of radium in the overburden and may indicate locations of very rapid groundwater discharge. An analytical model was also developed during Phase 1 to describe how a gas phase would migrate through a fracture zone in the bedrock to the surface if the gas was injected into an existing borehole in the discharge area. The model was used to predict travel time of the gas to the surface for two cases: 1) bedrock and 2) bedrock with an overburden cover (Gascoyne and Wuschke 1990).

In Phase 2 of the program, the analytical model was tested by injecting He gas into a fracture zone in borehole B-34 and monitoring its arrival and concentration distribution at the surface. This report describes the results of this work and additional geological, hydrogeological and geophysical studies that were performed in the area of B-34 to provide supporting information for the test and model. The results are interpreted in terms of mechanisms of gas phase migration in saturated fractured rock and in terms of the ability of a He gas injection test to assist in hydrogeological characterization of a groundwater discharge area.

2. GAS MIGRATION IN FRACTURED ROCK

2.1 MECHANISMS OF GAS MIGRATION

Gases are formed naturally in the subsurface by a variety of mechanisms, including biological activity, decomposition of organics, crust and mantle outgassing, acid-base reactions and radioactive decay. In most situations, because of the ambient hydrostatic pressure, the gases dissolve immediately in adjacent groundwater or hydrothermal fluids and only migrate to the surface at the speed of the host fluid. However, when this fluid approaches atmospheric pressure, such as near ground surface, the gases can exsolve and migrate rapidly through the remainder of the fluid column and an overlying unsaturated material, to the atmosphere. Because most gases are naturally present in groundwater in minor or trace quantities, the solubility of the gas is not exceeded until near the fluid surface when hydrostatic pressure is typically less than 100 kPa (1 atm). For instance, it was reported in Phase 1 of the UKDOE/AECL soil gas project that the range of He concentration observed in URL area groundwater was between

1 and 56 cm^3 He STP·L^{-1} H_2O, with a mean concentration of about 11 cm^3 He STP·$L^{-1}H_2O$. The solubility of He at STP is about 9.4 $cm^3 \cdot L^{-1}$ H_2O, and therefore most of the URL area groundwaters require only 1-2 atm of pressure (10-20 m of hydrostatic head) for the dissolved He to remain in solution. Only in borehole zone M4A-4 at the URL site, where the groundwater contains 56 cm^3 He·L^{-1}, would a hydrostatic head of 50 m be required to keep all He in solution.

In most natural situations, the migration of gases to the surface is likely to follow the above mechanism, i.e., dissolution at the source under hydrostatic pressure, upward flow with the groundwater velocity, exsolution of the gas from the groundwater within 20 m to 50 m of the water table and rapid vertical flow of the exsolved gas to the surface. If the rate of gas production at the source is sufficient, a gas phase will form and migrate upwards through pores and fractures because of buoyancy forces that exceed hydrostatic and capillary pressures. This is also the situation that describes the behaviour of a gas phase injected into a permeable fracture zone through an access borehole. As gas is injected, water is displaced laterally in the fracture zone along permeable pathways. Depending on fracture aperture, the gas may either break into bubbles and rise with little restriction or, as is more likely the case in fractured crystalline rock, it will continue to displace water from the fracture zone until an almost complete gas phase pathway is formed. The analytical model of the movement of an injected gas phase is described below.

2.2 MODEL DEVELOPMENT

The flow of gases in the fractured subsurface media has been modelled by a variety of methods over the last ten years, mainly for applications in the petroleum industry and, recently, for international nuclear waste disposal programs. Two approaches have been used. The first involves analytical modelling in which Darcy's Law is applied to describe fluid flow (gas or liquids) in single fractures. The model is then extended to give flow in a network of fractures (Braester and Thunvik 1982, Thunvik and Braester 1987). The second approach describes the migration of gas in space and time using permeabilities and porosities assigned to volume elements of the rock medium. This method is termed a "macroscopic" approach and uses finite difference or finite-element methods to represent the flow field. All models developed using the macroscopic approach (recently reviewed by Worgan et al. 1990) require extensive computing effort and detailed information on the properties of the rock media.

In the work performed for Phases 1 and 2 of this study, a simple analytical modelling approach was used. This approach is much easier to implement. It requires only estimates of the bulk properties of the system and is suitable when detailed information about the rock media, such as the distribution of fracture apertures and channelling, is not available.

2.3 MODEL DESCRIPTION AND PREDICTIONS

The analytical model developed to describe the transport of gas injected into the subsurface fracture zone at the study area was given in detail by Gascoyne and Wuschke (1990). The model was based on equations for the

conservation of mass and the equations of motion for liquid and gas phases. It assumes that the gas is confined to the fractures and separated from the water by a sharp interface. The interface is treated as a moving boundary. Equations were developed for the displacement of water by a gas in a single open fracture as a function of the injection pressure, fluid properties and the fracture aperture. This model was then extended to an idealized network of orthogonal fractures, whose properties could be calculated from bulk hydrogeological properties determined in field tests.

The model calculates

- the required threshold pressure for injection of He, taking into account both the hydrostatic pressure and the capillary pressure in the fracture network;

- the "breakthrough time", i.e., the time of initial arrival of the He at the surface as a function of the injection pressure, the properties of the fluid and of the fracture network, and the geometry of the system (i.e., the angle of the fracture zone to the horizontal, and the distance from the point of injection to the surface);

- the velocity of He after breakthrough, and its volumetric flow rate; and

- the position of the He water interface at any time.

In the area of the gas injection test, the fracture zone is overlain by a fractured clay overburden several metres thick. This overburden has lower permeability than the fractured rock. An extension of the model was developed, therefore, and calculations carried out to take into account both the fracture zone in the rock and the layer of overburden.

For these calculations, the injection test was conceptualized as shown in Figure 1. Gas is injected into the fracture zone (FZ2) through borehole B-34. This gas is transported through the fracture zone until it reaches the overburden. Flow through the overburden is assumed to be through vertical fractures. Transport through the fractured rock and overburden were modelled separately, matching boundary conditions at the rock/overburden interface.

The calculated threshold pressure for injection is the greater of the threshold pressures for the two layers; the calculated breakthrough time is the sum of the breakthrough times for the two layers. For the geometry and hydraulic properties of the system modelled (based on permeability tests of the fracture zone, and an estimate that the permeability of the overburden was a factor of 1000 lower), the total breakthrough time was found to be almost entirely dependent on the properties of the overburden.

Predicted breakthrough times for gas injection at a depth of 40 m in borehole B-34 range from about 3 to 8 d (Table 1) (Gascoyne and Wuschke 1990). Breakthrough times were found to be sensitive to gas overpressure at the injection point, fracture spacing, and the porosity of the fracture zone. Phase 2 of the program provided field data from a He gas injection

test to compare with these predictions and some modifications were made to the model.

3. PHYSICAL SETTING

The study was performed on the Underground Research Laboratory (URL) lease area situated on the western limb of the Lac du Bonnet granite batholith, southeastern Manitoba (Figure 2). Borehole B-34 was chosen as the gas injection site because it penetrated a major inclined thrust fault, FZ2, which has been encountered in many boreholes across the URL area (Figure 3).

The borehole is located close to the NW edge of the URL lease area near the area where FZ2 subcrops beneath overburden deposits. This area is also the discharge area for groundwater moving upwards along FZ2. Access to the subcrop area of FZ2 (to the northwest of the URL lease area) was obtained by agreement with the local landowner. Borehole B-34 lies in a dense bush area where access had to be provided by trail cutting. The subcrop area, however, was an open cultivated field and only required mowing of an alfalfa crop.

3.1 GEOLOGY AND STRUCTURE

Close to the surface in the URL lease area, the Lac du Bonnet batholith is a medium- to coarse-grained, pink granite (Figure 4), which alters to a red, hematite-rich rock close to low-dipping thrust faults, such as FZ2 (Brown et al. 1989). In the fracture zones, biotite and plagioclase have been altered to chlorite and illite, and hematite has been removed, leaving the rock bleached in appearance. Highly permeable "rubble" zones often occur within the fracture zones and are characterized by water-pressure loss during drilling, poor core recovery and presence of sand and gravel-sized fragments. These low-dipping fracture zones have been encountered in many of the boreholes in the URL lease area and have been shown, using a combination of geological mapping and hydrogeological testing, to be interrelated in a three-dimensional network (Figure 5). FZ2 is a prominent feature throughout the area and, in the location of the work described here, strikes NNE and dips about 20° to the ESE.

Near the surface, subvertical fracturing is common (Figure 5) and is largely a result of stress release due to unloading. The dominant direction of subvertical fractures in this area is also NNE (040°) and lies parallel to the direction of maximum horizontal stress.

3.2 HYDROGEOLOGY

The major low-dipping fracture zones largely control the patterns of groundwater movement in the URL lease area (Davison 1984, Davison and Kozak 1988). Groundwater is recharged by surface precipitation in the upland (largely exposed bedrock) part of the area (Figure 3) and flows down subvertical fractures to intersect FZ3 and the upper splay of FZ2 (FZ2.5, Figure 3). Evidence for penetration of recharge to depths of at least

350 m in FZ2 comes from hydraulic head data and the observation of relatively dilute groundwaters in this part of the zone (Davison 1984, Gascoyne et al. 1988). Prior to excavation of the URL shaft and underground levels, most groundwaters flowed upwards along the fracture zones, towards the surface. The area to the northwest of the lease area is an outcrop location for FZ2 and a main discharge site for groundwater moving upward along this zone.

Groundwater flow in this region of FZ2 is partly controlled by the presence of an overlying thick soil and sediment deposit. The overburden consists of a permeable basal sandy till capped by laminated clays and silts, which serve as an aquitard. Because of this cover and the strong upward hydraulic gradients in FZ2, artesian conditions exist in the bedrock. Recent excavation of the URL shaft and levels has reduced the amount of groundwater moving upward along FZ2, although the hydraulic conditions in this area are still artesian. The overburden sequence, hydraulic conductivities and effects of URL excavation are described in more detail below.

4. CHARACTERIZATION OF THE INJECTION TEST AREA

Several detailed geological, geophysical and hydrogeological studies were performed in borehole B-34 and the surrounding area prior to the gas injection test.

4.1 GEOLOGY OF THE BOREHOLE AND AREA

Fracture zone FZ2 is one of the larger thrust faults known in the Lac du Bonnet batholith. In the vicinity of the URL lease area, the location and, in part, the orientation of these faults are controlled by that of discontinuous but regularly oriented schlieric and xenolith-rich layers in the granite of the batholith (Brown et al. 1989). In some cases the geometric complexity of the faults can be traced to this fabric. Most information on FZ2 comes from boreholes close to the URL shaft (Figure 5a). Boreholes close to the fault subcrop (of which B-34 is one) are sparse. The exact location of the subcrop beneath the glaciofluvial sediments cannot be determined by extrapolation from deeper subsurface geological data. In part, this is because the zone of secondary fracturing and alteration around the zone widens near the surface. More locally specific methods, such as those described in Section 4.2, locate the fault subcrop better. The wide horizontal extent of the possible subcrop location is shown by comparing contours of the upper surface of the zone of secondary alteration (Figure 5a) with the subsurface topography of the bedrock (Figure 12).

Where intersected in the shaft, 270 m below the surface, FZ2 has a simple, dip-slip movement of 7.3 m reverse offset and a simple suite of fracture sets. Although there is evidence of reactivation, with development of both cataclasites and simple brittle fractures, there are essentially two sets: primary shear fractures dipping approximately 20°, and secondary, subhorizontal fractures, which may be extensional in origin but are more likely to

be shear fractures. The fault zone has several known subparallel splays below 190 m from surface, but the main fault zone, as opposed to the accompanying alteration zone, appears regularly planar on a large scale. Within the fault zone, however, channelling of groundwater occurs, because of spatial variation in the permeability within the plane of the zone, including interconnected regions of high permeability. In some cases these regions of higher or lower permeability correspond to other features of the zone such as flexures in the topography of the zone or the junctions of secondary splays. However, in other cases, there is no apparent correlation between the permeability pattern and other geological factors.

Little is known of the surface and near-surface (0-100 m depth) characteristics of this fault zone because this part of the zone is largely outside the URL lease area, but there is evidence from another, similar fault where the subcrop region was excavated elsewhere on the Lac du Bonnet batholith, and at FZ3 at the URL, which was intersected 130 m above FZ2 in the shaft and outcrops a short distance to the east of borehole B-34 (Figure 3). These fracture zones widen near the surface and the fracturing becomes complex. Secondary fractures, with low-intermediate dips and strikes perpendicular to that of the general fault zone occur and a strike-slip movement is superimposed on the original dip-slip shear planes. In addition, the fault zones enter the zone of near-surface, in situ stress-relief fracturing.

Commonly the near-surface fracturing consists of three orthogonal sets: a subhorizontal set, which dies out a few metres below surface; a subvertical set striking east-southeast, which dies out within 100 m of surface; and a subvertical set striking north-northeast, which persists sparsely to 250-m depth. In some locations the north-northeast-striking fractures are common in a narrow zone in the hanging wall of the fault zone. In addition, in FZ3, there is evidence near the surface of a strike-slip movement (and attendant secondary fracturing) superimposed on the dip-slip movement.

Although the near-surface portion of FZ2 is likely to have similar characteristics to those seen elsewhere, the outcrops adjacent to borehole B-34 exhibit mesoscopic fractures striking east-southeast and north. However, the high probability of complex fracturing and channelling of groundwater (and perhaps gas) in this upper section of the fault is shown by the TV fracture log of borehole B-34. This logging shows the presence of three fracture zones at depths of 19-23 m, 37-48 m, and 52-54 m. A break in the general attitude of the fracturing is found in the central fracture zone (Figure 5b,c). Above 36-m depth, the major set (143/48, dip direction/dip) has intermediate to high-intermediate dips. The strike varies locally; for example, in the fracture zone (19-23 m) the orientation is 160/48. There are no secondary fractures in the fracture zone, but above and below it there is a subhorizontal set (323/10) that has a dihedral angle of 58° with the major set. The subhorizontal set is parallel to the theoretical conjugate shear direction but may belong to near-surface relief fractures. Below 36 m, especially in the main fracture zone (37-48 m), the common attitude is 244/31, a low intermediate dip, parallel to the common thrust fault attitude. Secondary fractures again are sparse but do occur within the fault zone; their poorly defined set orientation is 317/57. With an approximate dihedral angle of 90° between the primary and secondary

sets, the relationship is difficult to interpret. Both of these two general attitudes (143/48 and 144/31) are steeper than the common FZ2 orientation (134/20 and they may represent splays.

The intersection line of a major splay (FZ2.5) encountered underground comes very close to borehole B-34 according to one possible interpretation. Alternatively, the fracture zone may be steepening near the surface, a phenomenon known from thrust faults elsewhere or those sets may all be secondary fractures due to the local stress field within the primary fault zone. The best updip projection of FZ2 places it at 210 m amsl in B-34. The collar of B-34 is at 270 m amsl, which suggests that either the major part of the zone lies below the bottom of the borehole or, more likely, the zone has steepened.

Because B-34 is a vertical borehole, the sparse evidence for subvertical fracturing cannot be relied on to represent the true state of fracturing in the rock, but subvertical fractures are present with both northeast and southeast strikes. A poorly defined, intermediate-dip fracture set (089/38 and 068/40) is seen in all three fracture zones, striking approximately perpendicular to the general strike.

4.2 GEOPHYSICAL INVESTIGATIONS

Several types of geophysical data have been used to gain a better understanding of the overburden and bedrock structures in the immediate vicinity of borehole B-34. Previously collected airborne geophysical data for the URL lease area have been used for the region lying within a 1-km radius of the borehole. Geophysical maps were plotted at the 1:10 000 scale describing total aeromagnetic intensity, calculated vertical magnetic gradient, apparent resistivity from 935 and 4600 Hz electromagnetic data (EM) and overburden thickness determined from EM data.

These airborne geophysical maps clearly indicate a sharp bedrock/overburden contact along the road from the URL access road towards the north (Figure 6). This sharp contact runs within 50 m to the north of borehole B-34 and is mapped with an ENE-WSW trend. The map indicates that overburden thickness varies from 2 to 26 m immediately WNW of B-34. It also indicates the possibility of a small ridge in the bedrock surface between 200 to 400 m west of B-34. The sharp overburden/bedrock contact in the airborne EM data is supported by a low magnetic anomaly (Figure 7), and may be due to a fracture zone or lithological contact in the bedrock. The total magnetic field aeromagnetic map (Figure 7) clearly shows three lineations of negative magnetic anomaly along shaded zones marked FZ1, FZ2 and FZ3. The magnetic low zones, FZ3 and FZ2, are supported by lower resistivity (map not shown here). These are considered to be the exposures of FZ3 and and FZ2 at the bedrock surface. The magnetic low, FZ1, lies in the area of thick overburden and low resistivity.

Ground geophysical surveys involving 2.5 line km of VLF-EM resistivity and 0.6 line km of seismic refraction surveys were conducted. These methods are described in detail in Appendix A (from Hayles et al., in preparation). The ground grid survey lines are shown by dotted lines on Figure 6. The ground geophysical surveys were designed to map bedrock relief more

precisely than the previous airborne survey and to delineate FZ2 outcrop in the bedrock under the soil cover if possible. The interpreted depth profile along ground survey lines 2+00W and 3+20W are reproduced in Figure 8. These profiles show that the EM-resistivity method has limited depth of penetration because of the presence of near-surface conductive clays in this section. Maximum depths interpreted by EM data are limited to 10 m owing to concentration of current flow in upper conductive layers. The refraction seismic survey was also limited to about 10 m because the energy levels from the 6-kg hammer were insufficient to give good refracted arrival signals when the overburden is thicker than about 10 m. The potential for damage to the field and local environmental concerns did not permit using high-energy dynamite sources to give better penetration of the overburden.

The basement ridge that is slightly visible from the airborne data has been clearly defined on two lines (line 1+50N, Station 0+80W to Station 2+50W and line 2+00W, Stations 0+80W to Station L2+00W respectively, Figure 9). The shallowest part of the ridge, centred around intersection of the L1+50N and L2+00W, is interpreted to be at 4-m depth. The interpreted ridge, overburden thickness contours and depth to the basement (determined by drilling) are also shown in Figure 9.

4.3 HYDROGEOLOGY OF THE OVERBURDEN

During 1981, two nests of groundwater monitoring wells (0-31/-32 and 0-33/-34/-42) were installed in overburden sediments near borehole B-34 (Figure 10) as part of the URL lease area hydrogeological characterization program. In 1988, two piezometer nests (0-88/-89/B-45 and 0-90/-94) were installed west of borehole B-34 to assist in monitoring shallow hydrogeological conditions in the discharge area of FZ2.

In 1989, seven additional shallow piezometer nests were constructed to the west of borehole B-34 to provide more detailed hydrogeological data in support of the soil gas injection test. For these investigations, sites for piezometer nests were selected to maximize areal coverage and provide the most effective use of existing monitoring boreholes and stratigraphic data. All piezometer nest locations are shown in Figure 10.

4.3.1 Overburden Stratigraphy

Boreholes 12.5 cm in diameter were augered to refusal using solid-stem augers and sediment samples were retrieved at 1.5-m intervals from the cuttings return or from the auger bit when the drill string was removed from the borehole. The samples were visually examined and a provisional stratigraphy log completed. Samples were bagged, marked and retained for additional laboratory analysis. Based on stratigraphy and borehole depth, groundwater monitoring intervals were selected within the boreholes and piezometers constructed. Typical piezometer nest and bedrock monitoring well installations are shown in Figure 11. Where overburden depths were greater than 10 m, an additional borehole was augered adjacent to the piezometer nest and a water table well constructed.

Geodetic elevations of piezometer standpipes were determined and stratigraphic logs completed with details, such as ground surface elevation, monitoring interval elevation and total depth recorded.

Within the study area, boreholes augered to refusal indicate that overburden deposit depths range from 3.0 to 25.5 m. At some locations the overburden thickness changes abruptly, indicating an uneven bedrock topography.

The uppermost stratigraphic unit consists of dark greyish brown silty clay with silt laminae. This unit is less than 0.5 m thick and is rich in organics (topsoil) at the surface. The silty clay is underlain by a pale olive clayey silt. This unit was most often about 1 m thick and at some locations is the surface stratigraphic unit. Some sand and clay are also present within the silt unit and at some locations silt laminae are interbedded with clay. This is particularly evident at boreholes 0-90 and 0-163 where these interbedded deposits were about 5.0 m thick. Carbonate pebbles are occasionally found throughout these deposits.

The predominant deposit of the study area is a generally massive 16-m-thick clay unit. Some silt laminae and beds are found throughout the clay deposit. Silt nodules, deposited as ice rafted material, are also scattered throughout the clay. Horizontal fractures and preferred parting planes are evident in some portions of the unit. Underlying the clay but directly on bedrock is a silty sand till. The till is discontinuous within the study area and was not intersected by two of the boreholes.

4.3.2 Hydraulic Properties

Grain-size analysis was completed on seven overburden samples retrieved with a split spoon from boreholes at piezometer nests 0-90 and 0-88 of this study area. These analyses were used to confirm field logs of stratigraphic units identified during the borehole drilling and sampling procedures. The stratigraphy of the study area is shown in Figure 12.

After completion of groundwater monitoring wells, five single well response tests were performed on selected monitoring intervals of the overburden deposits. The field tests were analyzed using Hvorslev's (1951) basic time log technique. Hydraulic conductivities for the overburden deposits ranged from 7.5×10^{-11} to 7.5×10^{-8} m/s. The shallow 3-m cored bedrock borehole (B-45) of this section has a hydraulic conductivity of 4.2×10^{-7} m/s.

4.3.3 Groundwater Flow Patterns

Water-level measurements have been made at weekly to monthly intervals following installation of all the groundwater monitoring wells described above. Hydrographs have been plotted from water level data and groundwater flow diagrams constructed.

Figure 13 illustrates the groundwater equipotentials and flow directions for the east-west cross section indicated in Figure 10. This section includes the longer term monitoring wells for which about nine years of water-level data are available as well as data for the recently constructed wells. Analysis of hydrograph records show that all groundwater levels in

the recently constructed wells have stabilized and the flow patterns are consistent with previously constructed flow diagrams (Thorne 1990).

The flow diagrams show that recharge occurs through thin overburden deposits at the easternmost segment of the piezometer cross section. Groundwater flow is then principally in a lateral direction with a slight upward component near piezometer nests 0-33, 0-34, 0-42 and borehole B-34. Long-term water-level monitoring records at this nest show that the hydraulic head for the upper part (0-32 m) of borehole B-34 is nearly identical to those measured in the overburden glacial till unit, directly overlying bedrock. The lower interval of borehole B-34 (33-60 m) indicates good hydraulic connection to FZ2 elsewhere in the URL lease area. This connection has been recorded from pump tests and water-level fluctuations associated with large drawdowns or dewatering of FZ2 in the URL facility (Thorne 1990).

The western segment of the piezometer cross section shows that groundwater flow is controlled by a zone of higher potentials in the clay unit. A gradational decrease of groundwater potential occurs towards bedrock at this location. This zone of higher hydraulic head is believed to be due to fracturing in the clay unit and, possibly, localized groundwater discharge from underlying bedrock.

The long-term records of monitoring hydraulic head in FZ2 at B-34 show a gradual decline in head over the period 1986 to 1989 (Figure 14). This decline has been observed in other boreholes accessing FZ2 on the URL lease area. It is largely a result of reduction in recharge to FZ2 by the dewatering of the overlying rock, which has resulted from drainage of FZ3 (Figure 3) into the URL facility. This has important implications for the discharge of FZ2 groundwater (and associated helium) in the study area.

4.4 HYDROGEOLOGICAL TESTING OF BOREHOLE B-34

Borehole B-34 is a 61-m-deep, 152-mm-diameter borehole, drilled vertically in 1982 as part of a program to establish a surface network of water-level monitoring boreholes (Figure 15). A packer at 32-m depth in an unfractured part of the borehole isolates FZ2 in the lower part of the borehole (B-34 Zone 2) from near-surface fracturing in the upper part (in B-34 Zone 1). A flexible PVC standpipe was attached to the packer from the surface shortly after drilling, and water-level measurements have been recorded continuously since then, in both zones, using downhole pressure transducers linked to a central data acquisition system at the URL facility (Davison 1984). All testing was conducted within B-34 Zone 2 using the installed monitoring and packer system.

Pulse tests and constant-rate pumping tests were performed in B-34 Zone 2 to measure the transmissivity of FZ2 at this location. Water levels in B-34 Zone 1 and a nearby borehole, M5A, were monitored for response to testing. The techniques used and the results are described in detail in Appendix B.

In summary, the hydraulic testing of B-34 Zone 2 shows that the transmissivity of FZ2 at that location is about 5×10^{-5} m^2/s, the storativity is

about 5 x 10^{-4} and the tests indicated the presence of an impermeable boundary detectable after 300 s of pumping. The testing also revealed the presence of a small leak in the original borehole packer system. The leak was verified when the packer system was removed from the borehole for inspection. It was repaired and the casing system replaced in the borehole. Hydraulic pressures were allowed to stabilize prior to injection of the gas.

5. THE GAS INJECTION TEST

Helium gas was injected into the isolated lower zone of borehole B-34 for an 11-d period in 1989 October. The arrival of the gas at the surface and its spatial distribution were monitored by sampling from temporary access tubes installed previously when measurements were made to determine natural He levels in the area. Monitoring continued for 38 d after injection had ceased. The following sections describe the techniques used and results of this test, and the results are compared with model predictions of gas flow to the surface.

5.1 SAMPLING AND ANALYTICAL METHODS

Soil gases were sampled using both the mobile sampling system described by Gascoyne and Wuschke (1990) and temporary access tubes, which were specifically installed for the duration of the test. Duplicate and often triplicate samples of soil gas were taken in 10-mL syringes from each site.

All samples were analysed within 24 h on a Veeco MS 18AB helium leak detector. The leak detector had been converted to function as a mass spectrometer by installation of a gas inlet system. The Veeco MS 18AB has an enhanced sensitivity over most other commercially available leak detectors and can potentially detect differences in He concentration as low as ±6 ppb* in atmospheric air. In practice, however, signal instability and drift, and the problem of signal attenuation due to sample evacuation (see Appendix C) resulted in a working sensitivity of about ±30 ppb. This proved to be quite adequate both for determining the natural He background levels and the elevated concentrations resulting from the gas injection test. A full description of the sampling and analytical methods used is given in Appendix C.

5.2 DETERMINATION OF BACKGROUND He

Because of the problems in mass spectrometric analysis experienced in the previous He survey of the gridded area near borehole B-34 (Gascoyne and Wuschke 1990), a detailed survey of background He level in soil gases was performed prior to the start of the injection test. Over 100 sites were sampled in the field grid area (Figure 16). These sites had been sampled for Rn in 1988. Samples were also obtained from access tubes installed in a radial grid around B-34 and in other tubes in adjacent areas to the field

---

* 1 ppb = 1 nL/L

grid (Figs. 16, 17, and 18). A radial array was also established in case the injected gas did not follow the predicted pathway (i.e., up the dip of FZ2 towards the field grid).

The results of the background He survey are listed in Table 2 and are shown as a contour diagram in Figure 19. It can be seen that the site of the Rn anomaly observed in the 1988 survey did not also have a detectable He anomaly, suggesting that the cause of the Rn anomaly was likely to be a localized excess of ^{226}Ra in the overburden rather than rapidly discharging groundwater at that location.

The survey showed that He was present in soil gases at above atmospheric levels, close to the road, as first observed in the 1987 survey (Gascoyne and Wuschke 1990). This time, however, the anomaly was concentrated in a much smaller area than previously seen (about 10 m x 10 m instead of about 100 m x 100 m in the 1987 survey). This may be due to a reduction in groundwater discharge caused by a gradual decline in hydraulic head of FZ2 over the 1987-1989 period (see Section 4.3). In the 1989 survey, maximum He concentrations observed were close to 4 ppm above atmospheric levels, whereas previously a maximum anomaly of only 0.5 ppm had been measured. This difference is probably due to the greater density of sampling sites in the 1989 survey, when a deliberate effort was made to locate the centre of the anomaly.

The survey of the radial grid sites and other sites adjacent to these areas revealed no other He anomalies.

5.3 GAS INJECTION EQUIPMENT

The equipment installed for injecting He gas into borehole B-34 Zone 2, is shown schematically in Figure 20. Three He cylinders (7.9 m^3 each) were connected to a manifold fitted with a low-range, pressure-reducing valve to allow precise control of He injection gas pressure and flow rate to the borehole. Gas flow was monitored by an Omega digital mass flowmeter (calibrated flow range 0-20 $L \cdot min^{-1}$) connected to a chart recorder for continuous monitoring. At the time, an Omega flowmeter calibrated for helium gas flow rates was not available from the supplier and so one calibrated for nitrogen was used instead. However, the manufacturer's user manual indicated that over the calibrated 0-20 $L \cdot min^{-1}$ range of the flowmeter, the helium flow rate could be obtained by multiplying the rate for N_2 by 1.454. In case of failure of the Omega flowmeter, a Matheson gas flowmeter (rising ball type, flow range 0-40 $L \cdot min^{-1}$) was installed for periodic manual readings. The Omega flowmeter performed without fault throughout the test and the manual readings were not used. During the injection, readings from the Omega digital display were recorded periodically, along with other test parameters (Table 3).

The injected gas was passed through each flowmeter, connected in series, before reaching the borehole casing. Except for the gas cylinders, the monitoring equipment was contained in a mobile trailer positioned near the borehole. Electrical power for the equipment and heating for the trailer was provided by a 10-kW diesel generator. Because of line voltage fluctuations from the generator output and the need to protect the recording

equipment from power failure, an auxiliary power supply (power purifier and battery backup) was installed in the trailer.

At the borehole head, a fluid-filled pressure gauge was installed on the casing cap to allow manual reading of gas pressure in the borehole. Comparison of pressure readings from gauges on the manifold regulator and casing top showed that there was no significant systematic pressure differential across the monitoring equipment (Table 3).

5.4 GAS INJECTION AND FLOW RATES

Pre-test conditions in the area were established by measuring water levels in B-34 and in adjacent field piezometers. The results for B-34 are shown in Figure 15 and piezometer levels are shown in Figure 21.

Prior to gas injection, all the installed equipment was tested by pressurizing the borehole zone with He to an equivalent depth of 30 m below normal hydrostatic level. In this way, gas leaks in the surface equipment could be detected and repaired before the start of the test. The absence of leaks in the equipment and in the borehole casing down to the top packer was verified by obtaining a zero gas flow once the depressed water level in B-34 Zone 2 had ceased downward movement. The integrity of the casing and top packer was also verified by observing the absence of gas bubbles at the water surface in the outside borehole casing (water was added to raise the piezometric surface to the top of the casing).

The gas injection test began on 1989 October 13. Gas was introduced to the casing in gradual steps while the increase and subsequent decrease in gas flow rate were being monitored on the chart recorder (Figure 22) for each pressure increment. When no gas was entering fractures in the rock mass, the gas flow rate returned to zero. However, as gas pressure was increased and more water was displaced from the borehole, the time to attain a zero flow rate increased significantly because of the hydraulic characteristics of the fracture network. It was decided, therefore, that, instead of waiting for a zero gas flow rate following each pressure increment, the pressure would be increased in frequent steps until continuous gas flow into the fracture was observed (region A in Figure 22). Gas pressure was then reduced slightly, in two steps, so that a flow of about 6 $L \cdot min^{-1}$ into the borehole zone was obtained (region B in Figure 22) about 5 h after injection began. This flow rate allowed for the possibility of precisely monitoring an increase or decrease within the range setting on the chart recorder, which might occur as a result of the response of the hydrogeological system. The response of B-34 Zone 1 to the gas injection was monitored by recording the adjusted water level in the outer casing of the borehole (Table 3).

Over the first 24 h of injection, the gas flow rate increased gradually to over 12 $L \cdot min^{-1}$ before the gas cylinders had to be changed. Flow rate dropped after the changeover, even though the manifold reducing valve was not adjusted during the change and gas pressure was maintained in the borehole. This may be due to a slight hydraulic recovery of the fracture zone during the 20 min of zero gas flow. This characteristic can be seen in most of the other cylinder changeovers (Figure 23), where the resulting

decreases in flow rate vary from near zero to several litres per minute. A distinct reduction in flow rate was observed after two periods of zero flow (~2 h each) when the cylinders ran out of gas in advance of the planned changeover (Figure 23). Despite these effects, gas flow into the zone continued to increase during the test, attaining over 20 $L \cdot min^{-1}$, 5 d after the test began. Flow rates between about 17 and 22 $L \cdot min^{-1}$ were maintained for the remainder of the test. Gas injection ended after 11 d, on October 24. Shut-in pressure was maintained until November 1, when the borehole was vented to the atmosphere. Throughout the test, the water level in B-34 Zone 1 slowly fell to about 40 cm below casing top (Table 3). No gas bubbles were observed during this period, indicating the absence of gas transport past the packer or through vertical fractures connecting Zone 1 to the injection zone.

The data in Table 3 were used to determine whether the variation in gas flow rate was related to changes in injection pressure, as determined by the pressure gauge on the borehole casing. The lack of correlation can be seen in Figure 24, indicating that periods of high and low gas flow are a function of the hydraulics of the fracture zone rather than variations in the gas injection characteristics.

5.5 SOIL GAS SURVEY RESULTS

Sampling of soil gases was performed daily at selected grid sites to detect gas breakthrough at the surface and its location. Because of the time required to sample gases using the removable sampler in the field grid site (about 5 min per site), only a selected number of sites were sampled and analysed on a daily basis. This number increased as the gas front was found to spread so that on the last day of injection, October 23, 33 radial and 58 field grid sites were sampled and analysed (Table 2).

The first clear indication of gas breakthrough at ground surface was seen about 48 h after injection began at two sites close to borehole B-34 in the radial array (sites 20M-1 and 10M-2, Figure 17). Helium concentrations of over 10 ppm were observed in soil gases at these sites (Table 2). On subsequent days, He concentrations increased rapidly at most of the radial grid sites and attained a maximum of 4% of total soil gas (i.e., 40 000 ppm He) at the initial breakthrough sites. Across the road, in the field grid sites, He concentrations increased above background between about 4 and 8 d after injection began. By October 23, 11 d after the start of injection, all field grid sites that were sampled were showing elevated He concentrations, although maximum concentrations were generally below 3 ppm above atmospheric levels. The distribution of He above background is shown for all sites in Figure 25. Two areas of maximum He concentration are evident at this stage of the injection, one centred on the neighbouring sites 20M-1 and 10M-2, close to the borehole, and one centred at site 40M-3, 40 m to the south of the borehole. In both areas, He attained 4% of total soil gas.

The difference in response and maximum concentrations attained between sites 20M-1 and 10M-2 and the more remote radial and field grid sites can be clearly seen in Figures 26 and 27. These diagrams also show the decline of He concentrations after injection ceased. Within 7 d, all field grid

sites had returned to background He levels. However, He concentrations of 20 ppm above background were still present in soil gases at 20M-1 and 10M-2 in the radial grid, 39 d after injection had ceased.

5.6 PIEZOMETER RESPONSE

Hydrographs for piezometers close to borehole B-34 are shown in Figure 21 for the period 1989 September to December. Pronounced variations in water level are seen in only one piezometer, 0-33, where an increase in level of about 1 m was observed soon after the start of the test. This well monitors the hydrostatic head in the sandy till at the base of the overburden, about 30 m from borehole B-34. No response was observed in higher piezometers in this nest, borehole M-5A or any other piezometers in the area.

6. DISCUSSION

The results of the injection test show that gas moved rapidly away from the injection location in the borehole and reached the surface between one and two days after injection had begun. Most of the gas came to surface within about 40 m to the south and east of the injection borehole. Only minor amounts appeared to migrate to the west, up the dip of FZ2. These results and their implications for gas migration in the subsurface are considered in greater detail below.

6.1 GAS INJECTION AND FLOW RATES

For a constant pressure of injection, the gas flow rate into B-34 Zone 2 increased from 6 to over 20 $L \cdot min^{-1}$ during the first 5 d of the test (Figure 23). A reduction in flow rate might be expected to occur because of the influence of the lower permeability boundary conditions detected during the hydraulic testing of the borehole (see Section 4.4). The increase that was observed in gas flow rate may be explained by a small displacement of water laterally, without incurring influence of the hydraulic boundary, while the gas penetrated permeable, steeply inclined fractures above FZ2. Eventually, a continuous gas phase formed along this upward migration path and lateral displacement of groundwater ceased. The reduction in hydrostatic pressure on the gas front as it rose allowed the gas to expand so that flow rates would ultimately be defined by the size of apertures the gas penetrates and not by hydrostatic head.

The relatively constant gas concentrations at the sampling sites during the latter part of the injection test indicate that the gas/water front had become almost stationary. Because of the greater permeability of the bedrock relative to the overburden, a large portion of the open fractures near borehole B-34 would, therefore, likely be dewatered and acting as conduits for He gas to pass through the rock to the lower permeability fractures in the clay overburden. At steady state, the gas phase might, therefore, resemble a dendritic drainage pattern in reverse, with most of the flow restrictions close to the outlets (Figure 28).

6.2 MODELLING THE RESULTS OF THE INJECTION TEST

The average minimum breakthrough time for gas injected into FZ2 was between 1 and 2 d and for modelling was assumed to be 1.5 d. This time is shorter than the "best estimate" of 3-8 d derived for transport through FZ2 and the overburden at this site in the model described by Gascoyne and Wuschke (1990). To compare the predictions of the model with results observed in the injection test, parameters in the model were first revised to more accurately reflect injection pressures used and actual flow path distances.

6.2.1 Flow Path Geometry

Two principal flow paths in the bedrock were inferred from the results of the test: 1) along steeply inclined fractures that intersect FZ2 relatively near the gas injection point, and 2) along the plane of FZ2 itself to distribute to near-surface intersecting fractures and the permeable till at the base of the overburden.

The transport paths through the high-permeability fractures above FZ2 were idealized for modelling purposes as shown in Figure 29, i.e., transport was assumed to be along a straight path characterized by its angle with the horizontal, in any plane (although it is recognized that the actual pathway will usually be more complex than this). This is an extension of the original model, which modelled transport along one pathway only, i.e., through the fracture zone via the shortest route to the surface (Figure 1).

The breakthrough time at any surface grid point is the sum of the transport times through the rock and overburden, and therefore depends on the properties of both the rock and overburden. The overburden is assumed to have uniform properties (hydraulic conductivity, fracture spacing, and thickness of the saturated zone) throughout the test area, and hence the transport time through the overburden is the same at all grid locations.

The breakthrough times for different points on the grid are therefore determined only by the properties of the fractured rock along the flow path to that point and by the geometry of the flow path, characterized by its angle with the horizontal (α). This angle can be obtained from the horizontal distance (Z) from the point of injection to the overburden/bedrock contact below the grid point (Figure 29), using the relationship

$$\alpha = \tan^{-1}\left[\frac{H}{Z}\right] \quad ,$$

where H is the vertical distance from the point of injection to the rock-overburden interface. The assumption is made that, for each grid point, the fractured rock has uniform properties all along the flow path to that grid point.

The input parameters for modelling the injection tests and the field test results are summarized in Table 4.

6.2.2 Threshold Pressure

The calculated threshold pressure for gas injection is 0.35 MPa, and the injection test was carried out at an injection pressure of ~0.37 MPa. The threshold and injection pressures are slightly lower than the previously calculated threshold pressure. This was because the previous calculation was based on 13 m of saturated overburden; in fact, field measurements have shown that only about 8 m of the overburden is saturated, so the hydraulic pressure and threshold pressure for injection are both lower than estimated by ~5 m of water pressure head (0.05 MPa). Gas flow through the remaining ~5 m of unsaturated overburden is assumed to be instantaneous.

6.2.3. Transport Time Through the Overburden

The highest concentration of He appearing at the minimum breakthrough time (1.5 d) occurred at grid point 20M-1, 20 m horizontally from the point of injection. The transport path through the fractured rock is therefore characterized by an angle of $\tan^{-1}(27/20)$ or 53.5°. Assuming the properties of this transport pathway are the same as the properties measured in the field tests of FZ2 (Gascoyne and Wuschke 1990), the "best estimate" of the breakthrough time along this pathway through the fractured rock is 0.3 d. The transport time through the overburden is therefore 1.5 - 0.3 = 1.2 d.

Using the model described by Gascoyne and Wuschke (1990), the hydraulic conductivity of the overburden can be calculated from the transport time through the overburden and estimates of the fracture spacing in the overburden. The calculated hydraulic conductivities of the overburden are approximately 5×10^{-12}, 5×10^{-11} and 5×10^{-10} $m \cdot s^{-1}$ for fracture spacings of 10, 1 and 0.1 m respectively.

6.2.4 Gas Concentrations

The maximum concentration of He gas was found to be 4% of total soil gas (at 0.5-m depth in the overburden) at three sites in the radial grid (10M-2, 20M-1 and 40M-3). Soil gases at other radial grid sites were significantly lower in He content, ranging from background up to 850 ppm (0.085%), and all field sites were less than 3 ppm above atmospheric levels. It is not possible to determine a He budget for steady-state conditions with any reasonable precision, because of the point nature of the gas sampling sites, the large spacing between them and the fact that gas flow rates at each of the sites were not measured. However, because He concentrations at a number of radial grid sites exceed all field sites by several orders of magnitude, it is likely that well over 90% of the injected gas emerged close to the site of injection, within ~50 m of the borehole.

6.2.5 Properties of the Transport Paths Through the Fractured Rock

The variation of breakthrough time with distance from the injection point is shown in Figure 30 for all grid points (40) at which He was measured above background levels within the 11-d period of gas injection. The error bars illustrate the uncertainty in the breakthrough times, arising because

gas samples were taken only once daily, at best. Superimposed on this plot are curves showing calculated values of breakthrough time as a function of the hydraulic conductivity of the fractured rock. The breakthrough times for all grid points at which He was measured are consistent with a hydraulic conductivity of between 2 x 10^{-8} and 5 x 10^{-5} $m \cdot s^{-1}$ for the fractured rock if the fracture spacing is 1.0 m, (i.e., if the fracture spacing is at the upper limit of its estimated range 0.4-1.0 m). If fracture spacing is at the lower end (0.4), the estimated hydraulic conductivity of the rock would be higher by a factor of 2.5.

Using the information shown in Figure 30, a best estimate of the hydraulic conductivity of the fractured rock was made for each grid point. Figure 31 illustrates these estimates for a fracture spacing of 1 m.

The estimates of hydraulic conductivity show a zone of high permeability southwest of injection borehole B-34 and just across the road, i.e., at grid points 7-11, 9-10, 11-11. The estimated hydraulic conductivity of the fractured rock along the pathways leading to these grid points is ~2 x 10^{-5} $m \cdot s^{-1}$ (assuming a fracture spacing of 1 m). Other grid points in the same general area (8-12.11, 8-12.2, 8-12.9) and outside it (2-8 and 15-7) indicate a slightly lower hydraulic conductivity of ~1 x 10^{-6} $m \cdot s^{-1}$. The large zone of higher permeability lies approximately above the outcrop of fracture zone FZ2, as predicted from geological information, and coincides with the area of localized groundwater discharge determined in the 1987 and 1989 soil gas He surveys. Flow paths to the remaining grid points at which injected gas was detected have estimated hydraulic conductivities in the range from ~2 x 10^{-8} to 5 x 10^{-7} $m \cdot s^{-1}$. Pathways to the few grid points at which gas was not detected probably have still lower hydraulic conductivities.

The analysis shows that the gas migration pathways to grid points near the injection well have relatively low estimated hydraulic conductivities of ~2 x 10^{-8} to 5 x 10^{-7}, even though some are within FZ2. However, because samples were taken only once a day, there are large uncertainties in the breakthrough times at these grid points (see error bars in Figure 30), and there is a correspondingly large uncertainty in the hydraulic conductivity of the pathways to them.

The results presented above and in Figure 31 apply to a fracture spacing of 1.0 m in the bedrock. As previously stated, if the fracture spacing is 0.4 m, estimated hydraulic conductivities of the fractured bedrock would be a factor of 2.5 larger.

7. SUMMARY AND CONCLUSIONS

Injection of He gas at about 40-m depth into a groundwater-saturated, low-dipping fracture zone in a granitic pluton was successfully performed during an 11-d period in 1989 October. For a constant injection pressure, the gas flow rate increased over this period from 5 $L \cdot min^{-1}$ to a relatively steady value of 20 $L \cdot min^{-1}$. The breakthrough of injected gas was detected in the surface soils within 2 d of the start of injection. Towards the end

of the test, a survey of the area around the injection borehole identified two areas of high gas discharge, one within 40 m to the south and east of the injection well, and a larger general area of trace levels of gas discharge, within 200 m to the west. The high discharge sites lie approximately on strike with steep northwest dipping fractures observed in borehole B-34 within the main fracture zone and the north-northeast strike of the most common set of near-surface, erosional-relief vertical fractures at the URL. This suggests that the preferential pathway for rapid gas migration was through inclined permeable fractures that intersect the fracture zone close to the injection point. In the high-discharge location, migration through the overburden appears to be the limiting factor in controlling the breakthrough time of gas at the surface. The larger, more diffuse region of gas discharge to the west corresponds to the projected outcrop of the low-dipping fracture zone beneath the overburden, indicating that some of the injected gas was also transported along the plane of the low-dipping fracture zone but in relatively minor amounts. The large differences in He gas content of soil gases close to, and distant from, the injection site suggest that well over 90% of injected gas was transported to the surface within ~50 m of the borehole through the network of steeply inclined fractures that intersect the low-dipping zone.

The data obtained from geophysical, hydrogeological and overburden stratigraphic measurements assisted in indicating the location of the fracture zone subcrop, and provided useful information on the local hydraulic regime and overburden thickness and type.

Gas arrival at the surface was somewhat faster than predicted by the model developed prior to the test, but this is partly because the injected gas followed shorter flow path distances in both bedrock and overburden than assumed in the original model. Revisions to the model, taking into account these differences, the actual injection pressure conditions and improved estimates of fracture spacing in rock and overburden, give a close fit with model breakthrough times for the high-discharge sites. The results indicate that the overburden has a relatively low hydraulic conductivity ($\sim 10^{-10}$ m$\cdot$s^{-1}).

The permeable pathways that the injected gas followed in migrating through the fractured rock have been identified by comparing gas breakthrough times at the sampling grid points and their distance from the point of injection. The hydraulic conductivity of these pathways has been calculated from the model and found to range from about 10^{-5} m$\cdot$s^{-1} to 10^{-8} m$\cdot$s^{-1}, assuming a fracture spacing of 1.0 m.

This work and the soil gas investigations performed in Phase 1 of the project demonstrate the usefulness of soil gas analyses and gas injection tests in determining areas where groundwater discharge is occurring from deeply penetrating fracture zones and also in detecting places where steeply inclined fractures in bedrock can be preferential pathways for gas migration out of these fracture zones. Modelling the gas injection test results has also been useful in estimating the hydraulic conductivities of gas flow paths through the fractured rock.

ACKNOWLEDGEMENTS

The assistance of Zain Lyall, Ken de Vos, and Martin Ridgway (Co-op students) and Alain Larocque, in various aspects of this project is greatly appreciated. Prof. E.M. Durrance (Dept. of Geology, University of Exeter/ Lincoln-Nebraska) has provided advice throughout this project. Comments and support of Cliff Davison, Denis McConnell, Tin Chan (of AECL) and N.T. Harrison and K.R. Butter (of UKDOE) is gratefully acknowledged. This work was jointly funded by AECL and the U.K. Department of the Environment.

REFERENCES

Banwell, G.M. and Parizek, R.R. 1988. Helium 4 and radon 222 concentrations in groundwater and soil gas as indicators of zones of fracture concentration in unexposed rock. Journal of Geophysical Research 93, 355-366.

Braester, C. and Thunvik, R. 1982. An analysis of the conditions of gas migration from a low-level radioactive waste repository. Swedish Nuclear Fuel Suuply Co., Division KBS Report, SKBF-KBS-TR-83-21.

Brown, A., Soonawala, N.M., Everitt, R.A. and Kamineni, D.C. 1989. Geology and geophysics of the Underground Research Laboratory site, Lac du Bonnet Batholith, Manitoba. Canadian Journal of Earth Sciences 26, 404-425.

Davison, C.C. 1984. Monitoring hydrogeological conditions in fractured rock at the site of Canada's Underground Research Laboratory. Ground Water Monitoring Review 4, 95-102.

Davison, C.C. and Kozak, E.T. 1988. Hydrogeological characteristics of major fracture zones in a granite batholith of the Canadian Shield. In Proceedings of the 4th Canadian/American Conference on Hydrogeology (Hitchon, B. and Bachu, S.,editors), Banff, AB, 1988, 52-59.

Everitt, R.A., Brown, A., Davison, C.C. and Martin, C.D. 1990. Regional and local setting of the Underground Research Laboratory. In Proceedings of the Symposium on Unique Underground Structures, Denver, CO, 1990, 64-1 - 64-23.

Gascoyne, M. and Wuschke, D.M. 1990. Fracture detection and groundwater flow characterization in poorly exposed ground using helium and radon in soil gases. U.K. Department of the Environment Report DOE/RW/90/079.

Gascoyne, M., Ross, J.D. and Watson, R.L. 1988. Geochemical and isotopic characterization of flow in fractured rocks: Examples from the Canadian Shield. In Proceedings of the 4th Canadian/American Conference on Hydrogeology (Hitchon, B. and Bachu, S.,editors), Banff, AB, 1988, 20-31.

Gregory, R.G. and Durrance, E.M. 1987. Helium, radon and hydrothermal circulation associated with the Carnmenellis radiothermal granite of southwest England. Journal of Geophysical Research 92 (B12), 12567-12586.

Hayles, J.G., Stevens, K.M. and Lodha, G.L. In preparation. Geophysical investigations for fracture detection and overburden mapping west of borehole B-34, Lee River Area, Lac du Bonnet, Manitoba. Atomic Ebnergy of Canada Limited Report, AECL-XXXXX.

Hvorslev, M.J. 1951. Time lag and soil permeability in groundwater observations. U.S. Army Corps. Eng., Waterways Experiment Stn. Bull. No. 36.

Larocque, J.P.A. and Gascoyne, M. 1986. A survey of the radioactivity of surface water and groundwater in the Atikokan area, northwestern Ontario. Atomic Energy of Canada Limited Technical Record, TR-379.*

Malmqvist, L., Isaksson, M. and Kristiansson, K. 1989. Radon migration through soil and bedrock. Geoexploration 26, 135-144.

Thorne, G.A. 1990. Hydrogeology of surficial materials of Permit Areas D and F and the Lee River Study Area in the Whiteshell Research Area. Atomic Energy of Canada Limited Technical Record, TR-498*.

Thunvik, R. and Braester, C. 1987. Calculation of gas migration in fractured rock. Swedish Nuclear Fuel and Waste Management Co. Technical Report, KBS-TR-87-18.

Worgan, K.J., Pearson, J. and Nunez-McNally, T. 1990. A review of modelling of gas migration in porous and fractured rock. U.K. Department of the Environment Report DOE/RW/89/101.

---

* Unpublished, report available from SDDO, AECL Research, Chalk River Laboratories, Chalk River, Ontario, Canada K0J 1J0.

TABLE 1

INJECTION PRESSURES AND ESTIMATED BREAKTHROUGH TIMES FOR GAS INJECTION TESTS

Case	Rock Only - Case 1	Rock & Overburden	
		Rock - Case 2	Overburden - Case 3
Input Parameters			
Depth of rock or overburden (m)	40	27	13
Hydraulic conductivity (m/s)	2×10^{-6}	2×10^{-6}	2×10^{-9}
Angle of inclination to horizontal (°)	20°	20°	90°
Fracture spacing (m)	27	27	1
Calculated Parameters			
Path length for gas (m)	117	79	13
Effective fracture width (m)	0.44×10^{-3}	0.44×10^{-3}	0.015×10^{-3}
Capillary pressure (MPa)	0.34×10^{-3}	0.34×10^{-3}	0.01
Threshold pressure (MPa)	0.39	0.39	0.40
Injection Pressure (MPa)	Breakthrough Time* (d)		
0.393	0.21	0.14	0.23
0.403	0.090	0.053	0.22
0.413	0.070	0.040	0.21
0.423	0.060	0.034	0.21
0.433	0.052	0.029	0.20
0.443	0.047	0.026	0.19
0.453	0.043	0.023	0.19
0.463	0.039	0.021	0.18
0.473	0.037	0.020	0.18
0.483	0.034	0.018	0.17
0.493	0.032	0.017	0.17

* Breakthrough times may be up to 100 times greater because of time taken to fill excess porosity in non-uniform cracks. "Best estimates" are 20-30 times greater than shown.

TABLE 2

CONCENTRATIONS OF HELIUM IN SOIL GAS SAMPLES OBTAINED FROM ALL SAMPLING SITES OVER THE PERIOD 1990 SEPTEMBER TO DECEMBER

DATE	TIME	SITE	Average He (ppb)	He #1 (ppb)	He #2 (ppb)	He #3 (ppb)
Sept 7 1989	10:30	1-1	-284	-103	-464	-
Sept 7 1989	11:00	2-1	-103	-376	17	51
Sept 7 1989	11:15	3-1	-129	253	-116	-68
Sept 7 1989	11:30	4-1	57	-68	0	240
Sept 7 1989	11:40	5-1	-60	-138	19	-
Sept 7 1989	11:45	6-1	-7	71	-55	-36
Sept 7 1989	11:55	7-1	-53	-69	-36	-
Sept 7 1989	12:00	8-1	-25	-37	-55	18
Sept 7 1989	12:10	9-1	160	337	-18	-
Sept 7 1989	12:15	10-1	23	207	-161	-
Sept 7 1989	12:25	11-1	-77	-120	-18	-92
Sept 8 1989	11:10	centre	-21	-21	-	-20
Sept 8 1989	11:20	11-2	-88	-62	-41	-161
Sept 8 1989	11:30	10-2	13	41	61	-62
Sept 8 1989	11:40	9-2	-41	83	-41	-164
Sept 8 1989	11:50	8-2	0	-62	62	-20
Sept 8 1989	11:56	7-2	-27	-41	-20	-21
Sept 8 1989	12:03	6-2	-21	-62	-41	41
Sept 8 1989	12:10	5-2	-101	-181	-20	-
Sept 8 1989	12:15	4-2	-7	41	20	-82
Sept 8 1989	12:17	3-2	-56	-120	-20	-116
Sept 8 1989	12:20	2-2	-47	-40	-100	0
Sept 8 1989	12:25	1-2	40	0	100	20
Sept 8 1989	12:30	1-3	-41	-20	-41	-61
Sept 8 1989	12:40	2-3	-36	-20	-197	102
Sept 8 1989	12:45	3-3	-6	40	0	-56
Sept 8 1989	12:50	4-3	13	100	-20	-40
Sept 8 1989	12:55	5-3	-47	-101	-39	0
Sept 8 1989	13:00	centre	-	-	-	-
Sept 11 1989	11:00	centre	-205	-83	-287	-246
Sept 11 1989	11:05	6-3	27	-20	20	81
Sept 11 1989	11:15	7-3	67	61	100	40
Sept 11 1989	11:20	8-3	-13	0	62	-100
Sept 11 1989	11:25	9-3	33	20	0	79
Sept 11 1989	11:30	10-3	0	-20	20	0
Sept 11 1989	11:35	11-3	13	0	20	20
Sept 11 1989	11:40	11-4	-14	80	-122	0
Sept 11 1989	11:45	10-4	27	20	20	40
Sept 11 1989	11:50	9-4	-34	-41	-40	-20
Sept 11 1989	11:53	8-4	21	-20	0	62
Sept 11 1989	11:56	7-4	-26	-118	20	20
Sept 11 1989	12:01	6-4	-26	-20	-20	-37
Sept 11 1989	12:50	5-4	20	-81	61	60

DATE	TIME	SITE	Average He (ppb)	He #1 (ppb)	He #2 (ppb)	He #3 (ppb)
Sept 11 1989	12:59	4-4	47	0	20	121
Sept 11 1989	13:02	3-4	20	20	-20	59
Sept 11 1989	13:06	2-4	59	139	-20	59
Sept 11 1989	13:10	1-4	14	79	-37	0
Sept 11 1989	13:13	1-5	-7	0	-39	19
Sept 11 1989	13:20	2-5	66	59	136	0
Sept 11 1989	13:28	3-5	-57	-20	-19	-132
Sept 11 1989	13:30	4-5	-86	-78	-40	-136
Sept 11 1989	13:35	5-5	-58	-58	-57	-58
Sept 11 1989	13:40	6-5	-82	0	-228	-19
Sept 11 1989	13:44	7-5	-51	-21	-37	-96
Sept 11 1989	13:49	8-5	19	20	19	19
Sept 11 1989	13:55	9-5	-46	-	-73	-19
Sept 11 1989	14:03	10-5	-0	-37	-19	55
Sept 11 1989	14:10	11-5	-79	-238	-36	36
Sept 11 1989	14:15	centre	-18	-18	-54	19
Sept 12 1989	11:46	centre	144	137	159	137
Sept 12 1989	12:02	1-6	-81	0	-228	45
Sept 12 1989	12:12	2-6	38	44	46	23
Sept 12 1989	12:20	3-6	68	-45	159	90
Sept 12 1989	12:28	4-6	45	68	0	68
Sept 12 1989	12:40	5-6	37	22	67	22
Sept 12 1989	12:50	6-6	89	158	22	90
Sept 12 1989	13:00	7-6	51	22	44	88
Sept 12 1989	13:10	8-6	-15	22	-89	22
Sept 12 1989	13:20	9-6	96	109	90	88
Sept 12 1989	13:30	10-6	15	66	-43	22
Sept 12 1989	13:38	11-6	-29	43	-175	44
Sept 12 1989	14:39	11-7	-1	-23	22	-
Sept 12 1989	14:48	10-7	0	-44	22	22
Sept 12 1989	14:56	9-7	15	-64	43	66
Sept 12 1989	15:07	8-7	0	65	-22	-43
Sept 12 1989	15:22	7-7	-16	0	-66	22
Sept 12 1989	15:33	6-7	-43	0	-21	-109
Sept 12 1989	15:43	5-7	14	-22	65	0
Sept 12 1989	15:57	centre	-161	-43	-22	-417
Sept 13 1989	8:38	centre	44	-	0	87
Sept 13 1989	8:43	4-7	1	-65	22	65
Sept 13 1989	8:48	3-7	44	22	109	0
Sept 13 1989	8:54	2-7	22	-65	110	22
Sept 13 1989	8:59	1-7	65	22	65	109
Sept 13 1989	9:03	1-8	-0	-22	43	-22
Sept 13 1989	9:11	2-8	7	-65	65	21

DATE	TIME	SITE	Average He (ppb)	He #1 (ppb)	He #2 (ppb)	He #3 (ppb)
Sept 13 1989	9:15	3-8	-14	0	-21	-22
Sept 13 1989	9:20	4-8	56	66	44	-
Sept 13 1989	9:27	5-8	-41	65	-163	-21
Sept 13 1989	9:29	6-8	-42	65	0	-192
Sept 13 1989	9:37	7-8	-145	-65	-64	-257
Sept 13 1989	9:41	8-8	28	22	42	21
Sept 13 1989	9:48	9-8	93	172	42	64
Sept 13 1989	10:33	10-8	50	21	64	66
Sept 13 1989	10:55	11-8	56	65	20	86
Sept 13 1989	11:00	11-9	-32	42	-60	-79
Sept 13 1989	11:05	10-9	21	-22	85	0
Sept 13 1989	11:08	9-9	64	129	21	42
Sept 13 1989	11:13	8-9	-7	-21	-60	61
Sept 13 1989	11:17	7-9	56	189	-42	20
Sept 13 1989	11:25	6-9	21	143	83	-164
Sept 13 1989	11:34	5-9	-34	20	-41	-82
Sept 13 1989	11:44	4-9	59	39	79	80
Sept 13 1989	11:52	3-9	-33	60	-298	130
Sept 13 1989	11:57	2-9	12	81	59	-104
Sept 13 1989	13:15	1-9	13	-19	78	-19
Sept 13 1989	13:23	1-10	46	97	99	-59
Sept 13 1989	13:29	2-10	78	-19	78	175
Sept 13 1989	13:41	3-10	-8	0	-39	20
Sept 13 1989	13:45	4-10	53	39	60	59
Sept 13 1989	13:52	5-10	19	0	39	19
Sept 13 1989	13:57	6-10	26	58	0	19
Sept 13 1989	14:02	7-10	19	39	0	19
Sept 13 1989	14:06	8-10	6	19	58	-59
Sept 13 1989	14:12	9-10	-138	-155	-39	-219
Sept 13 1989	14:18	10-10	32	19	78	0
Sept 13 1989	14:25	11-10	-32	-78	39	-58
Sept 13 1989	14:32	11-11	13	39	58	-58
Sept 13 1989	14:38	10-11	0	19	-19	0
Sept 13 1989	14:45	9-11	-32	0	0	-97
Sept 13 1989	14:50	centre		-96	19	-36
Sept 14 1989	10:51	centre	74	102	69	51
Sept 14 1989	11:32	5-11	63	17	172	0
Sept 14 1989	11:45	7-11	132	157	120	120
Sept 14 1989	11:52	6-11	45	66	-34	102
Sept 14 1989	12:02	5-11	-82	0	-102	-84
Sept 14 1989	12:12	4-11	34	34	-17	86
Sept 14 1989	12:21	3-11	12	69	-51	17
Sept 14 1989	12:41	2-11	40	52	70	17
Sept 14 1989	12:53	1-11	-34	34	-87	-68

continued...

TABLE 2 (continued)

DATE	TIME	SITE	Average He (ppb)	He #1 (ppb)	He #2 (ppb)	He #3 (ppb)
Sept 14 1989	13:00	1-12	-6	17	-69	35
Sept 14 1989	13:11	2-12	-22	0	17	-84
Sept 14 1989	13:22	3-12	-28	68	-67	-84
Sept 14 1989	13:32	4-12	-11	-118	0	84
Sept 14 1989	13:42	5-12	26	17	34	-
Sept 14 1989	13:50	6-12	35	-183	169	99
Sept 14 1989	14:01	7-12	112	100	135	100
Sept 14 1989	14:11	8-12	245	182	234	319
Sept 14 1989	14:30	centre	-78	-269	52	-17
Sept 18 1989	11:52	centre	-91	-166	-43	-64
Sept 18 1989	12:10	A1-2	-113	-254	0	-65
Sept 18 1989	12:21	A2-2	-106	-169	-106	-43
Sept 18 1989	12:30	A2-4	-55	-83	-83	0
Sept 18 1989	12:41	A1-4	-21	-42	-42	21
Sept 18 1989	12:48	A1-6	-75	-20	-164	-41
Sept 18 1989	12:58	A2-6	-48	-64	20	-61
Sept 18 1989	13:08	A3-6	-138	-100	-168	-121
Sept 18 1989	13:36	A3-8	-77	-42	-188	0
Sept 18 1989	13:46	A2-8	-14	21	-83	0
Sept 18 1989	13:56	A1-8	-34	-20	-61	-21
Sept 18 1989	14:08	A1-10	-115	-60	-146	-139
Sept 18 1989	14:17	A2-10	-54	-60	-81	-20
Sept 18 1989	14:27	A3-10	-40	-40	0	-80
Sept 18 1989	14:43	A1-12	-100	-120	-159	-20
Sept 18 1989	15:53	centre	-53	20	-40	-138
Sept 19 1989	8:36	centre	62	104	21	61
Sept 19 1989	9:40	5M-1	0	-	-	0
Sept 19 1989	9:52	5M-2	25	104	0	-20
Sept 19 1989	10:30	5M-3	14	0	-20	61
Sept 19 1989	10:03	5M-4	7	-20	-40	61
Sept 19 1989	10:10	5M-5	-87	61	-161	-161
Sept 19 1989	10:34	5M-6	7	-40	40	20
Sept 19 1989	10:17	5M-7	-40	0	-20	-101
Sept 19 1989	10:27	5M-8	20	-40	20	79
Sept 19 1989	10:40	10M-1	-28	-59	41	-59
Sept 19 1989	12:02	10M-2	-13	-39	-20	20
Sept 19 1989	11:13	10M-3	-28	-59	20	-40
Sept 19 1989	11:19	10M-4	-7	20	-60	20
Sept 19 1989	11:58	10M-5	-13	-40	-60	60
Sept 19 1989	11:25	10M-6	40	40	60	20
Sept 19 1989	11:35	10M-7	-73	-79	-60	-60
Sept 19 1989	11:49	10M-8	-20	0	-39	-20
Sept 19 1989	12:11	20M-1	5	0	40	-40

DATE	TIME	SITE	Average He (ppb)	He #1 (ppb)	He #2 (ppb)	He #3 (ppb)
Sept 19 1989	13:03	20M-2	0	-59	60	0
Sept 19 1989	12:50	20M-3	-7	-80	20	40
Sept 19 1989	13:06	20M-4	-33	-20	-59	-20
Sept 19 1989	13:15	20M-5	0	-	-	0
Sept 19 1989	12:57	20M-6	199	138	159	299
Sept 19 1989	13:27	20M-7	-73	-141	20	-98
Sept 19 1989	13:33	20M-8	-39	-162	-101	145
Sept 19 1989	13:39	40M-1	-63	40	-230	0
Sept 19 1989	13:49	40M-2	-61	-162	-	0
Sept 19 1989	13:55	40M-3	-87	-202	-101	41
Sept 19 1989	14:03	40M-4	0	-60	41	20
Sept 19 1989	14:10	40M-5	-176	-41	-224	-263
Sept 19 1989	14:15	30M-6	-34	21	-21	-103
Sept 19 1989	14:21	40M-7	-28	21	-62	-42
Sept 19 1989	14:23	40M-8	42	-63	84	105
Sept 19 1989	14:34	centre	0	-21	-21	43
Sept 21 1989	13:18	centre	25	19	0	56
Sept 21 1989	13:40	40M-1	56	111	0	56
Sept 21 1989	13:53	40M-2	-18	-91	19	18
Sept 21 1989	14:04	40M-3	0		0	0
Sept 21 1989	14:21	40M-4	-30	-36	18	-73
Sept 21 1989	14:31	40M-5	-	-	-	-
Sept 21 1989	14:43	30M-6	-72	-108	-36	-
Sept 21 1989	14:53	40M-7	-48	-108	-54	18
Sept 21 1989	15:06	40M-8	-12	-36	18	-18
Sept 21 1989	15:18	20M-1	-135	-126	-70	-210
Sept 21 1989	15:40	centre	-6	0	54	-73
Sept 22 1989	8:25	centre	33	65	0	33
Sept 22 1989	8:46	20M-2	55	0	99	65
Sept 22 1989	8:56	20M-3	49	33	16	98
Sept 22 1989	9:08	20M-4	22	-16	16	65
Sept 22 1989	9:20	20M-5	50	116	-33	66
Sept 22 1989	9:31	20M-6	-22	-82	49	-33
Sept 22 1989	9:39	20M-7	71	0	183	50
Sept 22 1989	9:48	20M-8	89	116	33	117
Sept 22 1989	9:58	10M-1	16	33	-50	66
Sept 22 1989	10:05	10M-2	66	66	50	83
Sept 22 1989	10:12	10M-3	22	-49	49	66
Sept 22 1989	10:22	10M-4	101	0	150	152
Sept 22 1989	10:32	10M-5	10	99	-61	-17
Sept 22 1989	10:43	10M-6	83	116	66	66
Sept 22 1989	10:52	10M-7	17	50	17	-17
Sept 22 1989	11:02	10M-8	17	116	50	-116

DATE	TIME	SITE	Average He (ppb)	He #1 (ppb)	He #2 (ppb)	He #3 (ppb)
Sept 22 1989	11:10	5M-1	78	17	84	134
Sept 22 1989	11:17	5M-2	11	66	-33	0
Sept 22 1989	11:28	5M-3	73	68	67	84
Sept 22 1989	11:36	5M-4	83	92	34	-
Sept 22 1989	11:53	5M-5	51	237	-102	17
Sept 22 1989	12:03	5M-6	88	66	101	70
Sept 22 1989	12:10	5M-7	-111	-	-169	-53
Sept 22 1989	12:24	5M-8	42	16	125	-16
Sept 22 1989	12:36	centre	116	237	125	-19
Oct 2 1989	8:35	centre	33	25	25	49
Oct 2 1989	8:50	8-12	295	277	395	276
Oct 2 1989	9:03	8-12.1	632	1378	283	258
Oct 2 1989	9:08	8-12.2	145	77	169	158
Oct 2 1989	9:14	8-12.3	83	332	257	-339
Oct 2 1989	9:18	8-12.4	3186	3330	3542	2685
Oct 2 1989	9:31	8-12.5	1668	1019	3201	755
Oct 2 1989	9:42	8-12.6	3468	3391	3590	3422
Oct 2 1989	9:47	8-12.7	1239	961	1381	1376
Oct 2 1989	10:12	8-12.8	60	121	48	70
Oct 2 1989	10:18	8-12.9	13	96	-	-71
Oct 2 1989	10:28	8-12.10	0	-	-24	24
Oct 2 1989	10:33	8-12.11	701	667	799	637
Oct 2 1989	10:45	centre	85	-24	146	132
Oct 12 1989	10:33	centre				
Oct 12 1989	10:40	11-11	-6	0	-79	60
Oct 12 1989	10:43	9-10	159	-61	430	128
Oct 12 1989	10:47	8-12.9	-26	-100	-19	42
Oct 12 1989	10:50	8-12.2	69	20	0	188
Oct 12 1989	10:53	8-12.11	9	0	-20	20
Oct 12 1989	10:57	8-12.4	21	20	102	-60
Oct 12 1989	10:59	8-12.5	13	-61	60	41
Oct 12 1989	11:01	7-11	21	20	63	-20
Oct 12 1989	11:04	4-12	-0	-20	39	-20
Oct 12 1989	11:07	2-8	-66	-59	-60	-80
Oct 12 1989	11:10	A1-6	14	0	41	0
Oct 12 1989	11:13	A3-10	-55	42	-208	0
Oct 12 1989	11:27	6M-1	-19	60	-137	20
Oct 12 1989	11:29	5M-3	-32	-137	0	40
Oct 12 1989	11:33	5M-4	-40	-41	-79	0
Oct 12 1989	11:36	5M-6	13	0	20	20
Oct 12 1989	11:39	10M-8	40	20	40	61
Oct 12 1989	11:43	10M-5	75	162	-20	62
Oct 12 1989	11:45	10M-4	67	20	122	60

continued...

TABLE 2 (continued)

DATE	TIME	SITE	Average He (ppb)	He #1 (ppb)	He #2 (ppb)	He #3 (ppb)
Oct 12 1989	11:47	10M-2	134	151	80	142
Oct 12 1989	11:49	10M-8	-6	-79	20	40
Oct 12 1989	11:53	20M-8	102	40	306	-41
Oct 12 1989	11:55	20M-1	46	40	32	60
Oct 12 1989	11:58	20M-3	43	-40	125	-
Oct 12 1989	12:03	20M-8	7	40	-20	0
Oct 12 1989	12:07	20M-7	68	125	20	60
Oct 12 1989	12:09	40M-7	20	41	-20	40
Oct 12 1989	12:14	40M-2	47	0	82	60
Oct 12 1989	12:18	40M-4	66	-83	81	205
Oct 12 1989	12:34	centre				
Oct 13 1989	15:17	centre	-8	0	-25	0
Oct 13 1989	14:58	5M-1	67	75	101	25
Oct 13 1989	15:02	5M-3	-8	25	-50	0
Oct 13 1989	15:04	5M-8	38	50	25	-
Oct 13 1989	15:08	10M-5	25	-25	0	99
Oct 13 1989	15:10	10M-2	-47	50	75	-266
Oct 13 1989	15:15	10M-8	34	101	0	0
Oct 13 1989	15:33	20M-1	61	-	121	0
Oct 13 1989	15:38	20M-3	-9	0	-50	24
Oct 13 1989	15:41	20M-8	7	48	-48	23
Oct 13 1989	15:45	40M-7	245	116	234	385
Oct 13 1989	15:48	40M-2	38	0	48	68
Oct 13 1989	15:54	40M-4	83	182	113	-47
Oct 13 1989	16:02	A3-10	-69	-162	47	-92
Oct 13 1989	16:05	4-12	45	66	70	0
Oct 13 1989	16:08	8-12.4	>3867	2678	5685	>3339
Oct 13 1989	16:19	11-11	350	464	361	226
Oct 13 1989	16:22	centre	39	137	-68	47
Oct 14 1989	10:45	centre	0	59	-59	-
Oct 14 1989	11:00	5M-1	139	99	179	-
Oct 14 1989	11:02	5M-3	49	59	39	-
Oct 14 1989	11:04	5M-8	99	39	159	-
Oct 14 1989	11:08	10M-5	213	387	39	-
Oct 14 1989	11:10	10M-2	39	59	19	-
Oct 14 1989	11:13	10M-8	79	118	39	-
Oct 14 1989	11:16	20M-1	-20	20	-59	-
Oct 14 1989	11:19	20M-3	0	-19	19	-
Oct 14 1989	11:25	20M-8	126	116	135	-
Oct 14 1989	11:28	40M-7	147	255	39	-
Oct 14 1989	11:42	40M-2	39	39	39	-
Oct 14 1989	11:47	40M-4	29	19	39	-
Oct 14 1989	11:53	A3-10	39	59	19	-

DATE	TIME	SITE	Average He (ppb)	He #1 (ppb)	He #2 (ppb)	He #3 (ppb)
Oct 14 1989	11:56	4-12	39	19	58	-
Oct 14 1989	11:58	8-12.4	>4229	8503	>1956	-
Oct 14 1989	12:01	11-11	327	440	214	-
Oct 14 1989	12:04	centre	49	0	98	-
						-
Oct 15 1989	11:45	centre	-77	-58	-96	-
Oct 15 1989	11:50	11-11	>2418	>1823	3013	-
Oct 15 1989	11:54	8-12.9	163	262	63	-
Oct 15 1989	11:58	4-12	67	96	37	-
Oct 15 1989	12:05	A3-10	-48	-96	0	-
Oct 15 1989	12:06	40M-7	87	20	154	-
Oct 15 1989	12:25	40M-2	10	0	19	-
Oct 15 1989	12:15	40M-4	-9	38	-55	-
Oct 15 1989	12:28	20M-1	>51920	>1060	102180	-
Oct 15 1989	12:33	20M-3	19	38	0	-
Oct 15 1989	12:37	20M-8	144	133	154	-
Oct 15 1989	12:41	10M-2	>9649	>1660	17637	-
Oct 15 1989	12:45	10M-5	86	171	0	-
Oct 15 1989	12:49	10M-8	28	18	37	-
Oct 15 1989	12:53	5M-1	46	146	-56	-
Oct 15 1989	12:58	5M-3	220	221	218	-
Oct 15 1989	13:00	5M-8	105	133	78	-
Oct 15 1989	13:10	centre	-9	19	-37	-
Oct 16 1989	10:45	centre	238	238	238	-
Oct 16 1989	11:07	40M-2	1763	1796	1731	-
Oct 16 1989	11:11	40M-4	230	139	320	-
Oct 16 1989	11:16	40M-7	600	485	715	-
Oct 16 1989	11:23	20M-7	1038	1224	847	-
Oct 16 1989	11:25	20M-8	702	572	832	-
Oct 16 1989	11:27	20M-1	>605220	>675860	>534480	-
Oct 16 1989	11:30	20M-3	3058	2953	3163	-
Oct 16 1989	11:33	20M-8	1162	1433	891	-
Oct 16 1989	11:37	10M-8	2518	2403	2632	-
Oct 16 1989	11:39	10M-2	>752298	1521846	>2749	-
Oct 16 1989	11:42	10M-4	1919	2047	1790	-
Oct 16 1989	11:44	10M-5	1711	1690	1731	-
Oct 16 1989	11:46	10M-8	1553	1878	1429	-
Oct 16 1989	11:50	5M-1	1900	1871	1928	-
Oct 16 1989	11:53	5M-3	>1905	>2495	1315	-
Oct 16 1989	11:56	5M-4	2059	2116	2001	-
Oct 16 1989	11:58	5M-8	1135	1285	985	-
Oct 16 1989	12:36	9-10	279	218	339	-
Oct 16 1989	12:45	11-11	624	331	887	-
Oct 16 1989	12:53	8-12.9	646	749	542	-

DATE	TIME	SITE	Average He (ppb)	He #1 (ppb)	He #2 (ppb)	He #3 (ppb)
Oct 16 1989	12:55	8-12.2	207	226	188	-
Oct 16 1989	12:58	8-12.11	874	1295	452	-
Oct 16 1989	1:00	7-11	252	257	246	-
Oct 16 1989	1:03	4-12	237	246	228	-
Oct 16 1989	1:05	2-8	151	248	113	-
Oct 16 1989	1:07	A1-8	86	95	76	-
Oct 16 1989	1:09	A3-10	76	75	76	-
Oct 16 1989	1:14	centre	-	-	-	-
Oct 17 1989	10:50	centre	142	126	157	-
Oct 17 1989	11:03	40M-2	3872	4018	3725	-
Oct 17 1989	11:09	40M-4	3509	3535	3483	-
Oct 17 1989	11:15	40M-7	360	312	408	-
Oct 17 1989	11:18	20M-7	316	312	320	-
Oct 17 1989	11:21	20M-8	244	80	408	-
Oct 17 1989	11:24	20M-1	8416024	-	8416024	-
Oct 17 1989	11:27	20M-2	99677	105314	94039	-
Oct 17 1989	11:30	20M-3	>6677	6707	>6646	-
Oct 17 1989	11:34	20M-8	1075	950	1200	-
Oct 17 1989	11:44	10M-8	722	730	713	-
Oct 17 1989	11:48	10M-2	4978000	-	4978000	-
Oct 17 1989	11:52	10M-4	2525	2604	2446	-
Oct 17 1989	11:54	10M-5	1600	1578	1622	-
Oct 17 1989	11:57	10M-8	785	686	884	-
Oct 17 1989	12:00	5M-8	1500	1598	1401	-
Oct 17 1989	12:03	5M-1	2317	2353	2281	-
Oct 17 1989	12:05	5M-3	5367	5556	5178	-
Oct 17 1989	12:08	5M-4	2256	2162	2349	-
Oct 17 1989	12:11	30M-1	363	279	447	-
Oct 17 1989	12:14	40M-1	169	157	181	-
Oct 17 1989	12:16	50M-1	143	94	192	-
Oct 17 1989	12:21	A3-10	95	64	126	-
Oct 17 1989	12:24	A1-8	121	150	92	-
Oct 17 1989	12:27	2-8	220	217	222	-
Oct 17 1989	12:31	1-12	306	361	250	-
Oct 17 1989	12:33	4-12	315	217	413	-
Oct 17 1989	12:36	6-12	307	480	333	-
Oct 17 1989	12:38	7-11	315	269	361	-
Oct 17 1989	12:42	8-12.2	110	-31	250	-
Oct 17 1989	12:45	8-12.11	1568	1494	1641	-
Oct 17 1989	12:48	8-12.9	491	446	535	-
Oct 17 1989	12:50	9-10	357	398	316	-
Oct 17 1989	12:52	11-11	446	469	428	-
Oct 17 1989	12:55	13-10	1217	1225	1209	-
Oct 17 1989	12:57	13.5-11	75	192	-42	-

continued...

TABLE 2 (continued)

DATE	TIME	SITE	Average He (ppb)	He #1 (ppb)	He #2 (ppb)	He #3 (ppb)
Oct 17 1989	13:01	14–6	180	231	128	–
Oct 17 1989	13:10	centre	159	85	233	–
			0			–
Oct 18 1989	13:03	centre	322	304	340	–
Oct 18 1989	13:16	5M–1	5208	5240	5176	–
Oct 18 1989	13:18	5M–2	21713	22371	21055	–
Oct 18 1989	13:20	5M–3	7029	4414	9663	–
Oct 18 1989	13:22	5M–4	4340	4468	4211	–
Oct 18 1989	13:24	5M–5	3824	3851	3797	–
Oct 18 1989	13:26	5M–6	3533	3504	3561	–
Oct 18 1989	13:28	5M–7	2041	2147	1934	–
Oct 18 1989	13:33	5M–8	2185	2181	2189	–
Oct 18 1989	13:35	10M–1	282811	162280	403342	–
Oct 18 1989	13:37	10M–2	2791765	4223585	1359945	–
Oct 18 1989	13:39	10M–3	7053	7144	6962	–
Oct 18 1989	13:41	10M–4	6464	6633	6295	–
Oct 18 1989	13:43	10M–5	5659	5629	5690	–
Oct 18 1989	13:45	10M–6	2264	2210	2318	–
Oct 18 1989	13:47	10M–7	1896	2237	1553	–
Oct 18 1989	13:51	10M–8	2605	2526	2684	–
Oct 18 1989	13:53	20M–1	15433303	17963154	12913452	–
Oct 18 1989	13:55	20M–2	322030	318724	325336	–
Oct 18 1989	13:57	20M–3	8194	7860	8528	–
Oct 18 1989	13:59	20M–4	2336	2336	2336	–
Oct 18 1989	14:02	20M–5	8617791	–	8617791	–
Oct 18 1989	14:04	20M–6	3587	3582	3592	–
Oct 18 1989	14:07	20M–7	936	899	973	–
Oct 18 1989	14:09	20M–8	1247	1318	1175	–
Oct 18 1989	14:11	30M–1	1540	1519	1560	–
Oct 18 1989	14:13	50M–1	717	618	816	–
Oct 18 1989	14:16	40M–1	925	997	852	–
Oct 18 1989	14:20	40M–2	8936	7837	10035	–
Oct 18 1989	14:22	40M–3	300	301	298	–
Oct 18 1989	14:25	40M–4	533	536	530	–
Oct 18 1989	14:28	40M–5	–125	–62	–187	–
Oct 18 1989	14:45	40M–6	–13	–51	25	–
Oct 18 1989	14:47	40M–7	434	305	563	–
Oct 18 1989	14:50	40M–8	741	814	668	–
Oct 18 1989	13:08	A3–10	60	60	60	–
Oct 18 1989	13:14	A2–11	411	394	427	–
Oct 18 1989	13:18	1–12	706	689	723	–
Oct 18 1989	13:20	4–12	797	797	797	–
Oct 18 1989	13:24	6–12	848	947	748	–
Oct 18 1989	13:28	13–10	872	840	903	–
Oct 18 1989	13:32	15–9	43	–28	114	–

DATE	TIME	SITE	Average He (ppb)	He #1 (ppb)	He #2 (ppb)	He #3 (ppb)
Oct 18 1989	13:35	9–11	591	699	482	–
Oct 18 1989	13:38	7–11	469	513	425	–
Oct 18 1989	13:42	5–11	634	705	563	–
Oct 18 1989	13:45	3–11	492	451	532	–
Oct 18 1989	13:48	A1–11	438	425	451	–
Oct 18 1989	13:56	A2–9	228	305	151	–
Oct 18 1989	14:01	A1–9	184	198	169	–
Oct 18 1989	14:03	2–9	408	255	561	–
Oct 18 1989	14:05	4–9	42	26	58	–
Oct 18 1989	14:08	6–9	436	507	364	–
Oct 18 1989	14:12	8–9	179846	0	359692	–
Oct 18 1989	14:15	10–9	517	557	476	–
Oct 18 1989	14:18	12–9	808	979	636	–
Oct 18 1989	14:26	17–7	323	308	338	–
Oct 18 1989	14:23	15–7	236	308	167	–
Oct 18 1989	14:29	13–7	459	476	441	–
Oct 18 1989	14:34	11–7	222	167	278	–
Oct 18 1989	14:37	9–7	408	364	451	–
Oct 18 1989	14:42	3–7	222	250	194	–
Oct 18 1989	14:47	1–7	256	258	254	–
Oct 18 1989	14:50	A1–7	232	179	285	–
Oct 18 1989	14:56	A1–6	139	83	194	–
Oct 18 1989	14:59	A2–5	138	194	82	–
Oct 18 1989	15:11	A1–5	98	167	28	–
Oct 18 1989	15:14	2–5	171	285	56	–
Oct 18 1989	15:17	4–5	153	110	196	–
Oct 18 1989	15:22	6–12.9	765	725	804	–
Oct 18 1989	15:25	8–12.2	239	228	250	–
Oct 18 1989	15:27	8–12.11	1902	1903	1900	–
Oct 18 1989	15:31	13.5–11	194	331	56	–
Oct 18 1989	15:33	14–6	606	659	552	–
Oct 18 1989	15:38	centre	279	279	279	–
						–
Oct 20 1989	8:40	centre	678	845	911	–
Oct 20 1989	8:56	60M–1	2230	2341	2118	–
Oct 20 1989	8:58	40M–1	5017	5015	5019	–
Oct 20 1989	9:01	40M–2	8770	9316	8223	–
Oct 20 1989	9:05	40M–3	1396823	1396823	–	–
Oct 20 1989	9:10	40M–4	620	620	620	–
Oct 20 1989	9:13	40m–5	5826	10536	1115	–
Oct 20 1989	9:16	30M–6	2997	1645	4348	–
Oct 20 1989	9:19	40M–7	1091	620	1561	–
Oct 20 1989	9:22	40M–8	1986	1820	2151	–
Oct 20 1989	9:25	30M–1	20587	19941	21232	–
Oct 20 1989	9:28	20M–1	40084690	40903851	39225529	–

DATE	TIME	SITE	Average He (ppb)	He #1 (ppb)	He #2 (ppb)	He #3 (ppb)
Oct 20 1989	9:31	20M–2	590121	590121	590121	–
Oct 20 1989	9:34	20M–3	381240	385066	377413	–
Oct 20 1989	9:37	20M–4	4425	4658	4192	–
Oct 20 1989	9:40	20M–5	1656141	1677486	1634516	–
Oct 20 1989	9:45	20M–6	6074	7945	6202	–
Oct 20 1989	9:48	20M–7	4492	4549	4434	–
Oct 20 1989	9:51	20M–8	1650	2671	629	–
Oct 20 1989	9:54	10M–1	518501	515093	521908	–
Oct 20 1989	9:57	6M–2	49348	49154	49542	–
Oct 20 1989	9:59	10M–2	17298831	4946832	29650999	–
Oct 20 1989	10:01	10M–3	27404	27361	27447	–
Oct 20 1989	10:03	10M–4	19312	19468	19155	–
Oct 20 1989	10:05	10M–5	19931	15748	24113	–
Oct 20 1989	10:07	10M–6	15425	15425	15425	–
Oct 20 1989	10:16	10M–7	4689	4705	5272	–
Oct 20 1989	10:19	10M–8	10093	9923	10262	–
Oct 20 1989	10:22	5M–1	18947	18780	19113	–
Oct 20 1989	10:24	5M–3	22424	22649	22199	–
Oct 20 1989	10:26	5M–4	16622	13796	19447	–
Oct 20 1989	10:29	5M–5	19564	19885	19283	–
Oct 20 1989	10:31	5M–6	9656	9662	9634	–
Oct 20 1989	10:33	5M–7	3690	3652	3727	–
Oct 20 1989	10:35	5M–8	10425	10460	10389	–
Oct 20 1989	8:44	1–12	1709	1886	1712	–
Oct 20 1989	8:46	4–12	1038	965	1090	–
Oct 20 1989	8:51	6–12	1414	1091	837	–
Oct 20 1989	8:55	8–12.2	3896	3891	3904	–
Oct 20 1989	8:58	8–12.9	1492	961	2023	–
Oct 20 1989	9:00	11–11	1349	1401	1297	–
Oct 20 1989	9:03	9–11	1310	1362	1258	–
Oct 20 1989	9:06	7–11	856	791	925	–
Oct 20 1989	9:08	5–11	1174	1090	1258	–
Oct 20 1989	9:10	3–11	986	986	986	–
Oct 20 1989	9:13	A1–11	996	1163	838	–
Oct 20 1989	9:15	A2–11	852	778	925	–
Oct 20 1989	9:18	A3–10	326	308	343	–
Oct 20 1989	9:27	8–10	1008	967	1048	–
Oct 20 1989	9:31	13–10	1180	1272	1088	–
Oct 20 1989	9:34	15–9	340	337	343	–
Oct 20 1989	9:38	12–9	986	1067	885	–
Oct 20 1989	9:41	10–9	797	803	791	–
Oct 20 1989	9:44	8–9	931	989	873	–
Oct 20 1989	9:46	6–9	913	913	913	–
Oct 20 1989	9:49	4–9	1125	1086	1164	–
Oct 20 1989	9:52	2–9	1037	1088	986	–

continued...

TABLE 2 (continued)

DATE	TIME	SITE	Average He (ppb)	He #1 (ppb)	He #2 (ppb)	He #3 (ppb)
Oct 20 1989	9:55	A1-9	693	761	625	-
Oct 20 1989	9:58	A2-9	372	395	349	-
Oct 20 1989	10:16	A1-7	262	330	194	-
Oct 20 1989	10:20	1-7	577	529	625	-
Oct 20 1989	10:23	2-8	743	708	778	-
Oct 20 1989	10:26	3-7	643	617	469	-
Oct 20 1989	10:30	9-7	742	721	762	-
Oct 20 1989	10:33	11-7	729	897	561	-
Oct 20 1989	10:36	13-7	697	967	427	-
Oct 20 1989	10:40	15-7	171	217	124	-
Oct 20 1989	10:43	17-7	238	-	238	-
Oct 20 1989	10:49	A1-6	77	154	0	-
Oct 20 1989	10:52	A2-6	161	240	82	-
Oct 20 1989	10:57	A1-5	178	200	156	-
Oct 20 1989	10:59	2-5	297	276	318	-
Oct 20 1989	11:03	4-5	467	496	437	-
Oct 20 1989	11:10	6-5	511	535	486	-
Oct 20 1989	11:16	8-5	585	378	791	-
Oct 20 1989	11:20	10-5	606	629	582	-
Oct 20 1989	11:25	11-3	565	594	535	-
Oct 20 1989	11:30	9-3	290	314	265	-
Oct 20 1989	11:35	7-3	476	476	476	-
Oct 20 1989	11:40	5-3	336	363	308	-
Oct 20 1989	11:50	3-3	265	265	-	-
Oct 20 1989	11:55	1-3	327	327	-	-
Oct 20 1989	11:58	A1-2	103	103	-	-
Oct 20 1989	12:02	2-1	-52	-52	-	-
Oct 20 1989	12:07	4-1	210	210	-	-
Oct 20 1989	12:10	6-1	314	314	-	-
Oct 20 1989	12:12	8-1	308	308	-	-
Oct 20 1989	12:14	10-1	308	308	-	-
Oct 20 1989	12:16	13-3	476	476	-	-
Oct 20 1989	12:20	13-5	308	308	-	-
Oct 20 1989	12:30	14-6	2490	2542	2438	-
Oct 20 1989	12:35	13.5-11	726	674	778	-
Oct 20 1989	12:40	centre	336	467	205	-
						-
Oct 23 1989	9:30	centre	1640	1820	1459	-
Oct 23 1989	10:27	50M-1	5957	6004	5909	-
Oct 23 1989	10:30	40M-1	10480	10756	10204	-
Oct 23 1989	10:33	30M-1	171043	173595	168491	-
Oct 23 1989	10:36	40M-2	8511	-	8511	-
Oct 23 1989	10:40	40M-3	43758606	43758606	-	-
Oct 23 1989	10:43	40M-4	2402	2293	2511	-
Oct 23 1989	10:47	40M-5	81	107	54	-

DATE	TIME	SITE	Average He (ppb)	He #1 (ppb)	He #2 (ppb)	He #3 (ppb)
Oct 23 1989	10:55	30M-6	58	321	-205	-
Oct 23 1989	10:58	40M-7	1283	1283	1283	-
Oct 23 1989	11:00	20M-7	4818	5240	4395	-
Oct 23 1989	11:01	20M-8	4354	4402	4325	-
Oct 23 1989	11:03	20M-1	42608396	-	42608396	-
Oct 23 1989	11:06	20M-2	239217	-	239217	-
Oct 23 1989	11:10	20M-3	218515	52763	384267	-
Oct 23 1989	11:13	20M-4	5134	5349	4919	-
Oct 23 1989	11:17	20M-5	205714	384363	27064	-
Oct 23 1989	11:20	20M-6	10624	11859	9388	-
Oct 23 1989	11:23	10M-1	848766	1003511	694021	-
Oct 23 1989	11:29	10M-2	484525	-	484525	-
Oct 23 1989	11:31	10M-3	-	-	-	-
Oct 23 1989	11:33	10M-4	-	-	-	-
Oct 23 1989	11:35	10M-5	-	-	-	-
Oct 23 1989	11:37	10M-6	-	-	-	-
Oct 23 1989	11:39	10M-7	-	-	-	-
Oct 23 1989	11:43	10M-8	20643	20643	-	-
Oct 23 1989	11:45	5M-1	20616	20039	21193	-
Oct 23 1989	11:47	5M-2	57783	57783	-	-
Oct 23 1989	11:51	5M-3	36084	36084	-	-
Oct 23 1989	11:55	5M-4	34138	44104	24171	-
Oct 23 1989	11:58	5M-5	-	-	-	-
Oct 23 1989	11:42	5M-6	-	-	-	-
Oct 23 1989	11:44	5M-7	12550	11999	13100	-
Oct 23 1989	14:21	40M-8	1261	1186	1336	-
Oct 23 1989	10:07	1-12	3299	3123	3475	-
Oct 23 1989	10:14	4-12	3002	2947	3057	-
Oct 23 1989	10:17	6-12	3482	3524	3440	-
Oct 23 1989	10:20	8-12.2	3014	3034	2994	-
Oct 23 1989	10:23	8-12.9	3319	3384	3254	-
Oct 23 1989	10:26	11-11	1600	1048	2151	-
Oct 23 1989	10:29	9-11	2539	2567	2511	-
Oct 23 1989	10:32	7-11	2247	2293	2201	-
Oct 23 1989	10:35	5-11	2437	2306	2567	-
Oct 23 1989	10:38	3-11	2367	2246	2488	-
Oct 23 1989	10:40	A1-11	1589	1467	1711	-
Oct 23 1989	10:43	A2-11	1510	1582	1438	-
Oct 23 1989	10:46	A3-10	448	476	419	-
Oct 23 1989	10:51	A2-9	764	794	734	-
Oct 23 1989	10:54	A1-9	1158	1310	1006	-
Oct 23 1989	10:57	2-9	1659	1677	1641	-
Oct 23 1989	10:59	4-9	2124	2064	2183	-
Oct 23 1989	11:02	6-9	1677	1641	1712	-
Oct 23 1989	11:05	8-9	1583	1525	1638	-

DATE	TIME	SITE	Average He (ppb)	He #1 (ppb)	He #2 (ppb)	He #3 (ppb)
Oct 23 1989	11:07	9-10	1694	1604	1783	-
Oct 23 1989	11:10	10-9	1560	1641	1497	-
Oct 23 1989	11:13	12-9	1271	1429	1112	-
Oct 23 1989	11:16	13-10	936	1153	719	-
Oct 23 1989	11:19	15-9	658	582	734	-
Oct 23 1989	11:22	17-7	739	848	629	-
Oct 23 1989	11:25	15-7	735	705	764	-
Oct 23 1989	11:28	13-7	1091	1193	989	-
Oct 23 1989	11:31	11-7	1189	1224	1153	-
Oct 23 1989	11:33	9-7	1258	1258	1258	-
Oct 23 1989	11:36	3-7	1048	1048	1048	-
Oct 23 1989	11:39	1-7	764	637	890	-
Oct 23 1989	11:42	A1-7	599	524	674	-
Oct 23 1989	11:45	A2-6	449	494	403	-
Oct 23 1989	11:48	A1-6	402	363	441	-
Oct 23 1989	11:50	A1-5	543	582	504	-
Oct 23 1989	11:53	2-8	686	1028	343	-
Oct 23 1989	11:55	2-5	755	938	571	-
Oct 23 1989	11:57	4-5	797	778	817	-
Oct 23 1989	12:40	8-5	847	988	705	-
Oct 23 1989	12:45	8-5	699	648	649	-
Oct 23 1989	12:53	10-5	949	1008	890	-
Oct 23 1989	12:56	11-3	822	719	925	-
Oct 23 1989	12:58	9-3	672	642	702	-
Oct 23 1989	13:02	7-3	684	605	763	-
Oct 23 1989	13:06	5-3	498	524	467	-
Oct 23 1989	13:10	3-3	555	467	642	-
Oct 23 1989	13:13	1-3	403	403	-	-
Oct 23 1989	13:16	A1-2	291	291	-	-
Oct 23 1989	13:19	2-1	358	358	-	-
Oct 23 1989	13:22	4-1	437	437	-	-
Oct 23 1989	13:25	6-1	549	549	-	-
Oct 23 1989	13:28	8-1	549	549	-	-
Oct 23 1989	13:39	10-1	571	571	-	-
Oct 23 1989	13:42	13-3	907	907	-	-
Oct 23 1989	13:47	13-5	838	838	-	-
Oct 23 1989	13:56	14-6	1069	962	1176	-
Oct 23 1989	13:58	13.5-11	265	371	159	-
Oct 23 1989	14:04	centre	779	865	692	-
						-
Oct 24 1989	8:40	50M-1	5833	5784	5502	-
Oct 24 1989	8:43	40M-1	11463	9293	13529	-
Oct 24 1989	8:46	30M-1	182113	-	182113	-
Oct 24 1989	8:49	40M-2	6565	4147	8982	-
Oct 24 1989	8:52	40M-3	14469545	14469545	-	-

continued...

TABLE 2 (continued)

DATE	TIME	SITE	Average He (ppb)	He #1 (ppb)	He #2 (ppb)	He #3 (ppb)
Oct 24 1989	8:55	40M-4	4730	5046	4414	-
Oct 24 1989	8:56	40M-5	1758	1789	1726	-
Oct 24 1989	9:01	30M-6	2771	2797	2746	-
Oct 24 1989	9:04	40M-7	1260	1359	1161	-
Oct 24 1989	9:07	40M-8	2289	2387	2191	-
Oct 24 1989	9:09	20M-1	16335542	-	16335542	-
Oct 24 1989	9:11	20M-2	167739	-	167739	-
Oct 24 1989	9:13	20M-3	56780	57447	56113	-
Oct 24 1989	9:15	20M-4	5902	6053	5751	-
Oct 24 1989	9:17	20M-5	174667	-	174667	-
Oct 24 1989	9:19	20M-6	10507	11318	9695	-
Oct 24 1989	9:21	20M-7	4430	4143	4716	-
Oct 24 1989	9:23	20M-8	3947	3817	4078	-
Oct 24 1989	9:25	10M-1	520265	-	520265	-
Oct 24 1989	9:27	10M-2	3840643	3840643	-	-
Oct 24 1989	9:29	10M-3	37114	35447	38780	-
Oct 24 1989	9:31	10M-4	28112	27683	28541	-
Oct 24 1989	9:33	10M-5	20001	16184	23818	-
Oct 24 1989	9:35	10M-6	17017	17236	16798	-
Oct 24 1989	9:37	10M-7	7308	7459	7153	-
Oct 24 1989	9:39	10M-8	10189	10598	9780	-
Oct 24 1989	9:41	5M-1	21601	21987	21215	-
Oct 24 1989	9:43	5M-2	50638	54760	46295	-
Oct 24 1989	9:45	5M-3	29629	29879	29378	-
Oct 24 1989	9:47	5M-4	28224	28530	27917	-
Oct 24 1989	9:49	5M-5	22126	22214	22037	-
Oct 24 1989	9:51	5M-6	16630	16550	16710	-
Oct 24 1989	9:53	5M-7	10677	-	10677	-
Oct 24 1989	9:55	5M-8	11993	11397	12588	-
						-
Oct 25 1989	8:47	centre	985	1059	911	-
Oct 25 1989	9:18	10M-2	2459472	2459472	-	-
Oct 25 1989	9:22	20M-1	13341316	-	13341316	-
Oct 25 1989	9:25	20M-2	118524	-	118524	-
Oct 25 1989	9:32	20M-5	99330	-	99330	-
Oct 25 1989	9:27	40M-3	5951683	5951683	-	-
Oct 25 1989	9:15	50M-1	5044	5128	4960	-
Oct 25 1989	9:11	1-12	1383	1449	1317	-
Oct 25 1989	9:07	8-12.2	3751	3743	3759	-
Oct 25 1989	9:02	11-11	1429	1409	1449	-
Oct 25 1989	9:04	8-9	1240	1183	1298	-
Oct 25 1989	8:57	17-7	520	538	502	-
Oct 25 1989	10:14	3-7	2293	4154	432	-
Oct 25 1989	9:58	13-5	644	644	644	-
Oct 25 1989	10:04	8-5	1118	655	1580	-

DATE	TIME	SITE	Average He (ppb)	He #1 (ppb)	He #2 (ppb)	He #3 (ppb)
Oct 25 1989	9:53	9-3	676	676	676	-
Oct 25 1989	9:48	4-1	346	390	302	-
Oct 25 1989	10:08	centre	801	789	813	-
						-
Oct 26 1989	8:33	centre	507	467	547	-
Oct 26 1989	8:48	4-1	273	287	259	-
Oct 26 1989	8:54	9-3	485	360	610	-
Oct 26 1989	8:58	13-5	525	537	514	-
Oct 26 1989	9:03	8-5	334	332	336	-
Oct 26 1989	9:08	17-7	397	336	458	-
Oct 26 1989	9:13	3-7	634	726	542	-
Oct 26 1989	9:16	1-12	1069	1162	976	-
Oct 26 1989	9:19	8-9	1113	1298	928	-
Oct 26 1989	9:22	8-12.2	878	925	830	-
Oct 26 1989	9:25	11-11	3020	3020	-	-
Oct 26 1989	9:33	40M-1	7556	6878	8234	-
Oct 26 1989	9:36	30M-1	122097	-	122097	-
Oct 26 1989	9:38	20M-1	83969091	83969091	-	-
Oct 26 1989	9:40	10M-2	1384589	1384589	-	-
Oct 26 1989	9:43	20M-2	98324	98324	-	-
Oct 26 1989	9:48	40M-3	5055868	-	5055868	-
Oct 26 1989	9:52	20M-5	60842	65336	52348	-
Oct 26 1989	9:58	centre	790	1080	500	-
Oct 26 1989	10:07	50M-1	4922	5079	4764	-
						-
Oct 27 1989	9:10	centre	293	382	204	-
Oct 27 1989	9:16	4-1	271	169	372	-
Oct 27 1989	9:23	9-3	1	34	-33	-
Oct 27 1989	9:28	13-5	33	33	33	-
Oct 27 1989	9:33	8-5	84	101	67	-
Oct 27 1989	9:39	17-7	122	174	69	-
Oct 27 1989	9:43	11-11	185	167	202	-
Oct 27 1989	9:47	8-12.2	83	33	133	-
Oct 27 1989	9:50	8-9	906	863	1209	-
Oct 27 1989	9:53	3-7	236	167	304	-
Oct 27 1989	9:56	1-12	136	204	67	-
Oct 27 1989	10:15	10M-2	-	-	414056	-
Oct 27 1989	10:17	20M-1	-	4788500	-	-
Oct 27 1989	10:20	30M-1	77697	78447	78947	-
Oct 27 1989	10:23	40M-1	4015	2858	5172	-
Oct 27 1989	10:25	20M-2	39371	41887	36855	-
Oct 27 1989	10:30	40M-3	-	-	2028311	-
Oct 27 1989	10:34	20M-5	-	-	-	-
Oct 27 1989	10:37	centre	201	148	253	-
Oct 27 1989	10:47	50M-1	1656	463	2849	-

continued...

TABLE 2 (concluded)

DATE	TIME	SITE	Average He (ppb)	He #1 (ppb)	He #2 (ppb)	He #3 (ppb)
						-
Oct 30 1989	8:35	centre	30	0	60	-
Oct 30 1989	8:43	4-1	45	60	30	-
Oct 30 1989	8:48	9-3	59	148	-30	-
Oct 30 1989	8:53	13-5	60	30	90	-
Oct 30 1989	8:58	8-5	373	595	150	-
Oct 30 1989	9:04	17-7	135	150	120	-
Oct 30 1989	9:07	11-11	75	120	30	-
Oct 30 1989	9:10	8-12.2	104	59	148	-
Oct 30 1989	9:14	8-9	330	273	487	-
Oct 30 1989	9:16	3-7	259	427	150	-
Oct 30 1989	9:18	1-12	196	148	244	-
Oct 30 1989	9:23	40M-1	934	868	1000	-
Oct 30 1989	9:26	30M-1	21658	22064	21251	-
Oct 30 1989	9:28	20M-1	1642179	1642179	-	-
Oct 30 1989	9:30	20M-2	10967	-	10967	-
Oct 30 1989	9:33	10M-2	122119	122119	-	-
Oct 30 1989	9:37	40M-3	243069	243069	-	-
Oct 30 1989	9:41	20M-5	10114	9119	11108	-
Oct 30 1989	9:45	centre	90	120	60	-
Oct 30 1989	9:52	50m-1	1859	1787	1931	-
						-
Nov 3 1989	7:27	centre	78	155	0	-
Nov 3 1989	7:37	4-1	45	30	60	-
Nov 3 1989	7:45	9-3	821	1457	185	-
Nov 3 1989	7:52	13-5	184	120	247	-
Nov 3 1989	7:57	8-5	156	187	125	-
Nov 3 1989	8:03	17-7	150	125	187	-
Nov 3 1989	8:11	11-11	105	150	60	-
Nov 3 1989	8:14	8-12.2	251	412	89	-
Nov 3 1989	8:17	8-9	120	120	120	-
Nov 3 1989	8:21	3-7	44	0	88	-
Nov 3 1989	8:24	1-12	241	361	120	-
Nov 3 1989	8:28	40M-1	272	305	238	-
Nov 3 1989	8:32	30M-1	7612	7922	7302	-
Nov 3 1989	8:35	10M-2	59760	59760	59760	-
Nov 3 1989	8:40	20M-1	350641	350641	-	-
Nov 3 1989	8:43	20M-2	4666	4758	4574	-
Nov 3 1989	8:47	40M-3	67176	67127	67224	-
Nov 3 1989	8:53	20M-5	3761	3674	3847	-
Nov 3 1989	8:56	centre	89	119	59	-
Nov 3 1989	9:07	50m-1	351	439	263	-
						-
Nov 7 1989	8:35	centre	75	64	85	-
Nov 7 1989	8:50	40M-1	125	42	208	-

DATE	TIME	SITE	Average He (ppb)	He #1 (ppb)	He #2 (ppb)	He #3 (ppb)
Nov 7 1989	8:53	30M-1	10645	12740	8549	-
Nov 7 1989	8:55	20M-1	201293	201293	-	-
Nov 7 1989	8:58	10M-2	49253	48310	50195	-
Nov 7 1989	9:00	20M-2	2895	2854	2935	-
Nov 7 1989	9:03	40M-3	34027	34468	33586	-
Nov 7 1989	9:08	20M-5	2988	2765	3212	-
Nov 7 1989	9:12	centre	210	335	84	-
Nov 7 1989	9:22	50M-1	94	83	104	-
						-
Nov 14 1989	8:35	centre	139	21	256	-
Nov 14 1989	8:50	40M-1	249	151	346	-
Nov 14 1989	8:55	30M-1	14612	14682	14742	-
Nov 14 1989	8:58	20M-1	154623	154623	-	-
Nov 14 1989	9:01	10M-2	39425	38851	39999	-
Nov 14 1989	9:04	20M-2	3585	3723	3447	-
Nov 14 1989	9:07	40M-3	8793	8180	9405	-
Nov 14 1989	9:10	20M-5	764	786	742	-
Nov 14 1989	9:15	centre	-	-	-	-
Nov 14 1989	9:35	50M-1	335	239	430	-
						-
Nov 21 1989	8:35	centre	160	99	221	-
Nov 21 1989	8:50	40M-1	174	124	224	-
Nov 21 1989	8:55	30M-1	14672	16169	13175	-
Nov 21 1989	8:57	20M-1	74300	74854	73746	-
Nov 21 1989	8:59	10M-2	13176	13175	13176	-
Nov 21 1989	9:03	20M-2	2016	2098	1933	-
Nov 21 1989	9:08	40M-3	5531	5240	5822	-
Nov 21 1989	9:10	20M-5	567	609	524	-
Nov 21 1989	9:15	centre	106	70	142	-
Nov 21 1989	9:30	50M-1	157	144	169	-
						-
Dec 1 1989	8:40	centre	370	393	346	-
Dec 1 1989	8:55	40M-1	199	377	21	-
Dec 1 1989	8:58	30M-1	10073	10184	9961	-
Dec 1 1989	9:01	20M-1	22381	24093	20669	-
Dec 1 1989	9:04	10M-2	19329	19543	19108	-
Dec 1 1989	9:07	20M-2	1317	1031	1602	-
Dec 1 1989	9:10	40M-3	3613	3668	3558	-
Dec 1 1989	9:14	20M-5	942	809	1074	-
Dec 1 1989	9:18	centre	309	271	347	-
Dec 1 1989	9:35	50M-1	132	244	20	-

TABLE 3

MEASUREMENTS AND MONITORING INFORMATION RECORDED DURING THE GAS INJECTION TEST IN BOREHOLE B-34

(N = DATA NOT RECORDED)

Date (1989)	Time	Pressures (kPa) Regulator	Casing	He Flow Rate ($L \cdot min^{-1}$)	Total He Injected (m^3)	Zone 1 Level* (cm)
13 Oct.	10.15	P increased to 103			0	0
	10.25	P increased to 262				
	10.39	P increased to 290				
	10.40	290	290	8.72	N	N
	10.42	290	303	7.46	N	N
	10.46	296	303	6.22	N	N
	10.52	296	303	3.64	0.16	N
	11.03	300	303	1.77	0.18	N
	11.07	P increased to 324				
	11.08	324	317	27.9	N	N
	11.10	328	317	23.0	N	N
	11.17	328	328	11.6	N	N
	11.21	331	324	8.53	N	N
	11.22	P increased to 352				
	11.23	355	345	33.3	N	N
	11.28	359	355	22.5	N	N
	11.35	362	362	12.7	N	N
	11.40	P increased to 383				
	11.41	383	379	32.1	N	N
	11.50	390	390	18.2	N	N
	12.00	393	393	11.0	N	N
	12.05	P increased to 407				
	12.06	407	400	30.2	N	N
	12.14	414	407	21.2	1.44	N
	12.25	417	414	18.2	1.66	-2.0
	13.27	410	403	18.8	2.83	N
	13.30	P dropped to 400				
	13.34	396	396	0	2.90	N
	13.42	390	390	0	2.90	N
	13.46	386	386	0	2.90	-2.5
	13.57	P increased to ~385				
	14.02	384	382	8.65	2.97	N
	14.24	386	386	8.01	3.14	N
	14.26	14.31	P dropped to give ~3 $L \cdot min^{-1}$			
	14.32	377	377	3.29	3.17	
	16.28	372	365	8.3	3.89	-3.9
	21.17	376	383	9.8	6.62	-5.1
	21.35	376	383	10.2	6.78	N

continued...

TABLE 3 (continued)

Date (1989)	Time	Pressures (kPa) Regulator	Casing	He Flow Rate ($L \cdot min^{-1}$)	Total He Injected (m^3)	Zone 1 Level* (cm)
14 Oct.	05.45	372	390	12.3	12.49	-7.7
	06.40	372	393	12.3	13.13	N
	09.30	372	390	12.0	N	N
	10.35	372	390	11.3	16.04	N
	11.33	372	376	10.4	16.67	-8.3
	12.37	372	362	9.2	17.32	-8.3
	16.25	372	372	10.7	19.59	-9.4
	16.29	cylinders changed				
	16.55	376	376	16.7↓	19.70	N
	17.28	376	383	8.2	20.02	N
	22.01	376	383	10.9	22.66	N
	22.40	376	383	11.0	22.97	-10.1
15 Oct.	09.24	372	386	13.5	31.62	N
	11.28	376	400	13.3	33.31	-11.8
	13.02	372	393	12.9	34.56	N
	21.38	376	390	14.5	41.51	N
	21.40	cylinders changed				
	21.58	381	396	16.7↓	41.84	-13.3
16 Oct.	08.04	379	400	17.3	50.11	-14.5
	10.58	376	403	16.4	52.95	-14.5
	13.48	383	383	15.1	55.63	-15.3
	15.48	379	379	16.4	57.51	N
	19.32	383	396	17.3	61.28	N
	20.06	cylinders changed				
	20.10	396	396	16.6	61.52	N
17 Oct.	08.50	379	393	16.1	72.81	N
	10.35	383	403	16.6	74.51	-18.1
	13.55	379	376	15.3	77.77	-18.6
	20.22	372	396	11.9	84.40	N
	20.40	cylinders changed				
	20.56	383	400	20.1	84.77	-20.6
18 Oct.	07.32	393	400	20.1	97.38	-20.7
	11.25	379	386	18.2	101.9	-22.1
	14.54	376	369	17.3	105.6	N
	19.11	cylinders changed (out of gas for 1-2 h)				
	19.38	383	393	18.9↓	107.7	N
19 Oct.	08.05	393	400	15.7	117.2	N
	09.50	393	393	15.7	118.9	-26.0
	13.22	379	359	14.7	122.1	N
	20.40	379	386	17.2	129.3	N
	21.00	cylinders changed				
	21.15	386	386	21.7↓	129.7	N

continued...

TABLE 3 (concluded)

Date (1989)	Time	Pressures (kPa) Regulator	Casing	He Flow Rate ($L \cdot min^{-1}$)	Total He Injected (m^3)	Zone 1 Level* (cm)
20 Oct.	08.25	383	396	21.4	143.1	-31.5
	11.52	379	369	17.7	147.1	N
	11.55	cylinders changed				
	12.26	379	365	16.7	147.4	N
21 Oct.	08.00	393	393	19.9	169.5	N
	08.15	cylinders changed				
	11.36	379	372	18.3	173.4	N
	21.12	379	383	20.5	184.4	N
	21.24	one cylinder changed (gas shortage)				
	21.42	379	376	26.0↓	N	N
22 Oct.	08.20	379	386	15.1	197.4	N
	08.30	cylinders changed				
	09.48	386	390	13.2	198.5	N
	17.02	379	372	16.1	204.4	N
23 Oct.	09.20	cylinders changed (out of gas for 2 h)				
	09.44	386	400	9.1↓	220.6	N
	10.00	386	400	7.1	220.7	N
	11.00	386	390	6.6	221.1	N
	11.55	379	386	6.6	221.4	N
	13.50	379	372	8.2	222.3	N
	14.55	383	369	9.6	222.9	-40.0
	16.19	383	369	10.8	223.7	N
24 Oct.	08.08	393	393	18.0	239.4	N
	09.00	injection ended		240.5	N	N
			Shut-in pressures			
24 Oct.	10.42		362			
	16.20		352			
25 Oct.	10.35		352			
26 Oct.	08.20		348			
27 Oct.	08.25		338			
30 Oct.	08.27		338			
31 Oct.	14.30		334			
1 Nov.	borehole vented					

N = Data not recorded
* = Water level below top of outer casing (topped up to 0 cm at start of test)

TABLE 4

INPUT PARAMETERS FOR MODELLING GAS INJECTION TESTS AND TEST RESULTS

Physical Properties of Fluids (Literature Values)

temperature (T)	10°C
water viscosity (μ_w)	1.307×10^{-3} N·s·$^{-2}$
water density (ρ_w)	0.999×10^{3} kg·m^{-3}
helium viscosity (μ_g)*	1.90×10^{-5} N·s·m^{-2}
helium density (ρ_g)*	0.37 kg·m^{-3}
helium-water n6erfacial tension (σ) (value for hydrogen; value for helium not available)	0.07422 N·m^{-1}
acceleration of gravity (g)	9.81 m·s^{-2}

* At T = 10°C, P = 0.2 MPa (average pressure of gas in fracture zone)

Experimentally Determined and Derived Parameters

	Fractured Rock	Overburden
Fracture spacing (m)	0.4-10[a]	0.1-10[b]
Height of transport zone (m)	27	8
Horizontal distance from injection to sampling points (m)	5-178	5-178
Angle of fractures to the horizontal (°)	79.5-8.6	90
Path length for gas transport (m)	27.5-180	8
Transport time (d)	0.3-7.3	1.2
Hydraulic conductivity (m·s^{-1})	2×10^{-8}-5×10^{-5}	5×10^{-12}-5×10^{-10}
Threshold pressure (calculated, MPa)	0.35	
Injection pressure (experimental, MPa)	0.37	

a Estimates obtained from A. Brown, Applied Geoscience Branch, AECL Research, Whiteshell Laboratories, Pinawa, MB.
b Estimates obtained from G. Thorne, Applied Geoscience Branch, AECL Research, Whiteshell Laboratories, Pinawa, MB.

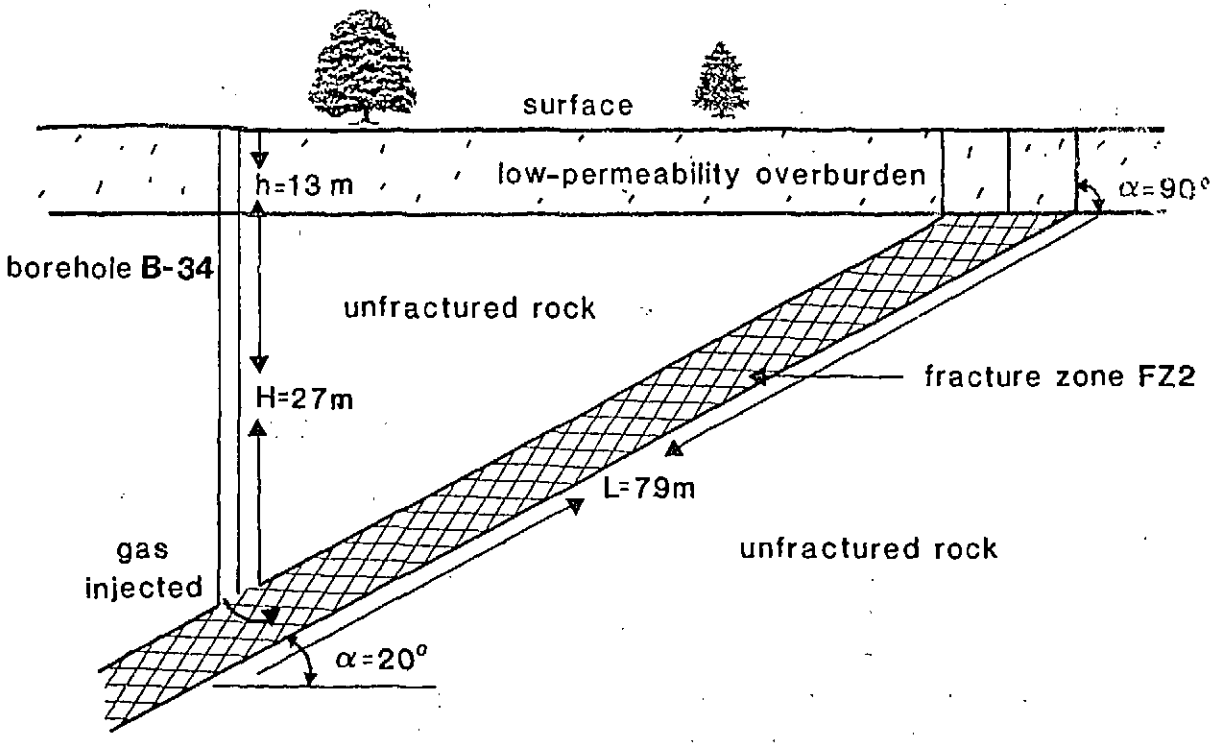

FIGURE 1: Model of Gas Transport in a Fracture Zone with Low-Permeability Overburden (from Gascoyne and Wuschke 1990)

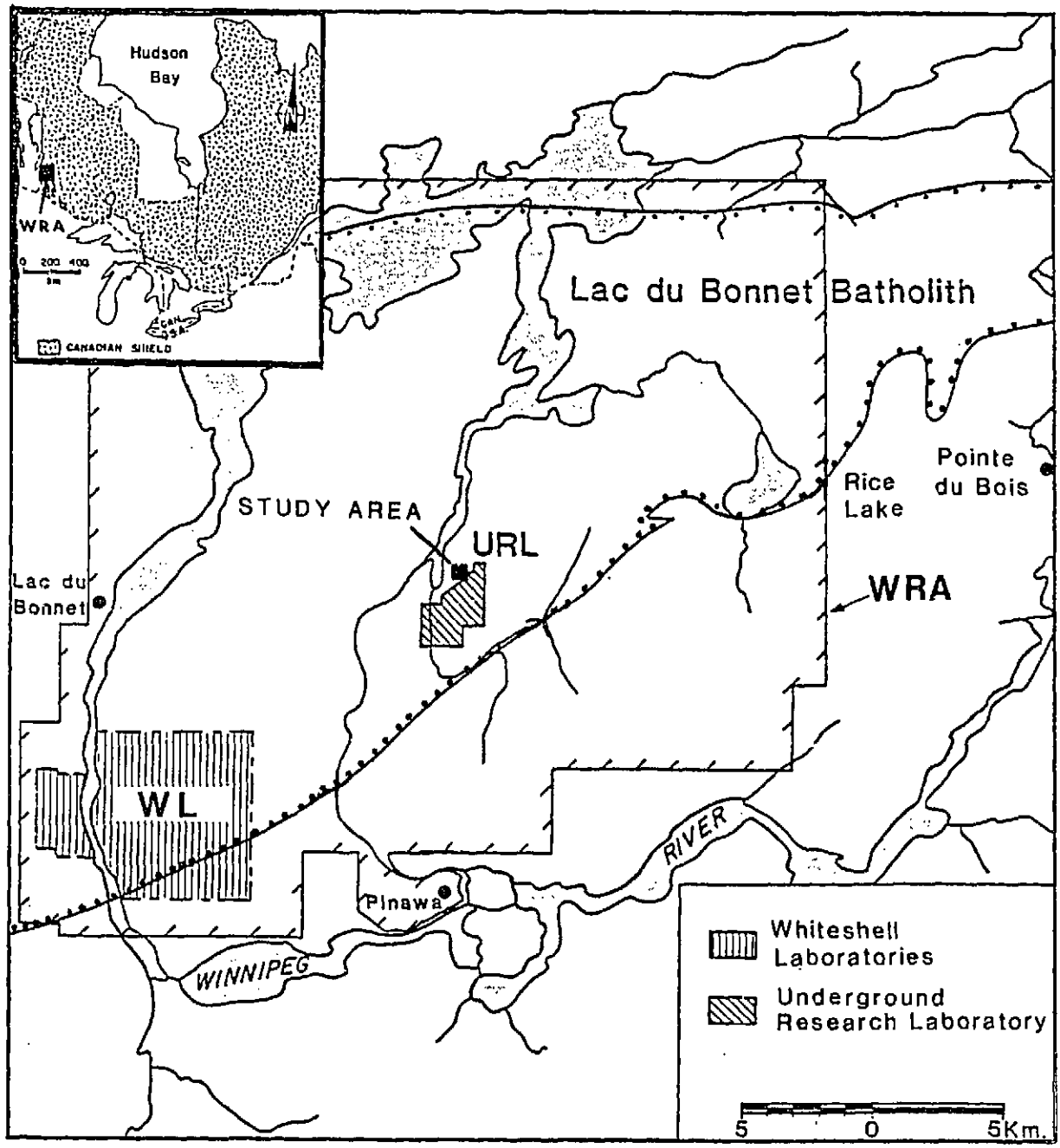

FIGURE 2: Location of the Underground Research Laboratory (URL) with Respect to the Whiteshell Laboratories (WL), the Whiteshell Research Area (WRA) and the Outcrop of the Lac du Bonnet Granite Batholith (dotted boundary). The inset shows the location of this region with respect to the Canadian Shield.

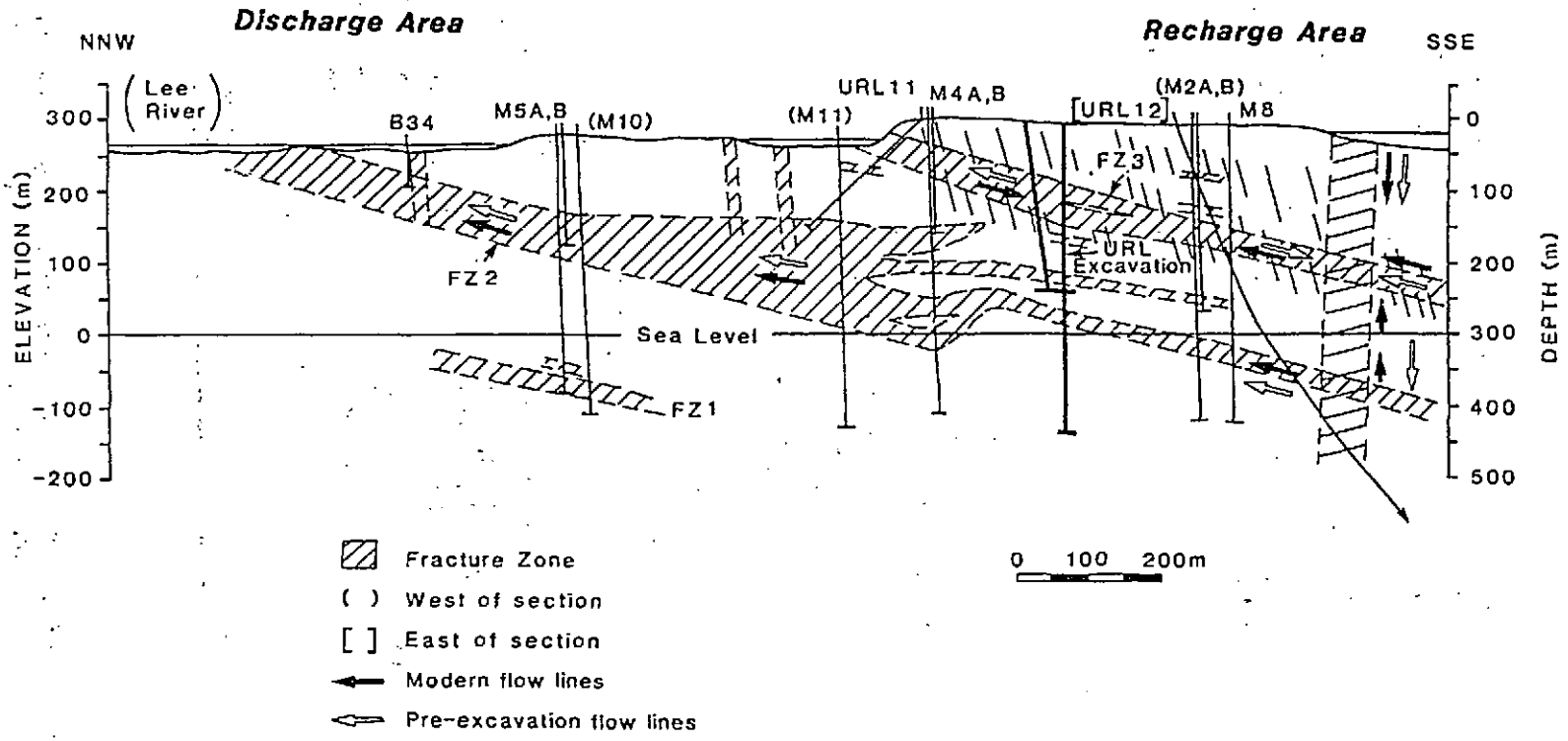

FIGURE 3: Cross Section Through the URL Showing Groundwater Flow Paths in Relation to the Recharge and Discharge Areas. Boreholes (numbered) are shown as steep or vertical lines.

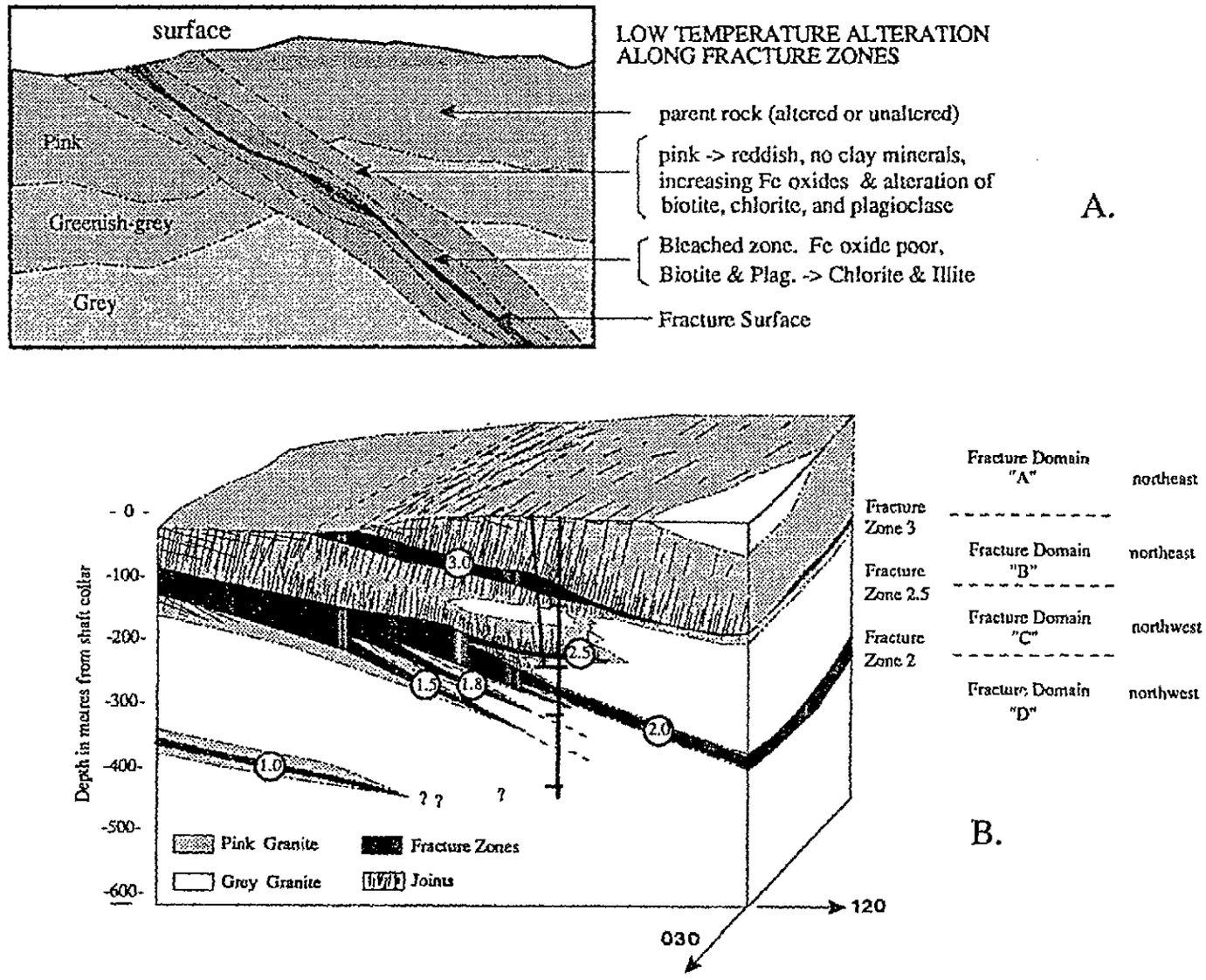

FIGURE 4: a) Typical Field Relationships for Alteration Associated with Fracture Zones in the Lac du Bonnet Granite, and b) Isometric Projection Showing the Location of the Underground Research Laboratory with Respect to the Fracture Zones (numbered) and Areas of Pink Alteration (from Everitt et al. 1990)

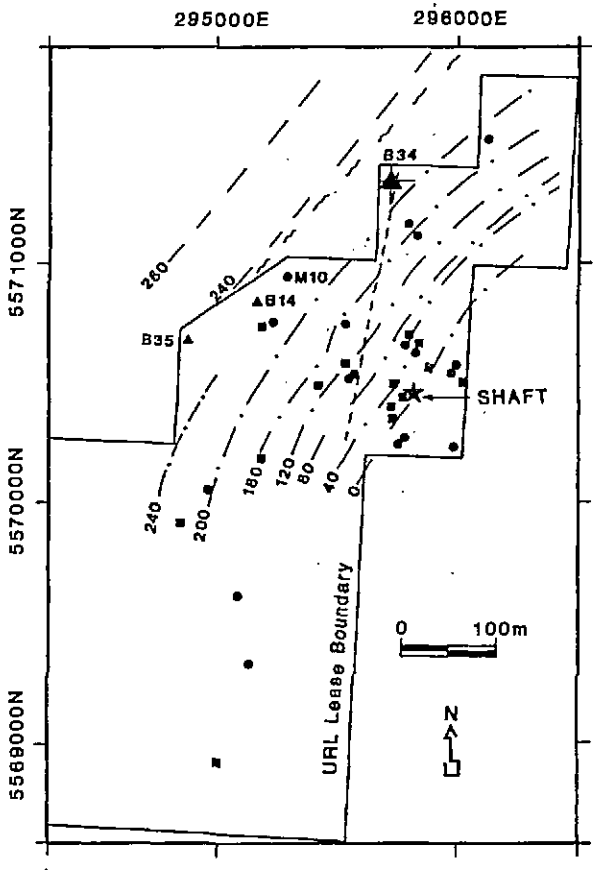

inferred outcrop of FZ2 from regional and lease area mapping,

contour of upper surface extrapolated from the URL shaft and boreholes near the shaft,

contour of upper surface from all boreholes,

collar locations of all cored URL-series boreholes (■), all major percussion-drill M-series boreholes (●), and some of the B-series boreholes drilled near the FZ2 subcrop (▲).

FIGURE 5a: Contours (in metres above mean sea level) of Upper Surface of FZ2 in the URL Lease Area

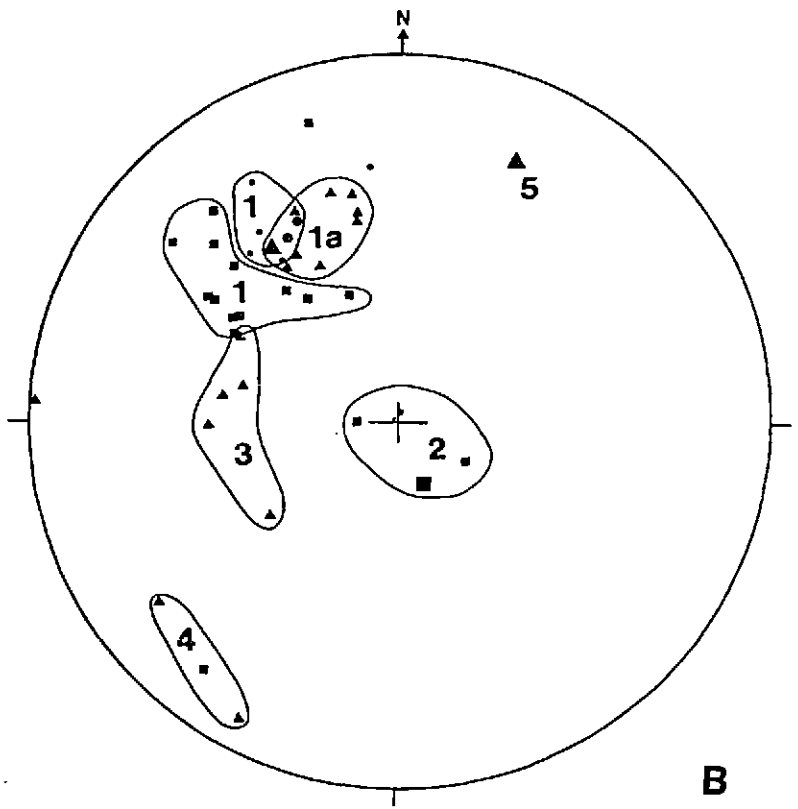

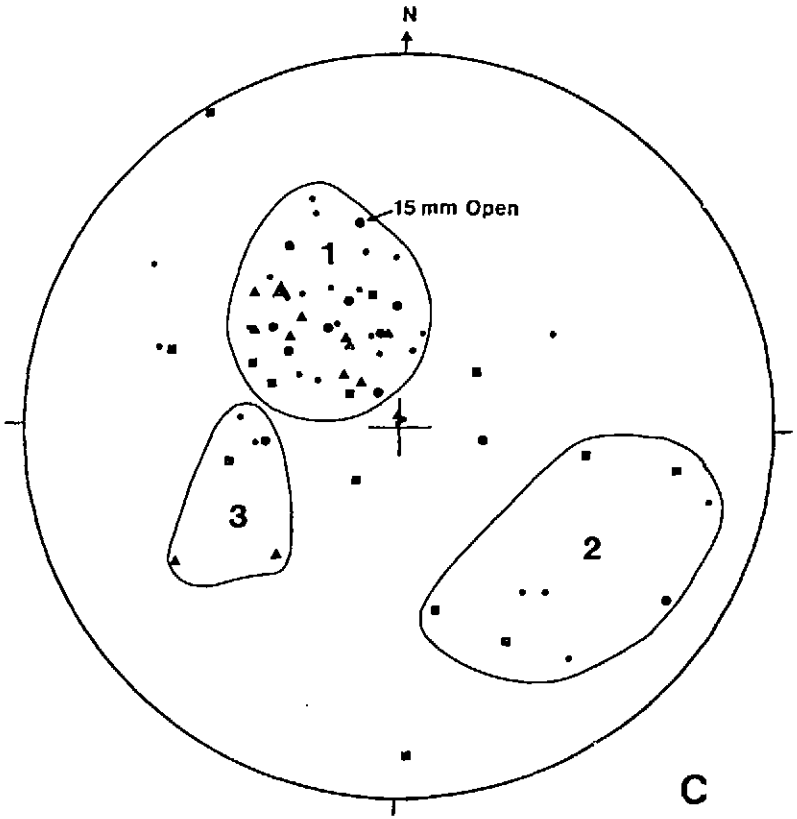

FIGURE 5b and c: Stereograms of Poles to Fractures in Borehole B-34 Measured by Downhole Televiewer (lower hemisphere Schmidt net). Large symbols indicate fractures with widths logged as ≥1 mm. (Depths are from surface along the borehole; sets are indicated by enclosed areas and given as follows in dip direction/dip:

(b) ● 0-18 m; ▲ 19-23 m; ■ 24-36 m.
sets: (1) 143/48 ((1a) 160/48 for ▲); (2) 323/10; (3) 089/38; (4) 040/74; 204/66.

(c) ● 37-48 m; ▲ 49-54 m; ■ 55-60 m sets: (1) 144/31; (2) 317/57; (3) 068/40.

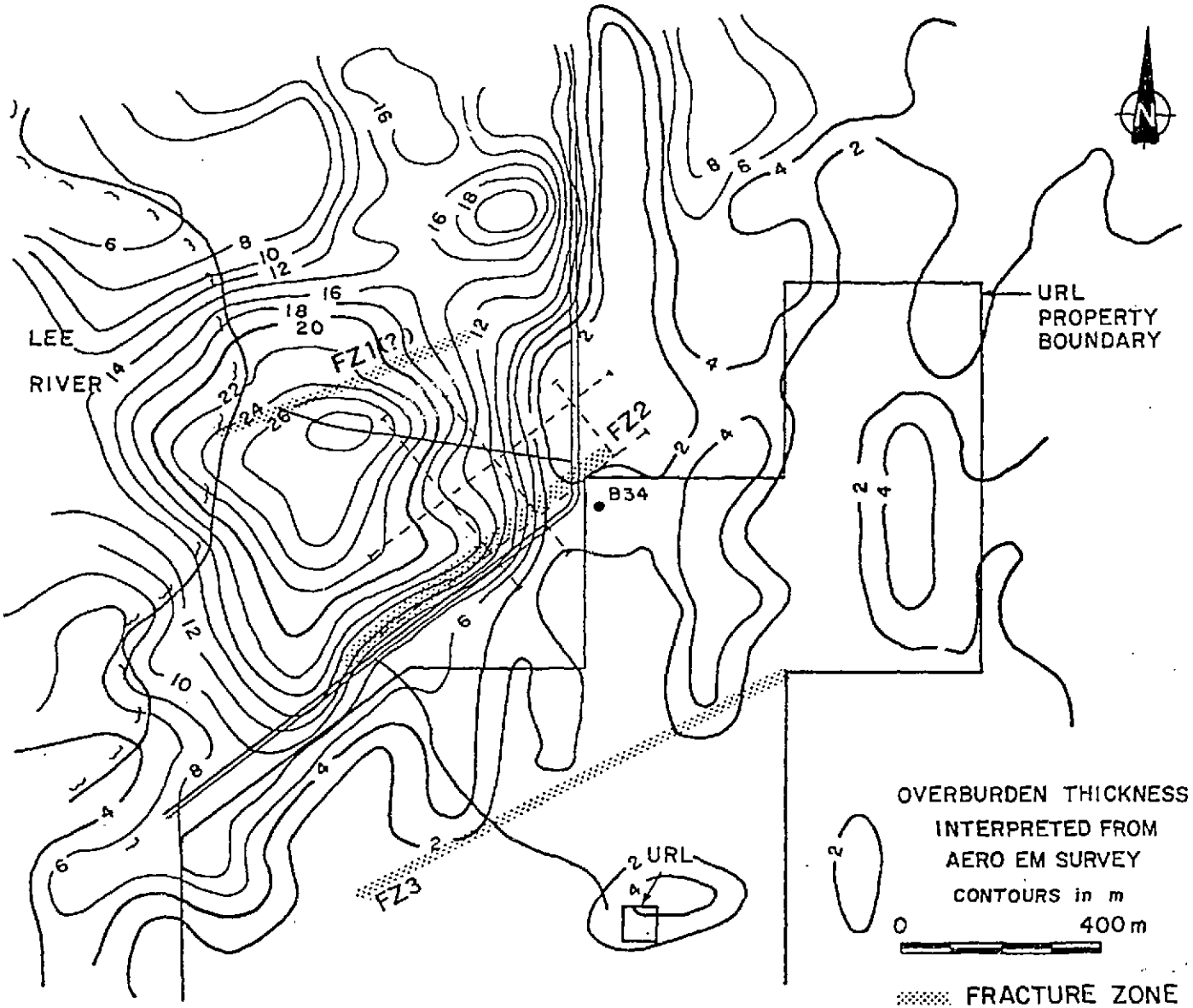

FIGURE 6: Overburden Thickness Map of the Study Area Interpreted from Airborne EM Data at 935 Hz and 4600 Hz. The location of outcrops of the fracture zones FZ1, 2 and 3 is determined from interpretation of all geophysical data.

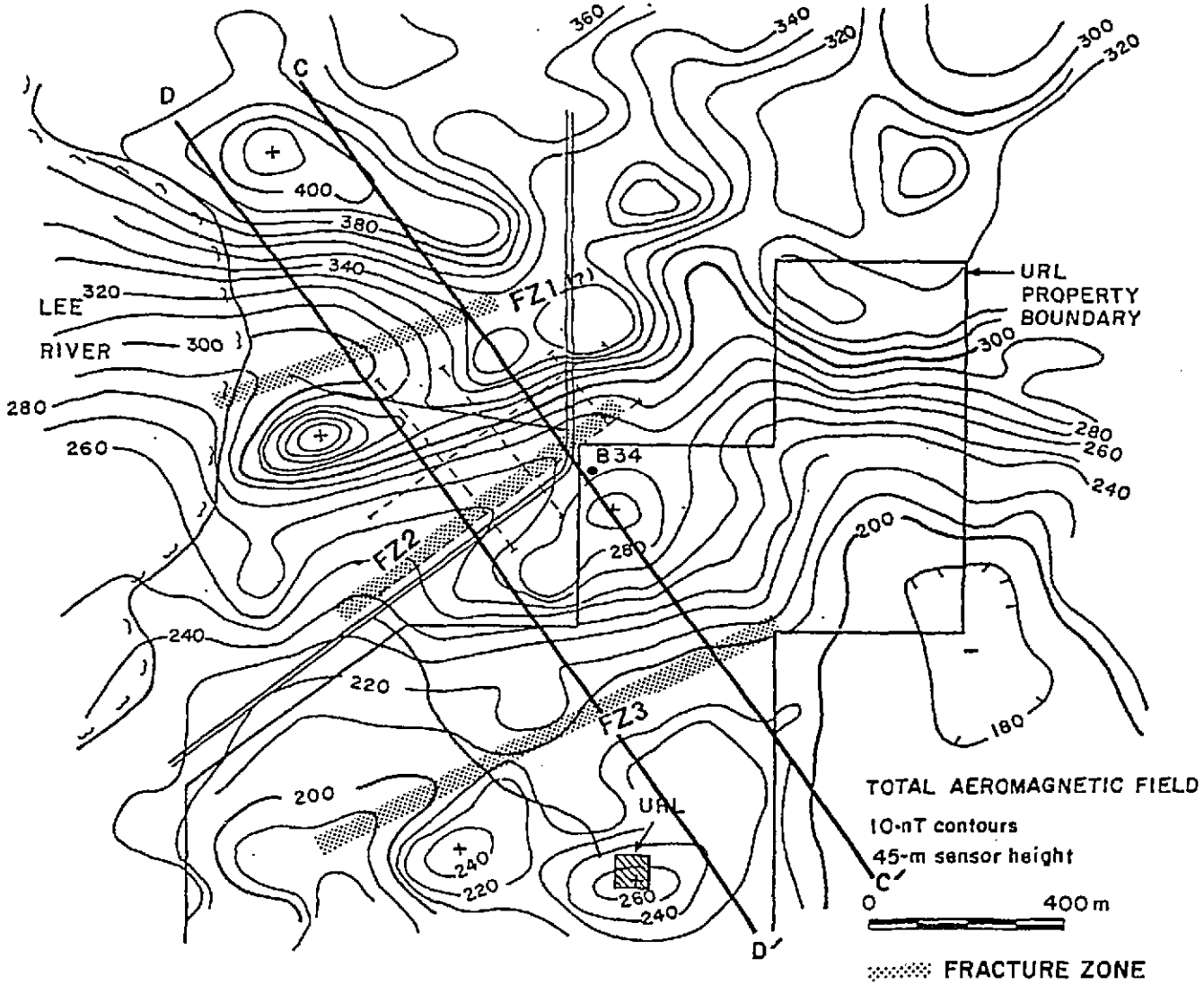

FIGURE 7: The Total Field Aeromagnetic Map of the Study Area. Magnetic lows indicate the surface exposure of fracture zones.

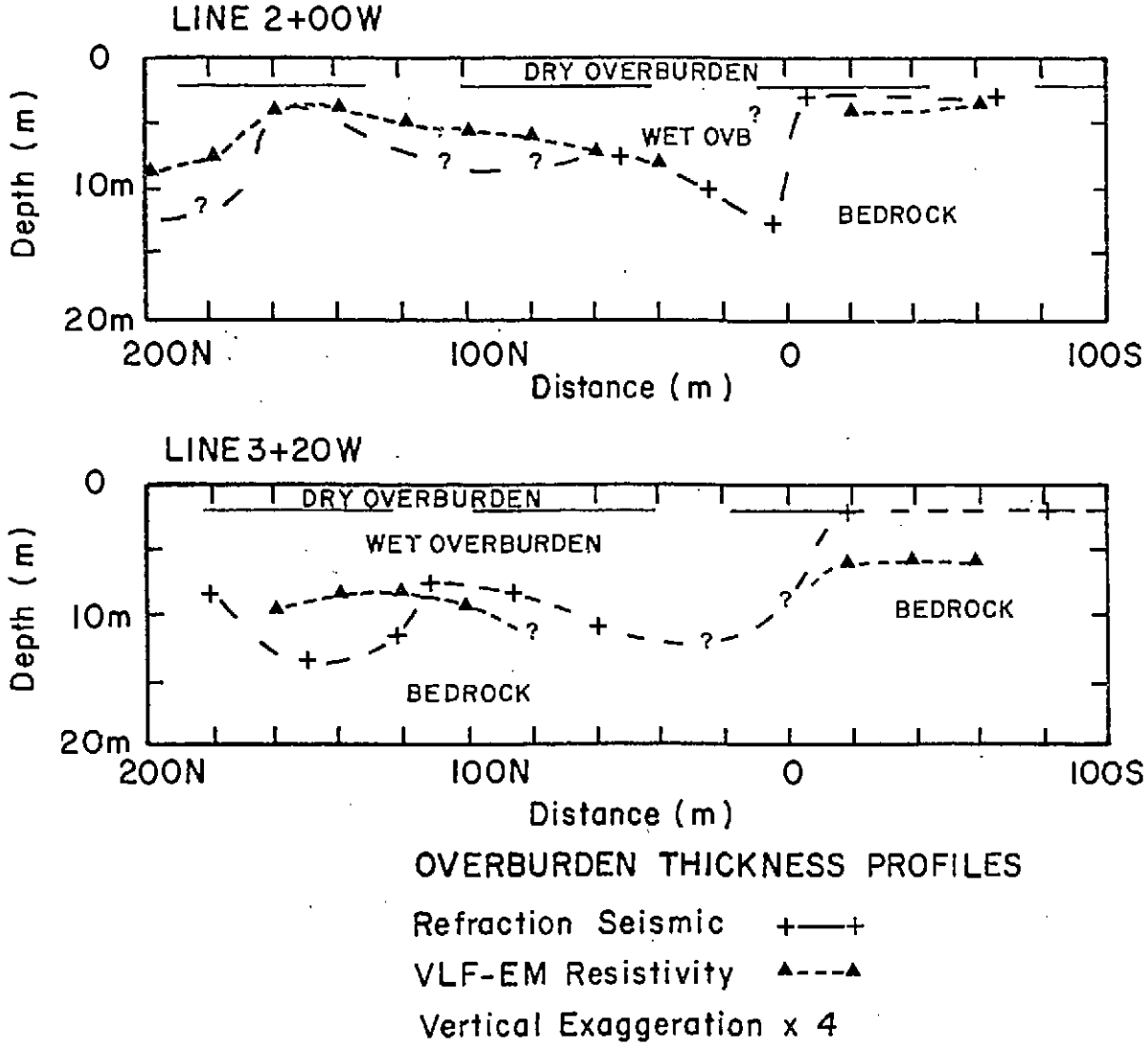

FIGURE 8: Comparison of Overburden Thicknesses Determined from Ground Measurements of VLF-EM Resistivity and Hammer Seismic Refraction Data along Profiles L2+00W and L3+20W

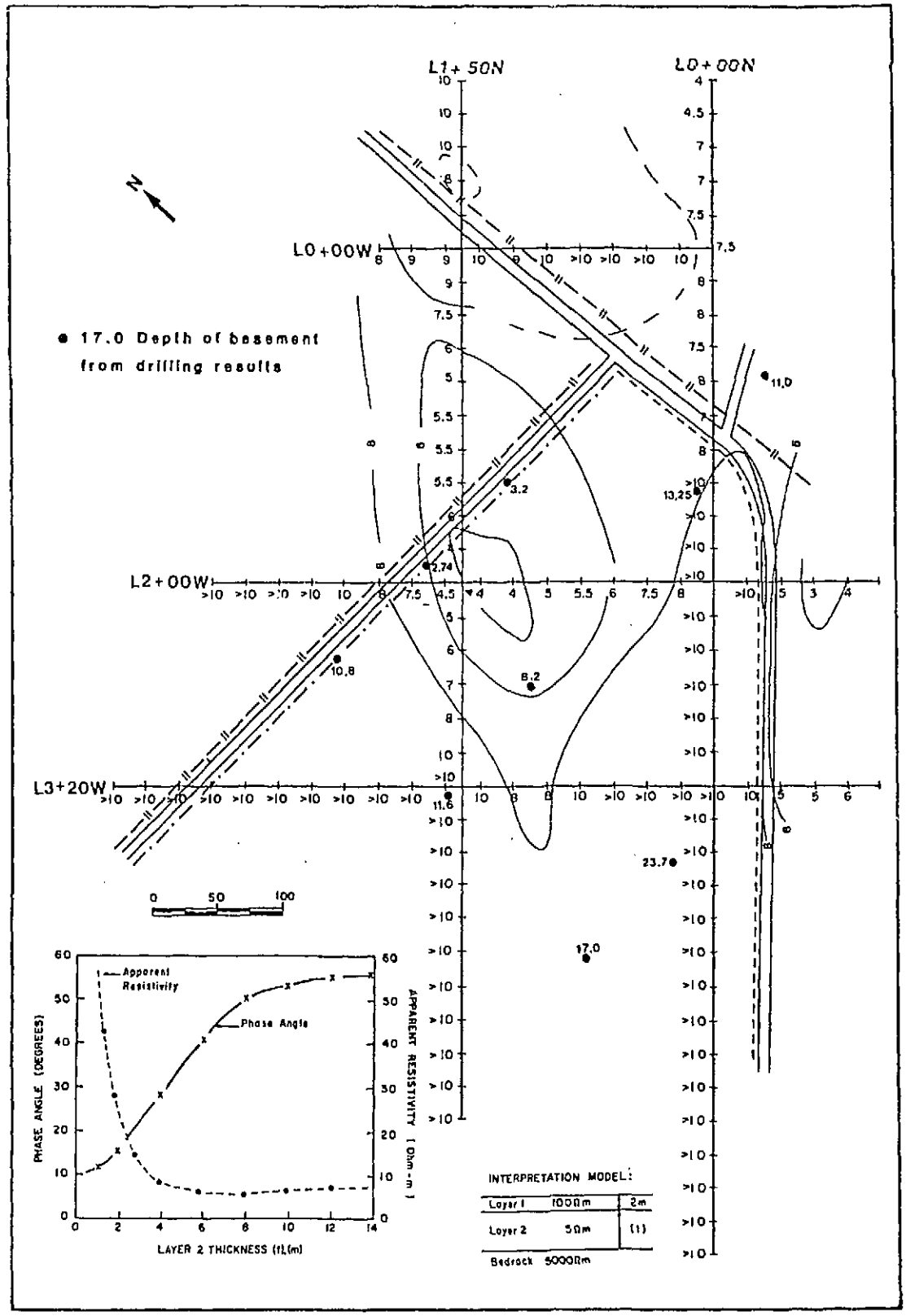

FIGURE 9: Comparison of Overburden Thicknesses Determined from VLF-EM Resistivity Surveys (contours) and Borehole Data (isolated points)

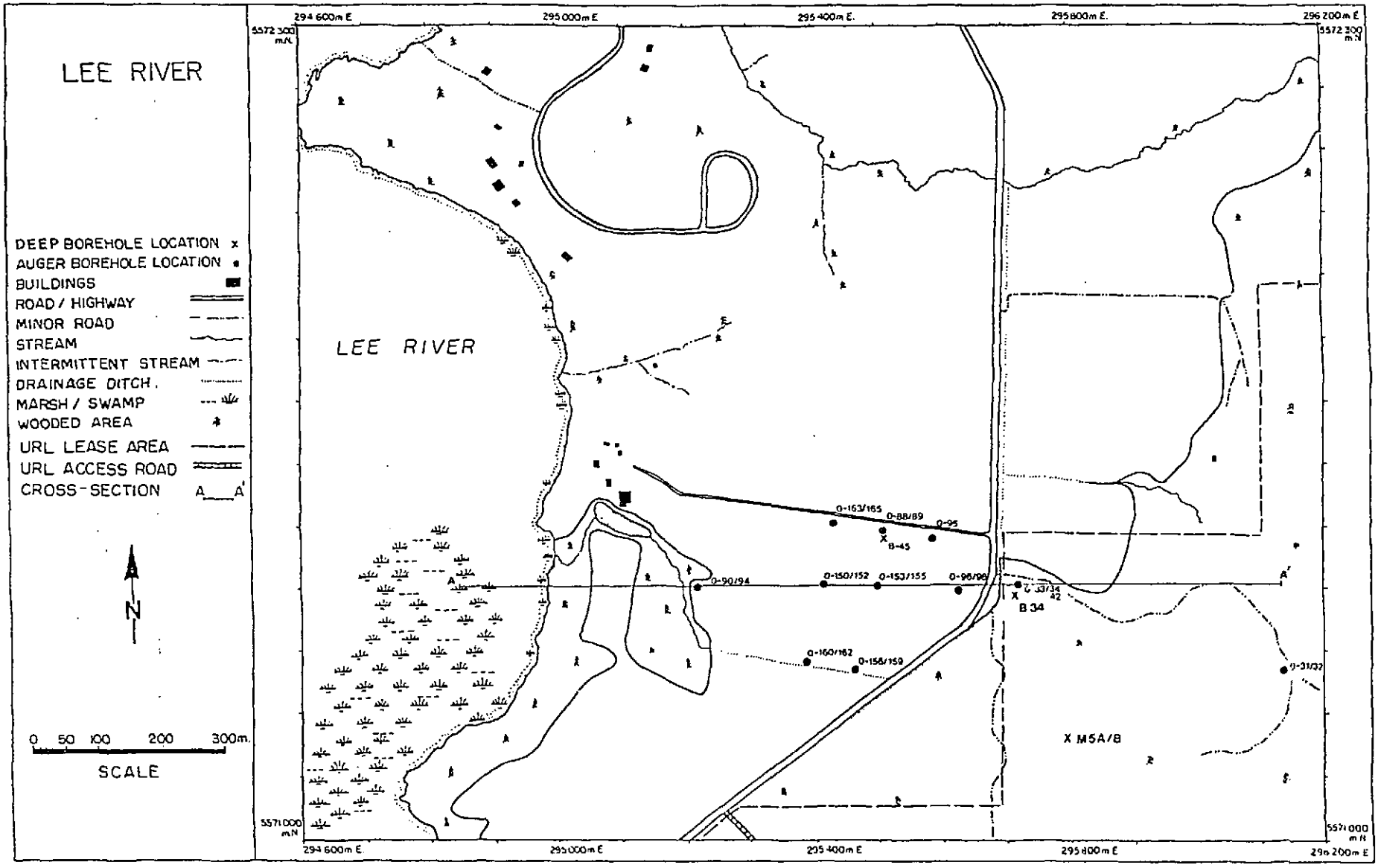

FIGURE 10: Locations of Overburden Piezometers and Boreholes in the Study Area

CONSTRUCTION OF A TYPICAL PIEZOMETER NEST

CONSTRUCTION OF A TYPICAL BEDROCK MONITORING WELL

Top of Pipe Elevation: 277.6 m ASL
Surface Elevation: 276.7 m ASL

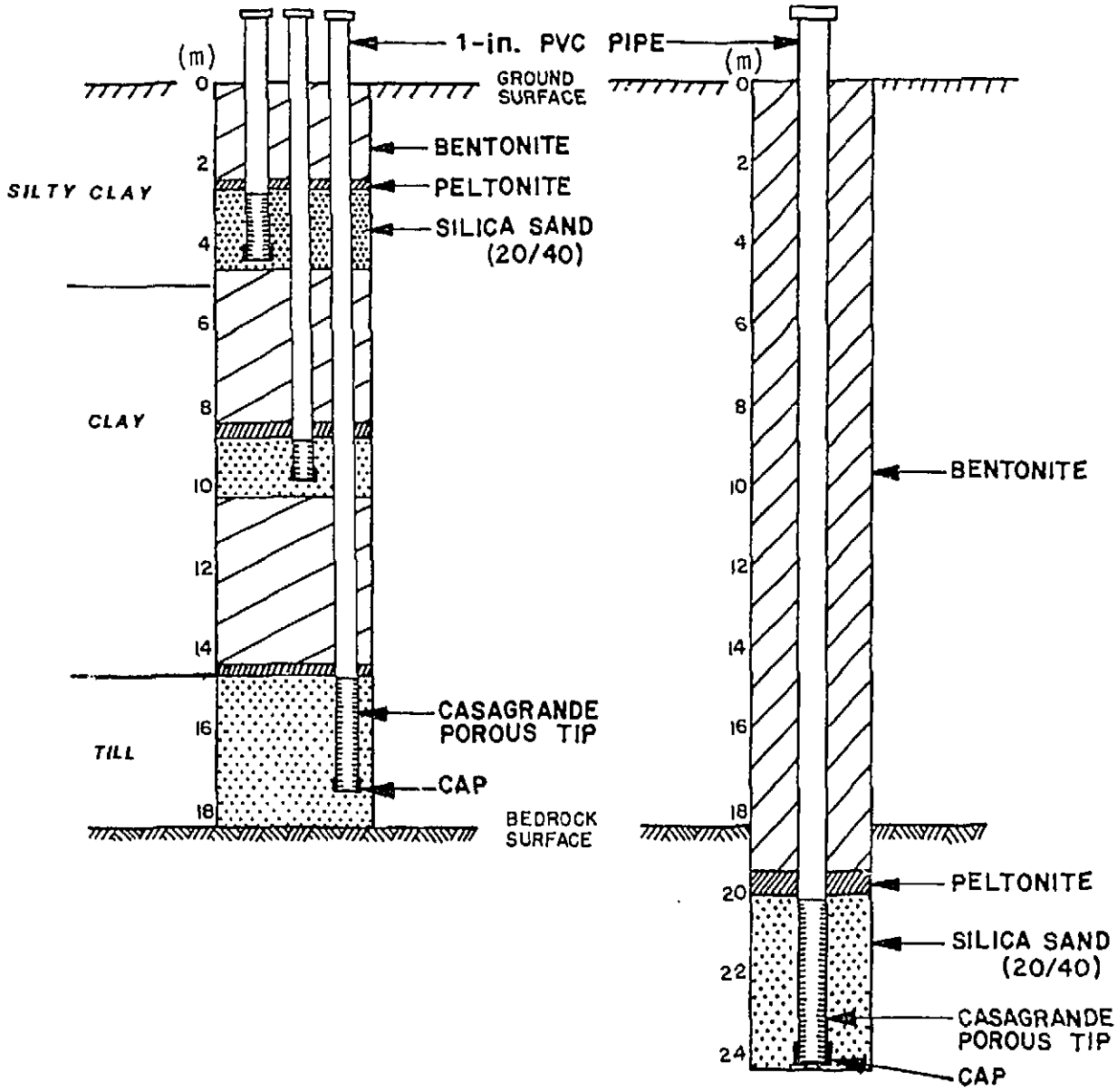

FIGURE 11: Typical Installations for Overburden Piezometers and Bedrock Monitoring Wells

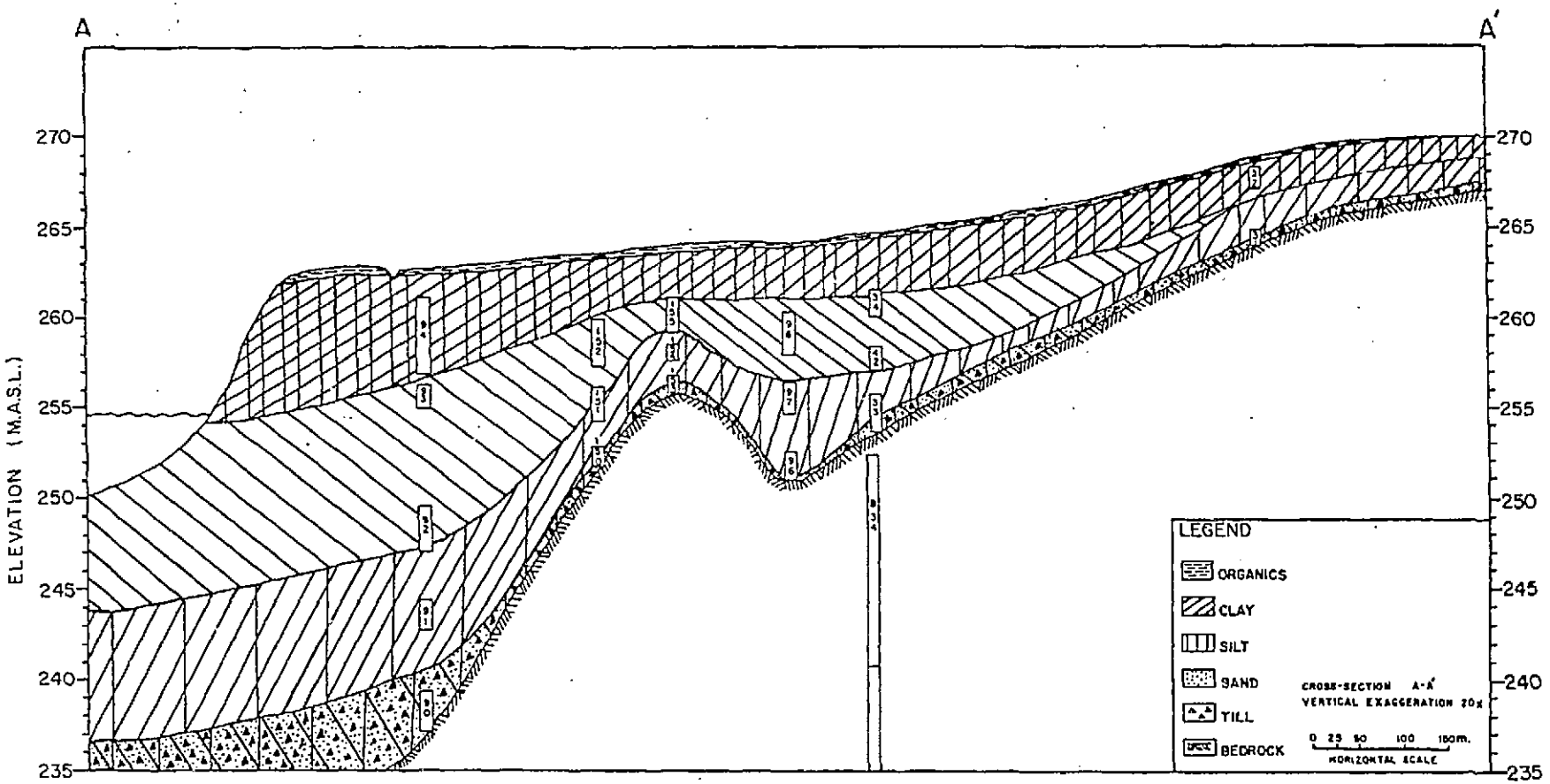

FIGURE 12: Stratigraphic Section Through the Overburden in the Study Area. Locations of piezometers and borehole B-34 are shown.

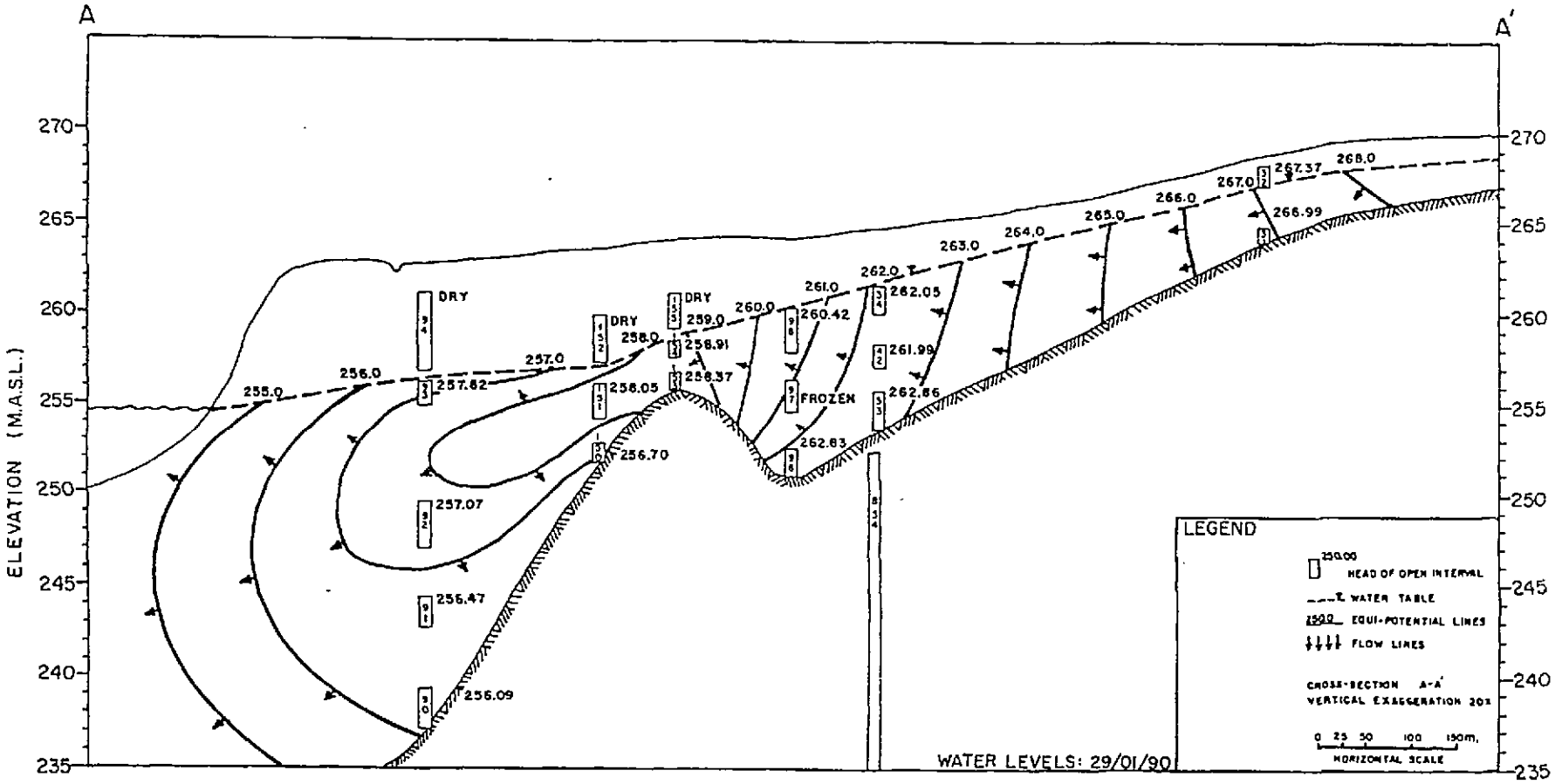

FIGURE 13: Flow Patterns of Groundwater in the Overburden in the Study Area from Piezometer and Bedrock Well Data

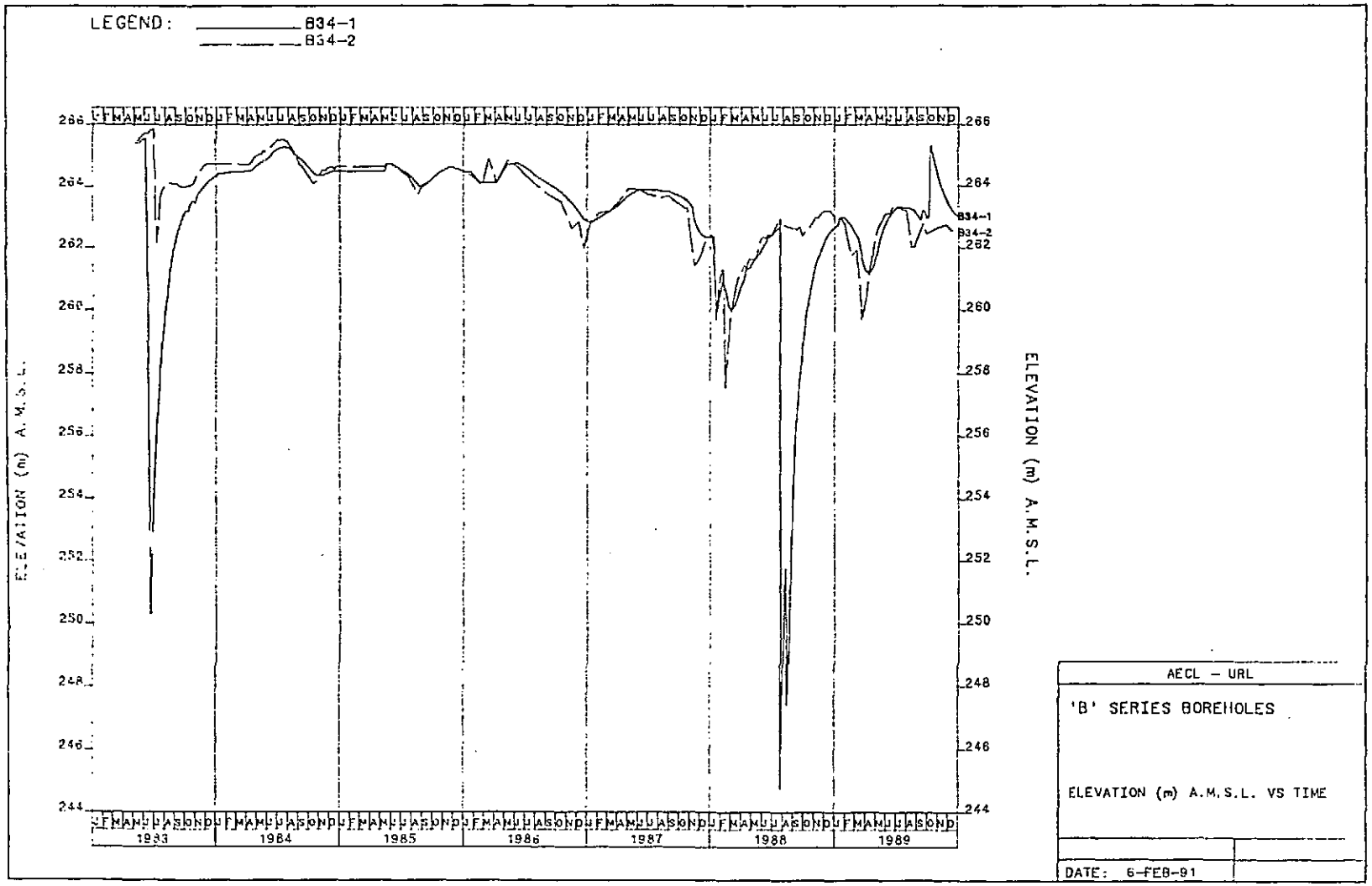

FIGURE 14: Records of Hydraulic Head for the Upper (-1) and Lower (-2) Zones in Borehole B-34 for the Period 1983-1989. The large drawdowns are due to groundwater sampling from the borehole or to activities in the URL.

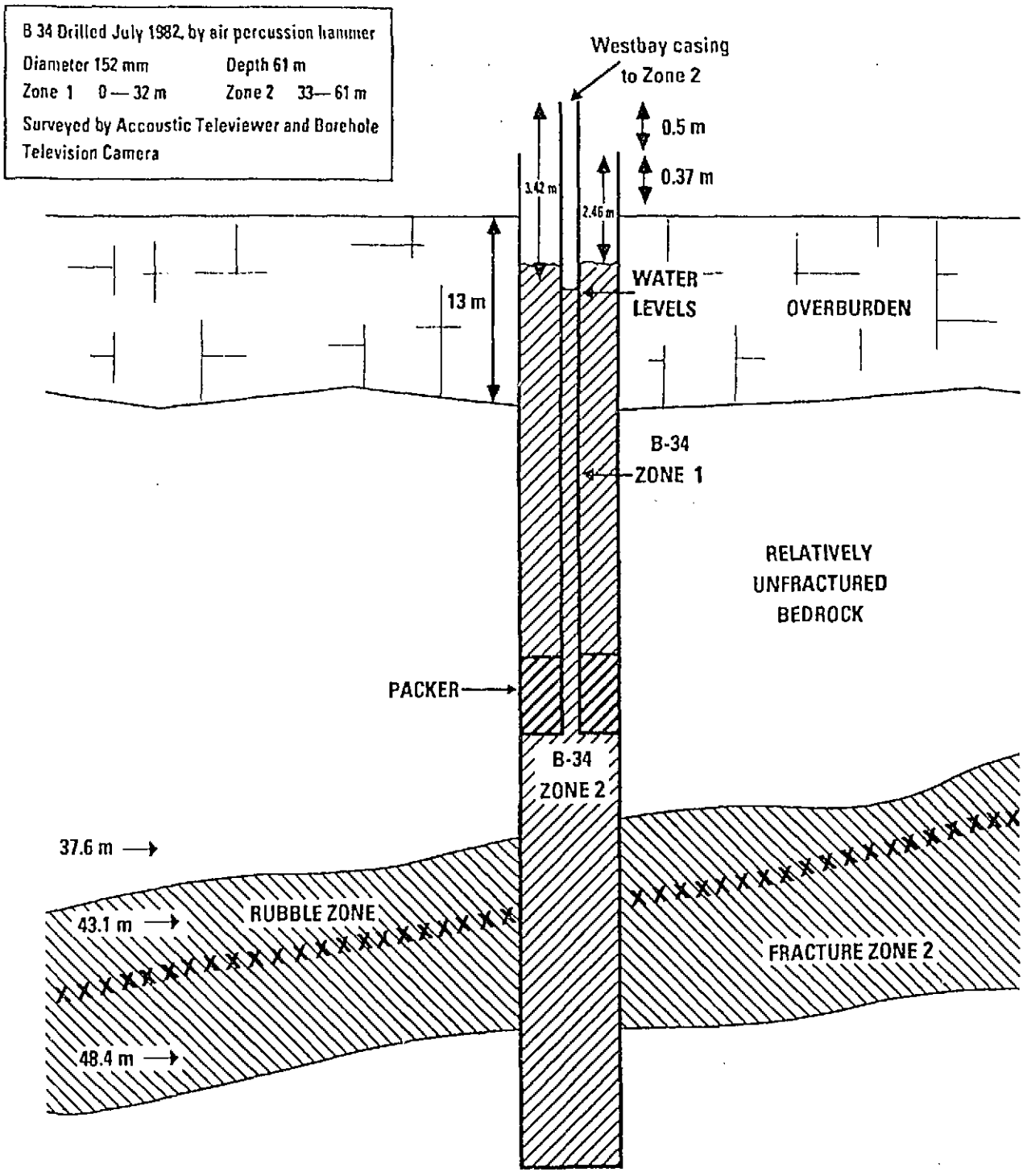

FIGURE 15: Detail of Borehole B-34 Installation Showing Piezometric Levels and Borehole Dimensions

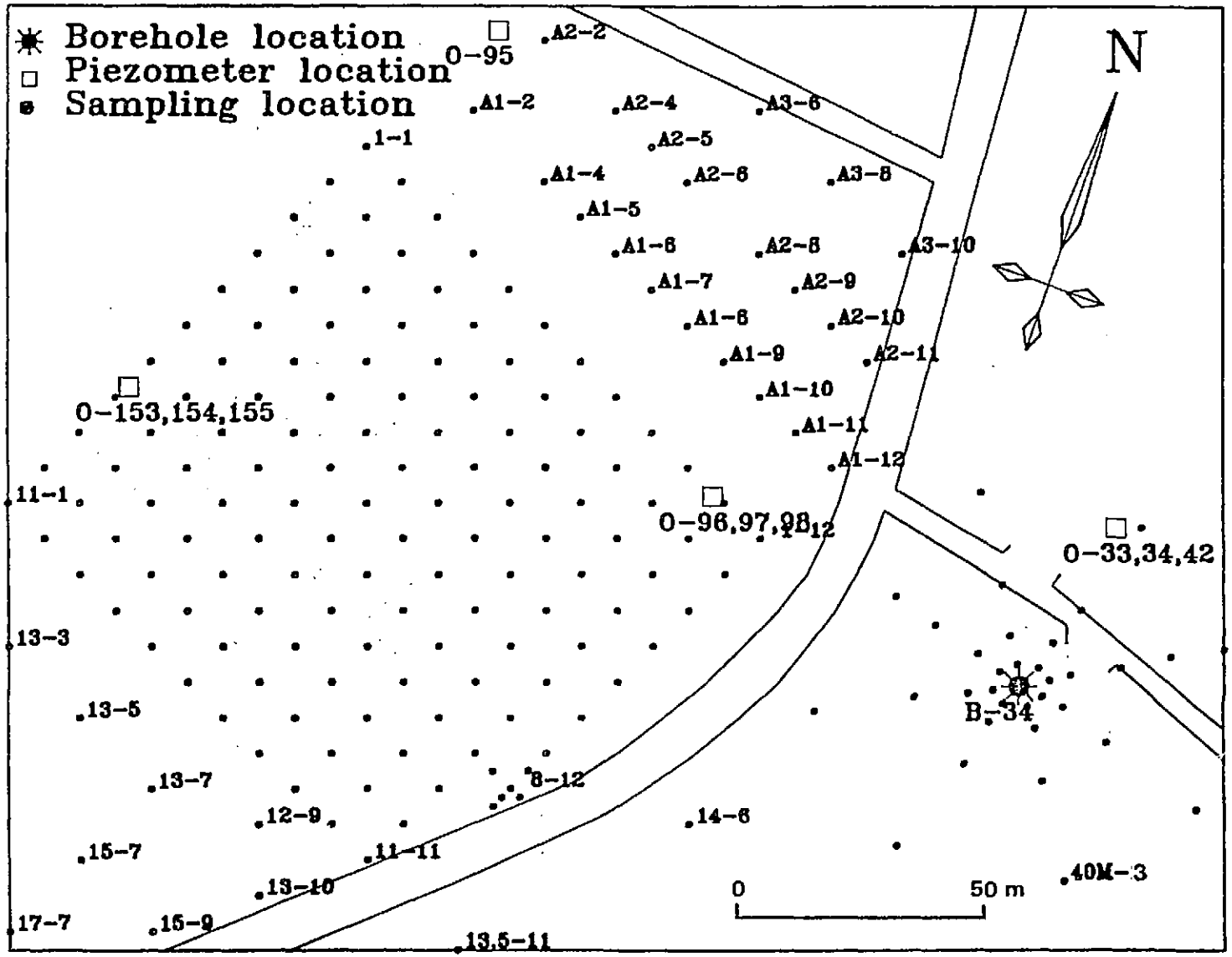

FIGURE 16: Location of Piezometers and Soil Gas Sampling Sites in the Field Grid and Radial Array Around B-34, in Relation to Access Roads

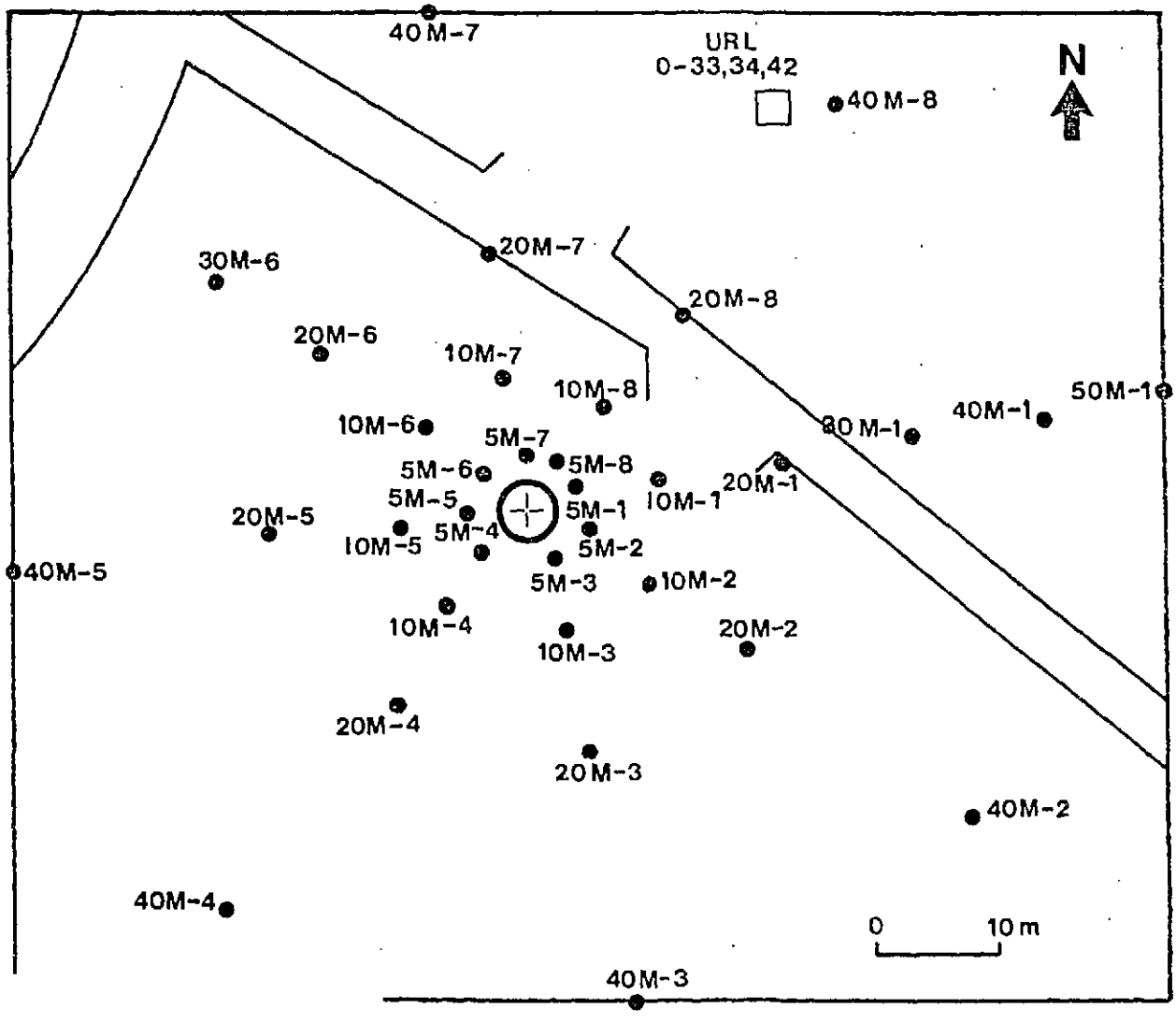

FIGURE 17: Location Details of the Radial Soil Gas Sampling Sites Around Borehole B-34

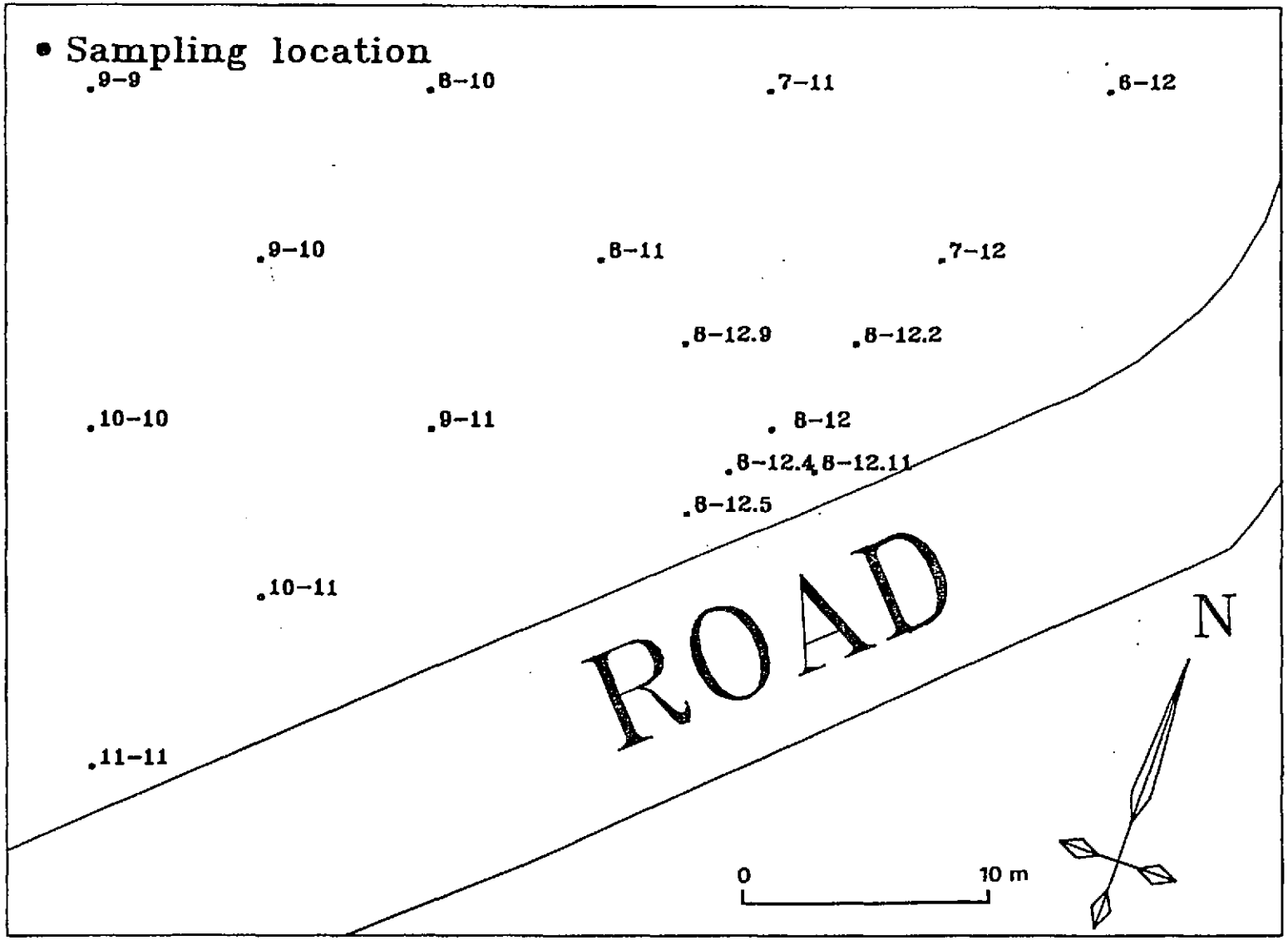

FIGURE 18: Location Details of Soil Gas Sampling Sites in the He Anomaly Area of the Field Grid

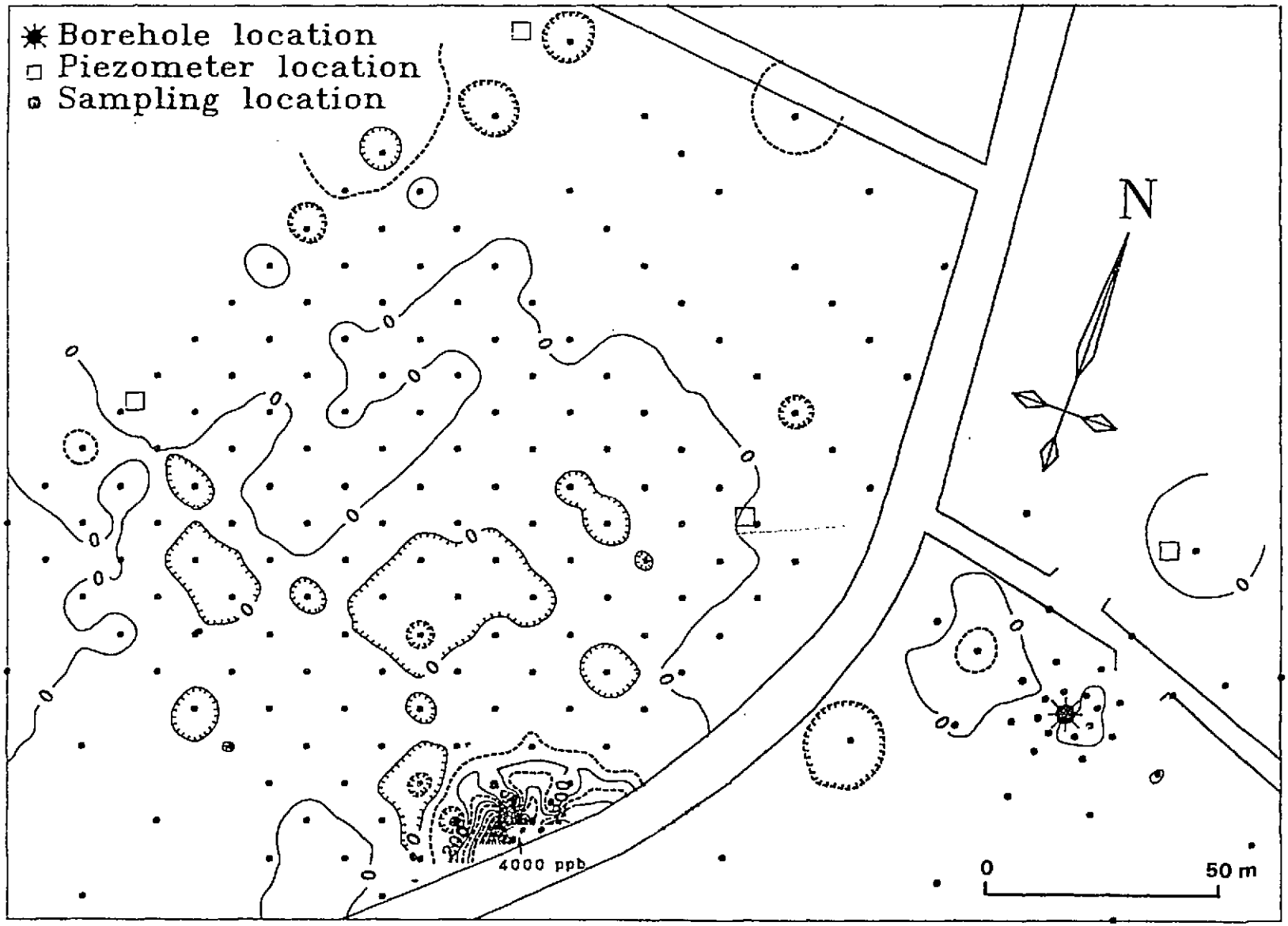

FIGURE 19: Helium Concentrations Above Atmospheric Levels (plotted as parts per billion, ppb) in Soil Gases Prior to the Gas Injection Test

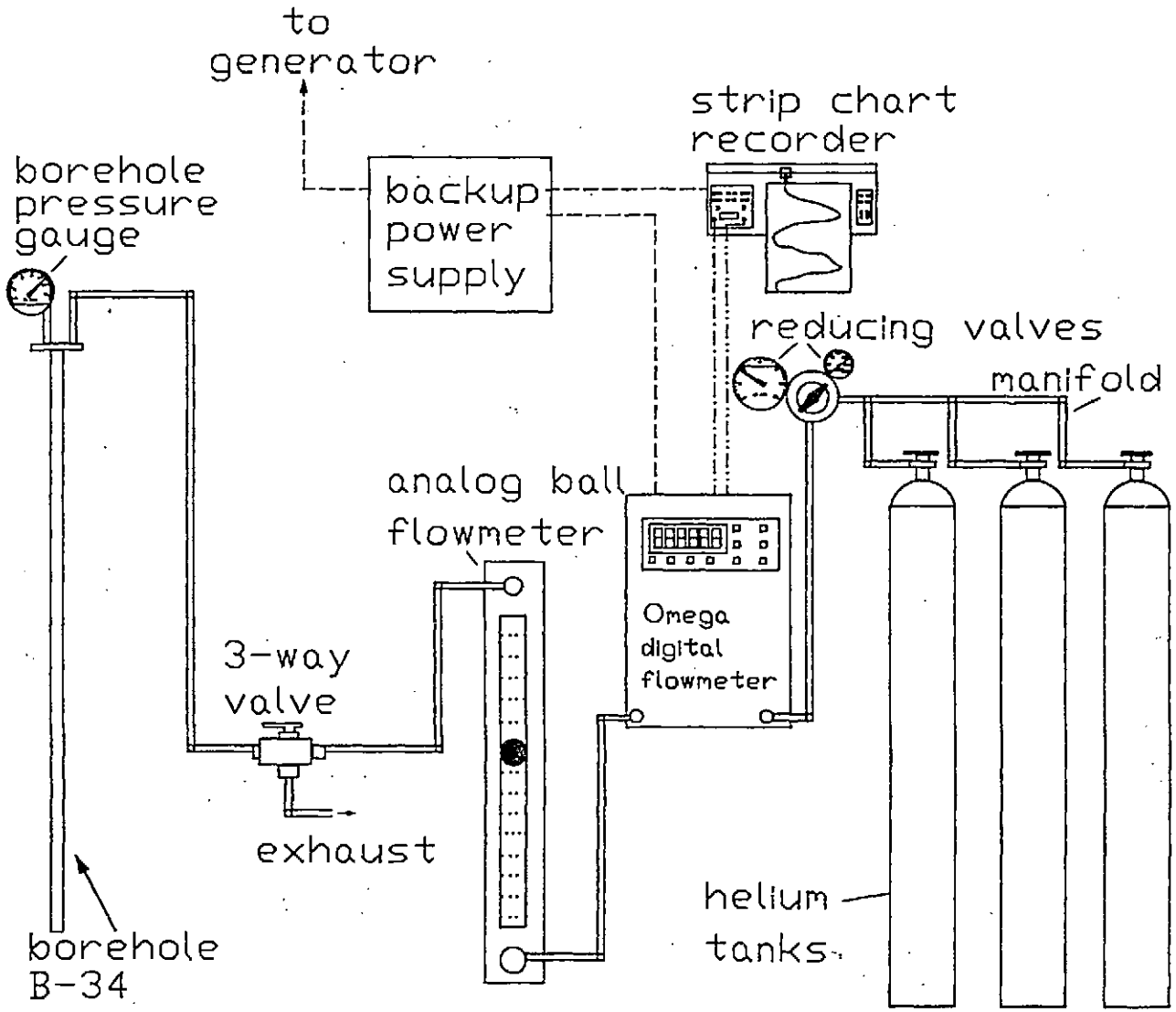

FIGURE 20: Schematic Diagram Showing the System for Gas Injection and Monitoring of Pressures and Flow Rates

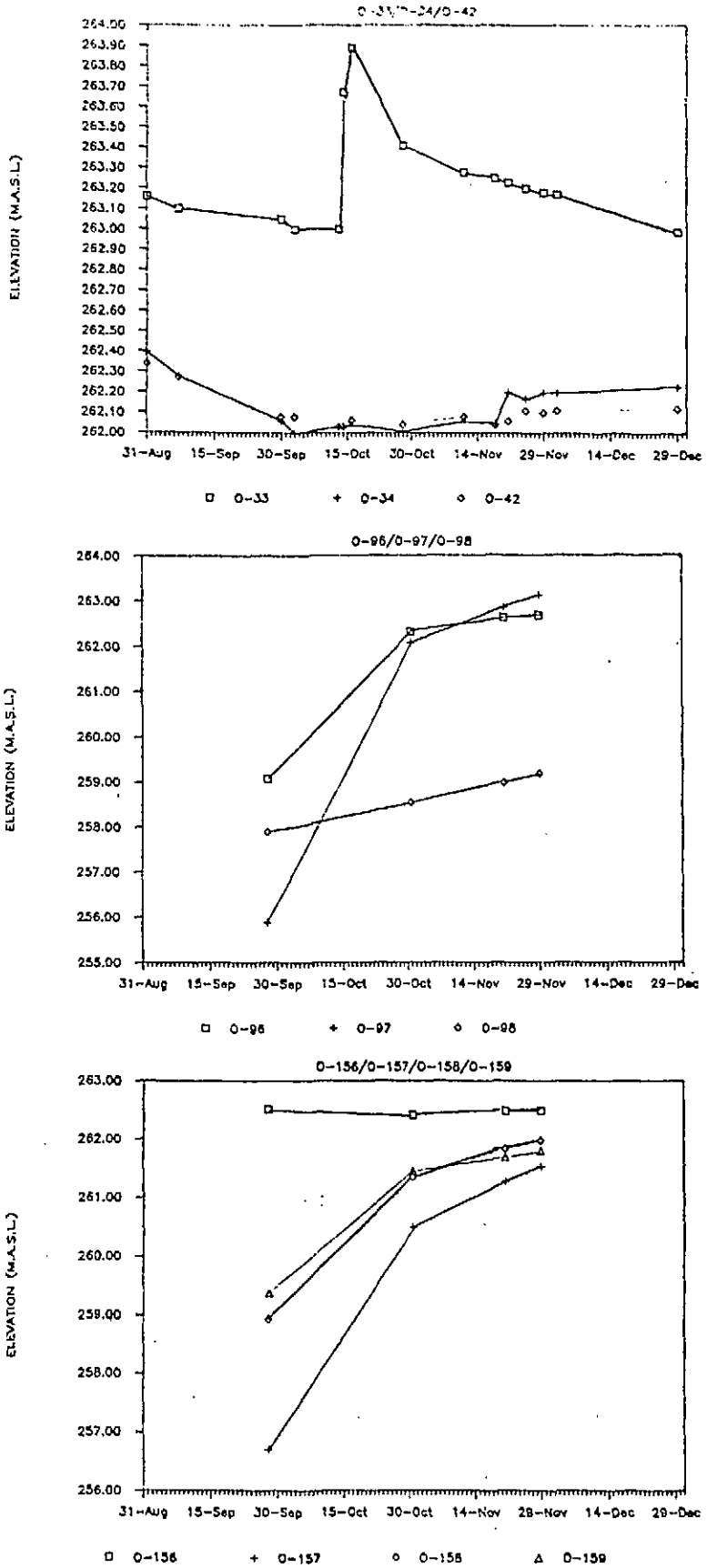

FIGURE 21: Hydrographs of Overburden Piezometers near Borehole B-34, for the Period 1989 September to December

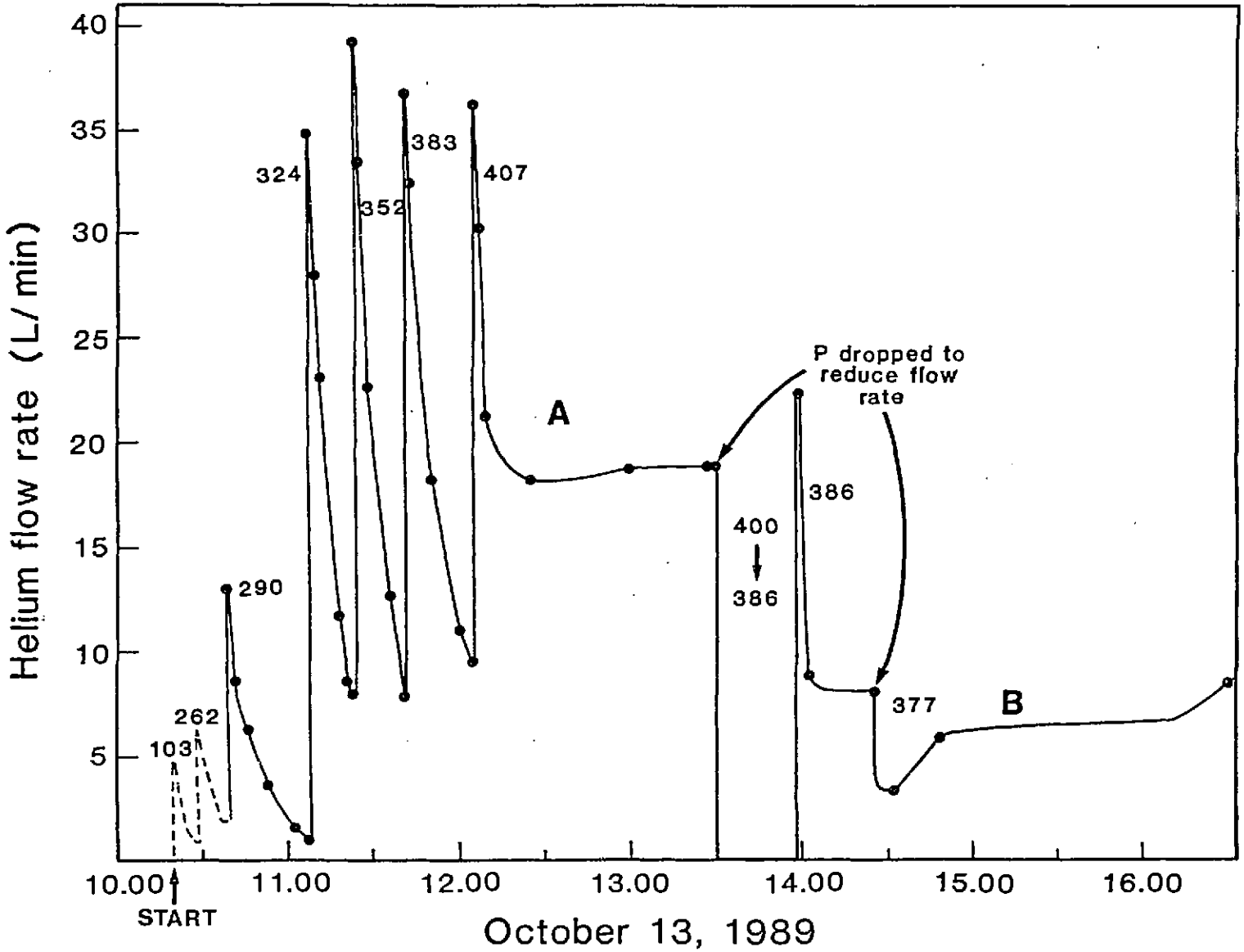

FIGURE 22: Record of Gas Flow Rate for the Beginning of the Injection Test. Areas A and B are described in the text

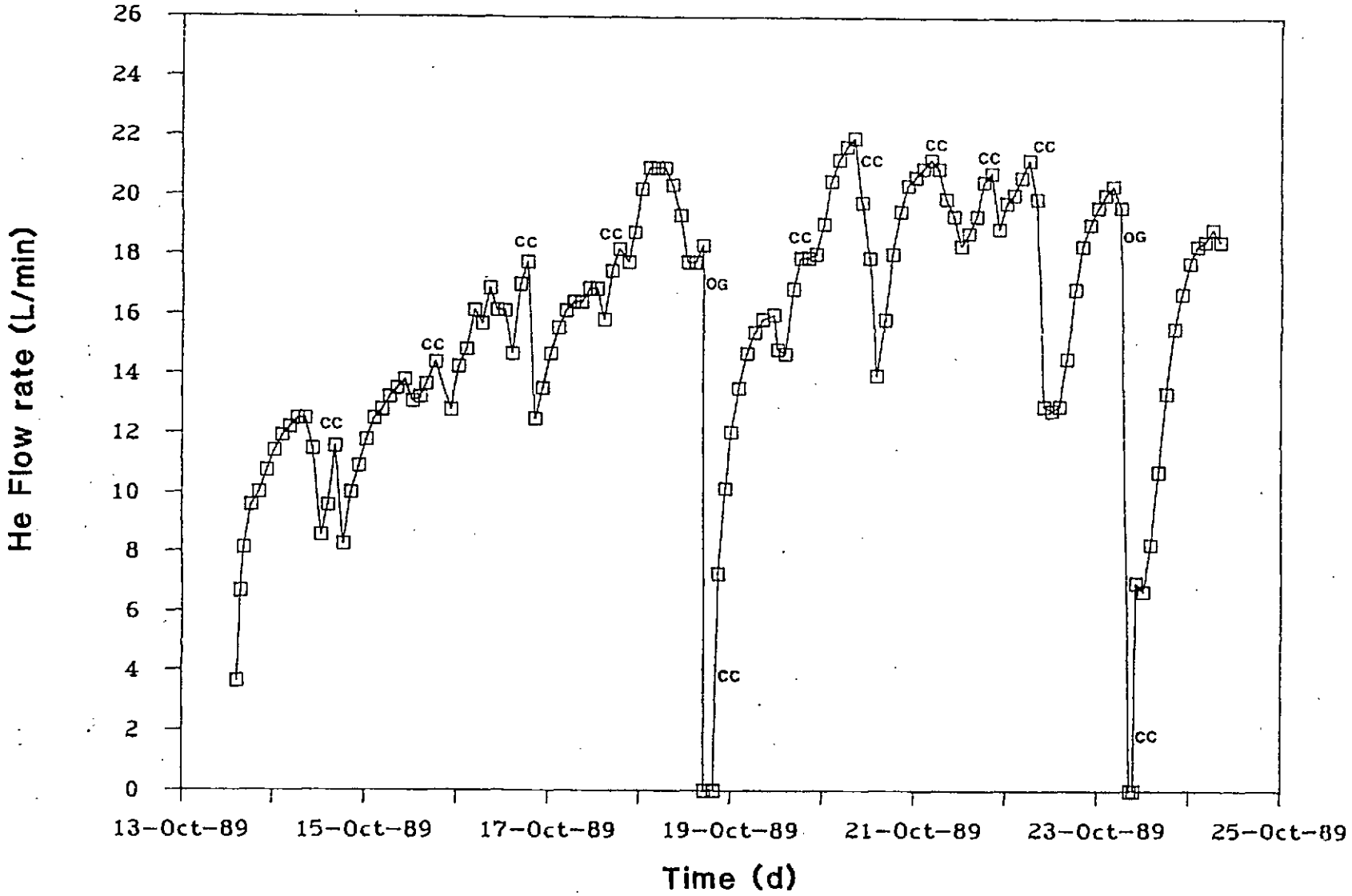

FIGURE 23: Record of Gas Flow Rates for the Period of Gas Injection in Borehole B-34. Times of changing gas cylinders (CC) and periods when the system was out of gas (OG) are indicated.

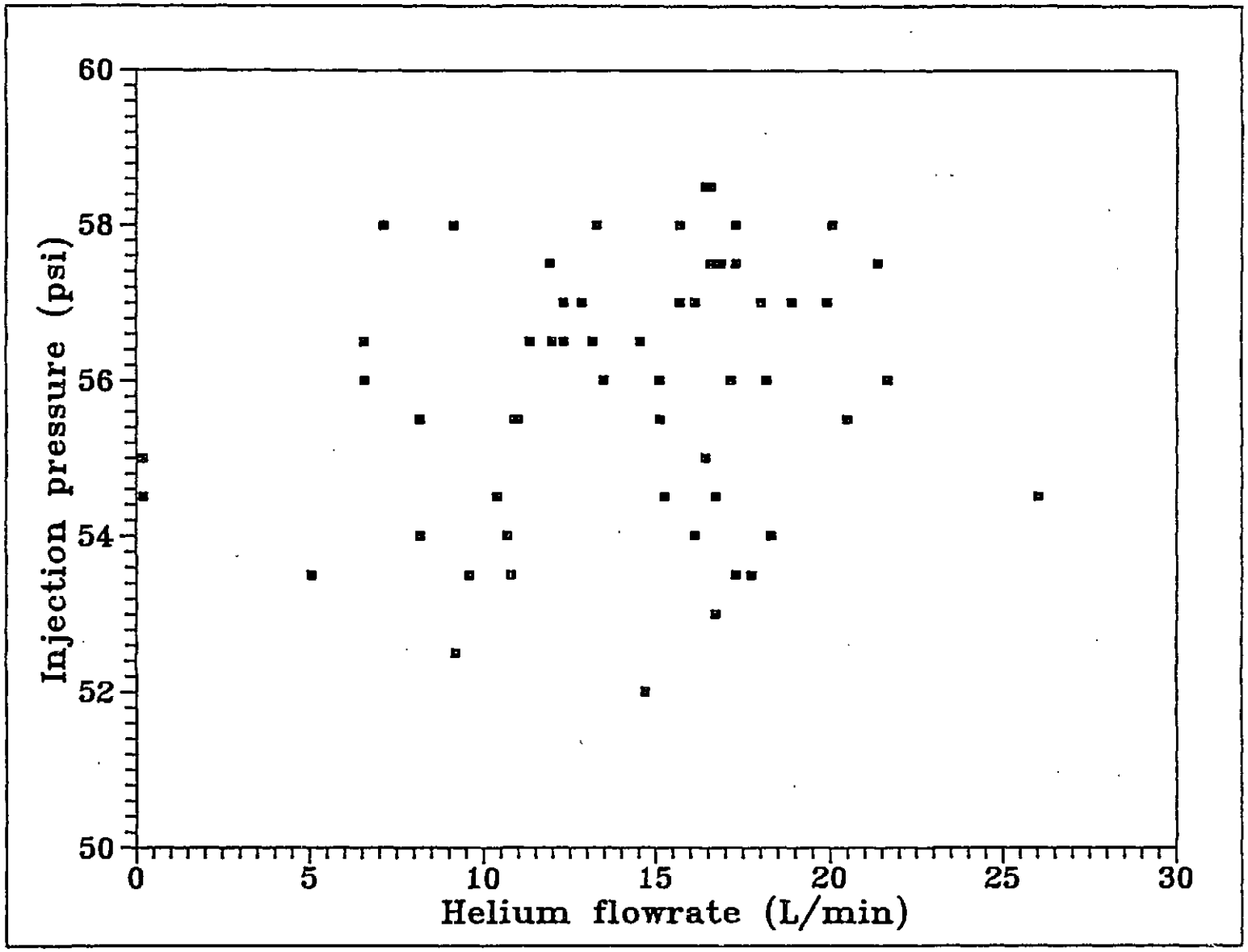

FIGURE 24: Variation of He Injection Pressure with Flow Rate for the Period of the Injection Test

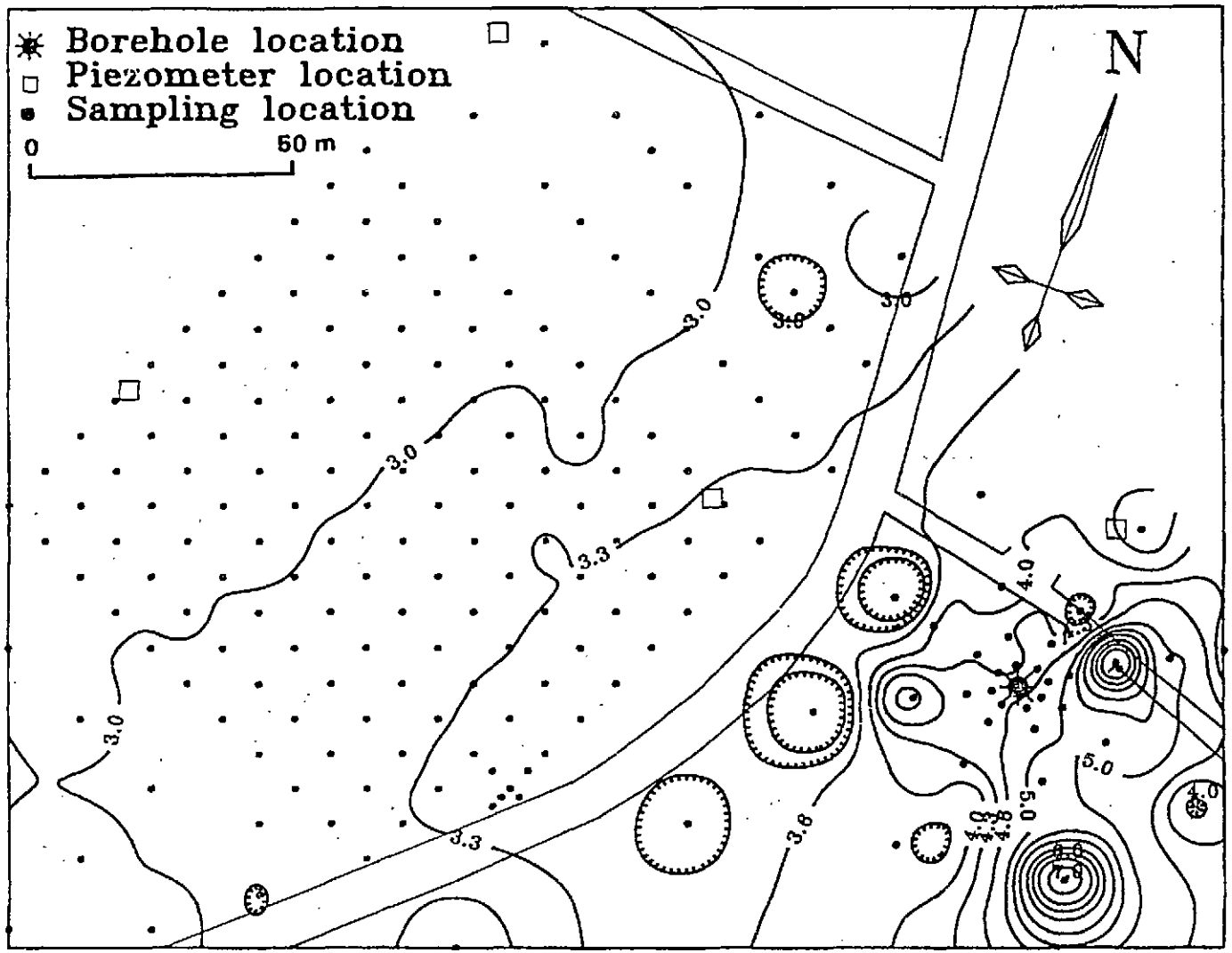

FIGURE 25: The Distribution and Concentration of He (expressed as log He (ppb)), in Soil Gas Samples Taken at Selected Sites on 1989 October 23

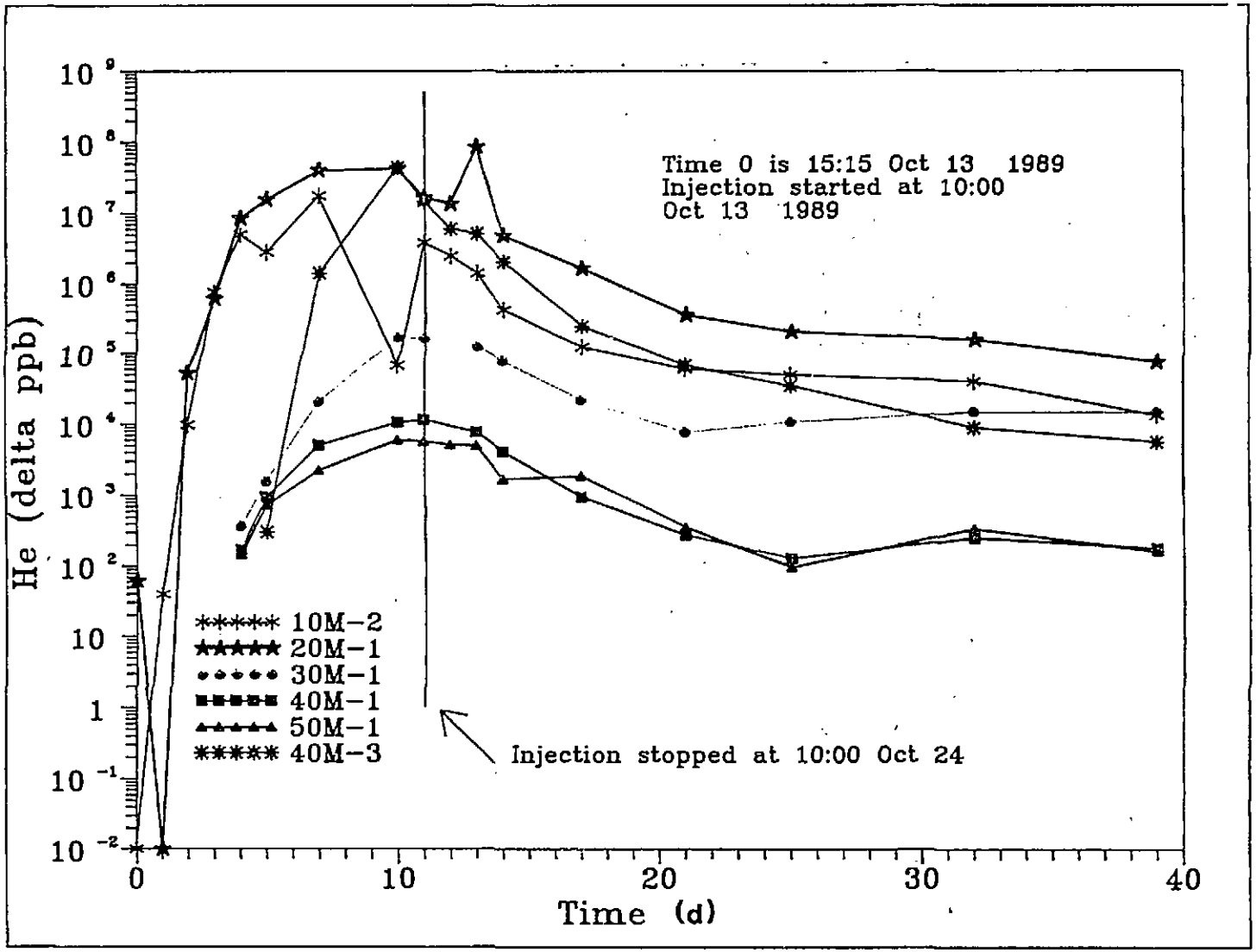

FIGURE 26: Helium Concentrations Above Background (expressed as Δ, in parts per billion) in Soil Gases at Selected Sites in the Radial Array over the Entire Test Period

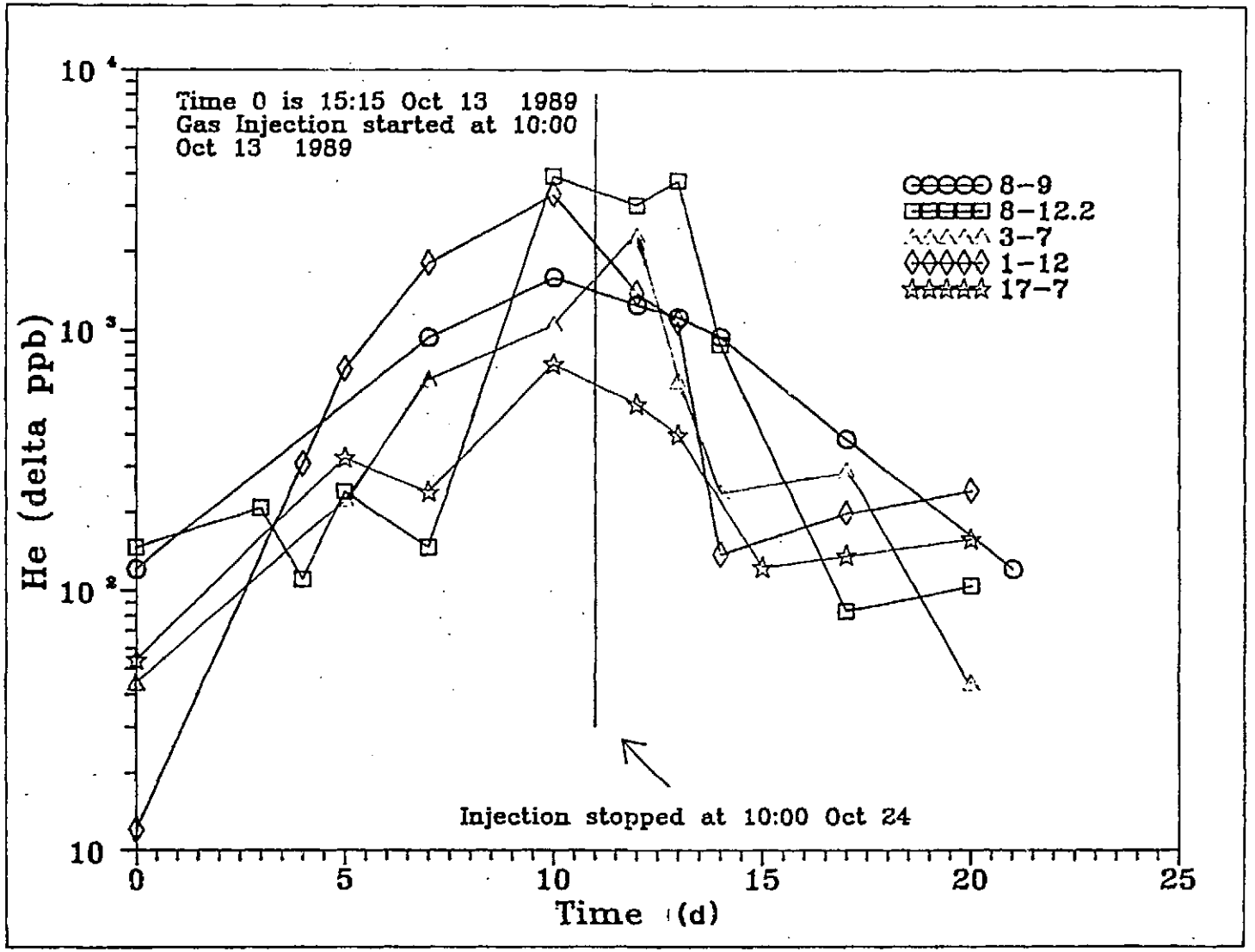

FIGURE 27: Helium Concentrations Above Background (as Δ, parts per billion) in Soil Gases at Selected Sites in the Field Grid over the Entire Test Period

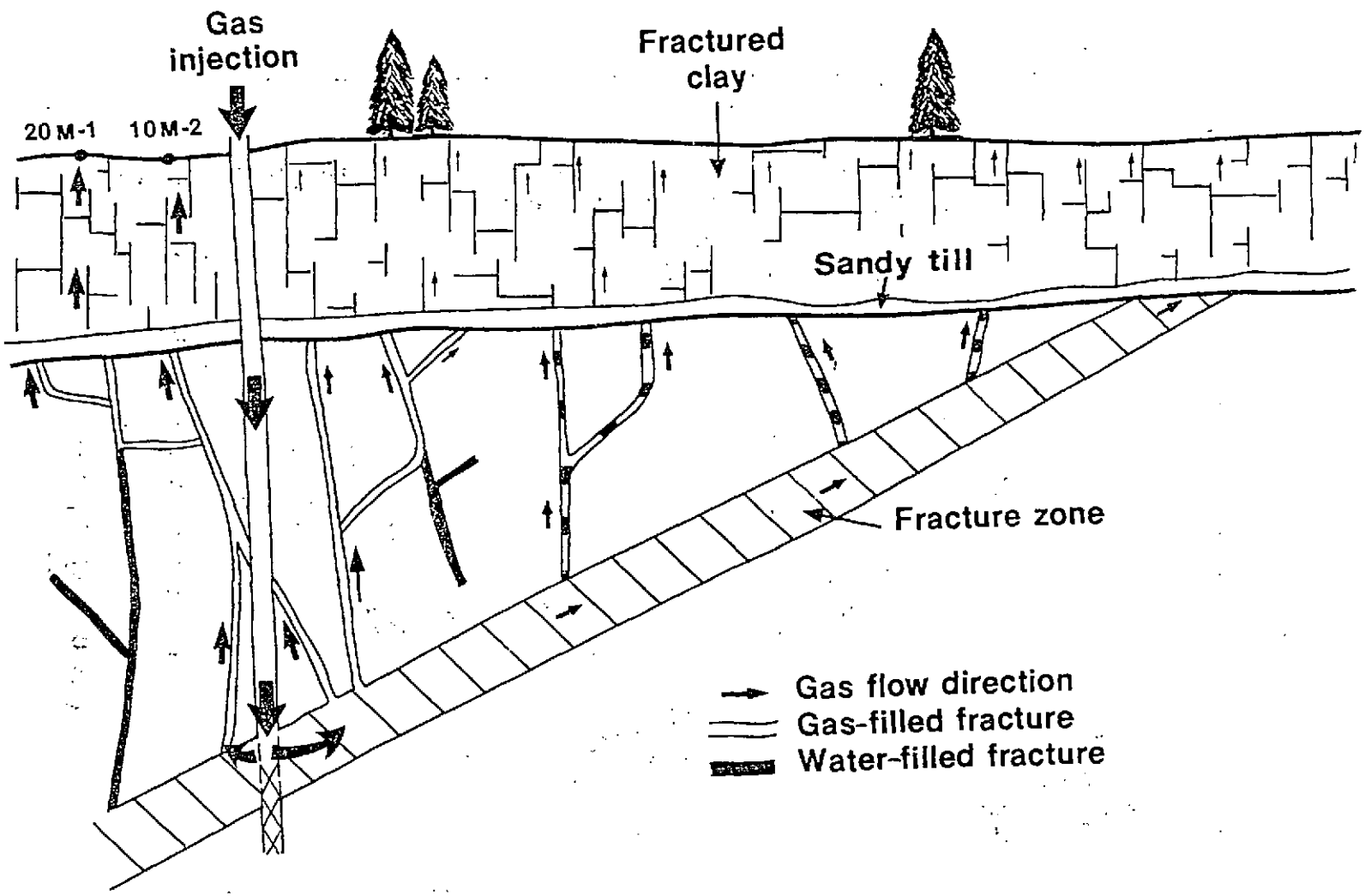

FIGURE 28: Schematic Section Through Borehole B-34 and the Sampling Areas Indicating Possible Gas Migration Pathways That Might Account for the Observed Gas Distributions. The size of arrow indicates the relative amount of He gas in transport.

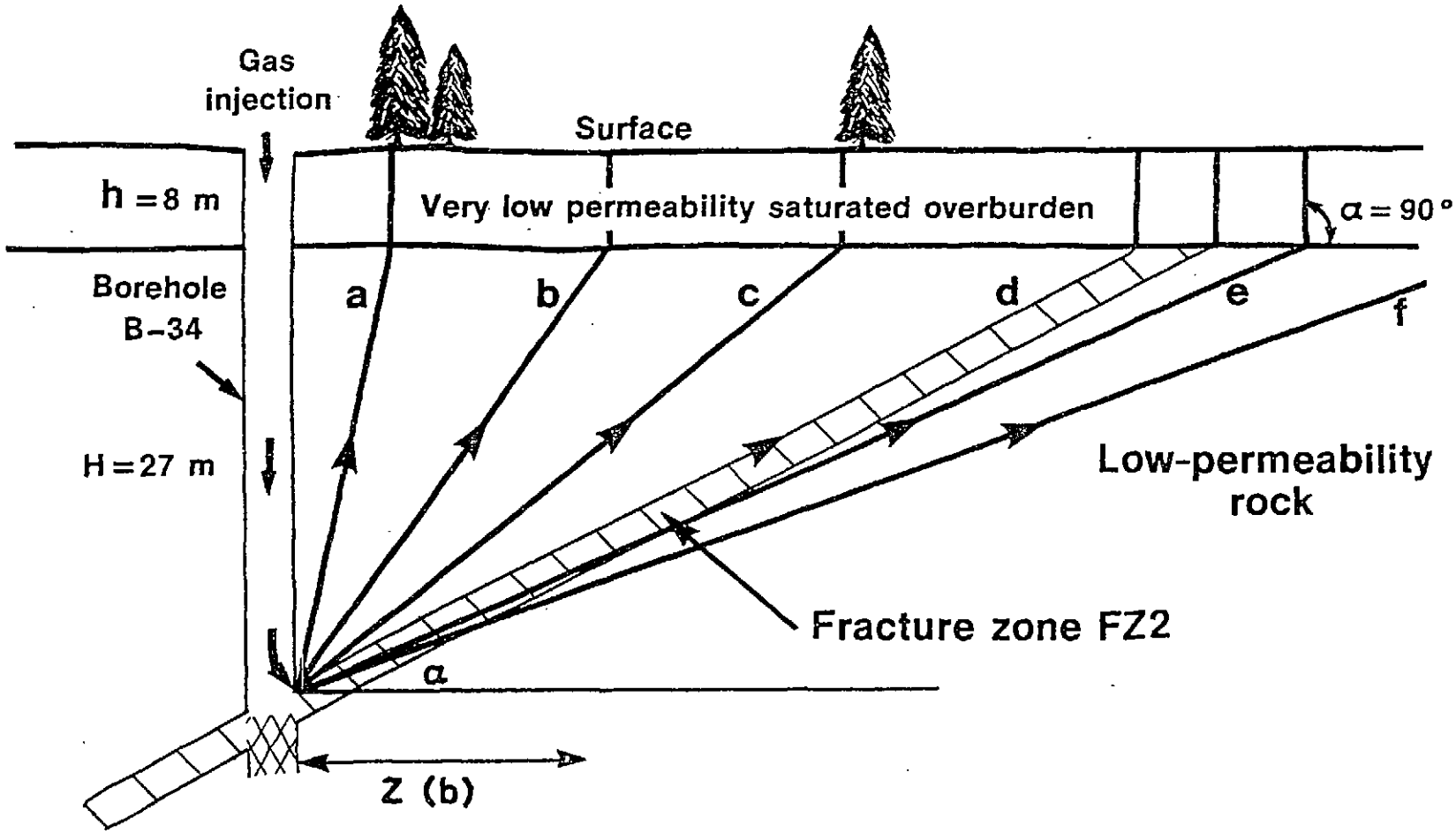

FIGURE 29: Diagram Showing Revisions to the Gas Flow Model Derived by Gascoyne and Wuschke (1990). Flow paths a-f, the angle they subtend to the horizontal (α) and a lower overburden thickness are considered in the revised model.

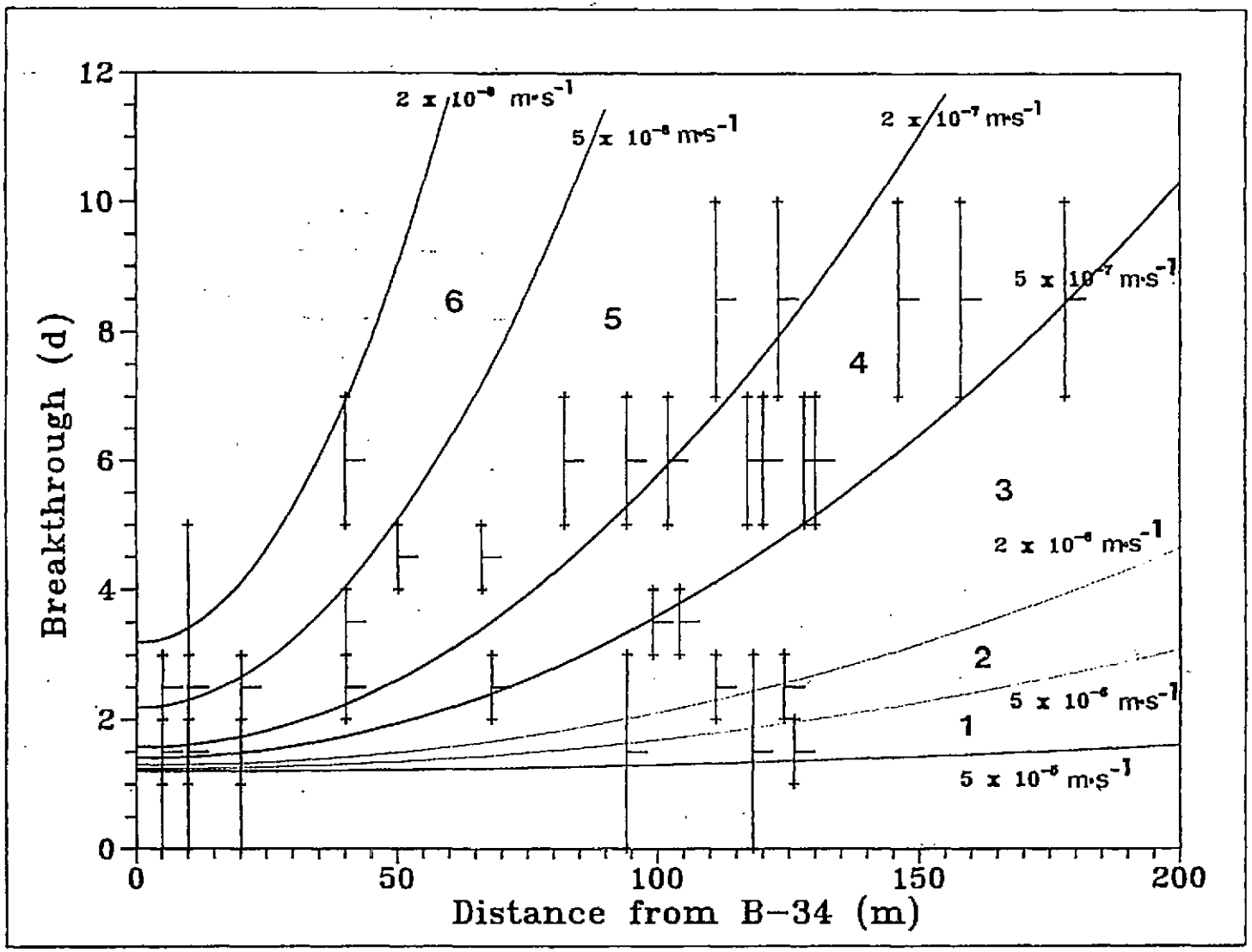

FIGURE 30: Variation of Breakthrough Time of Injected He Gas with Horizontal Distance from Borehole B-34 for 40 Sampling Sites in the Field and Radial Arrays. Error bars indicate the uncertainty of breakthrough time. Relationships derived from the model for selected bedrock hydraulic conductivities are shown by the curved lines and intervals between the lines are numbered for reference in Figure 6.

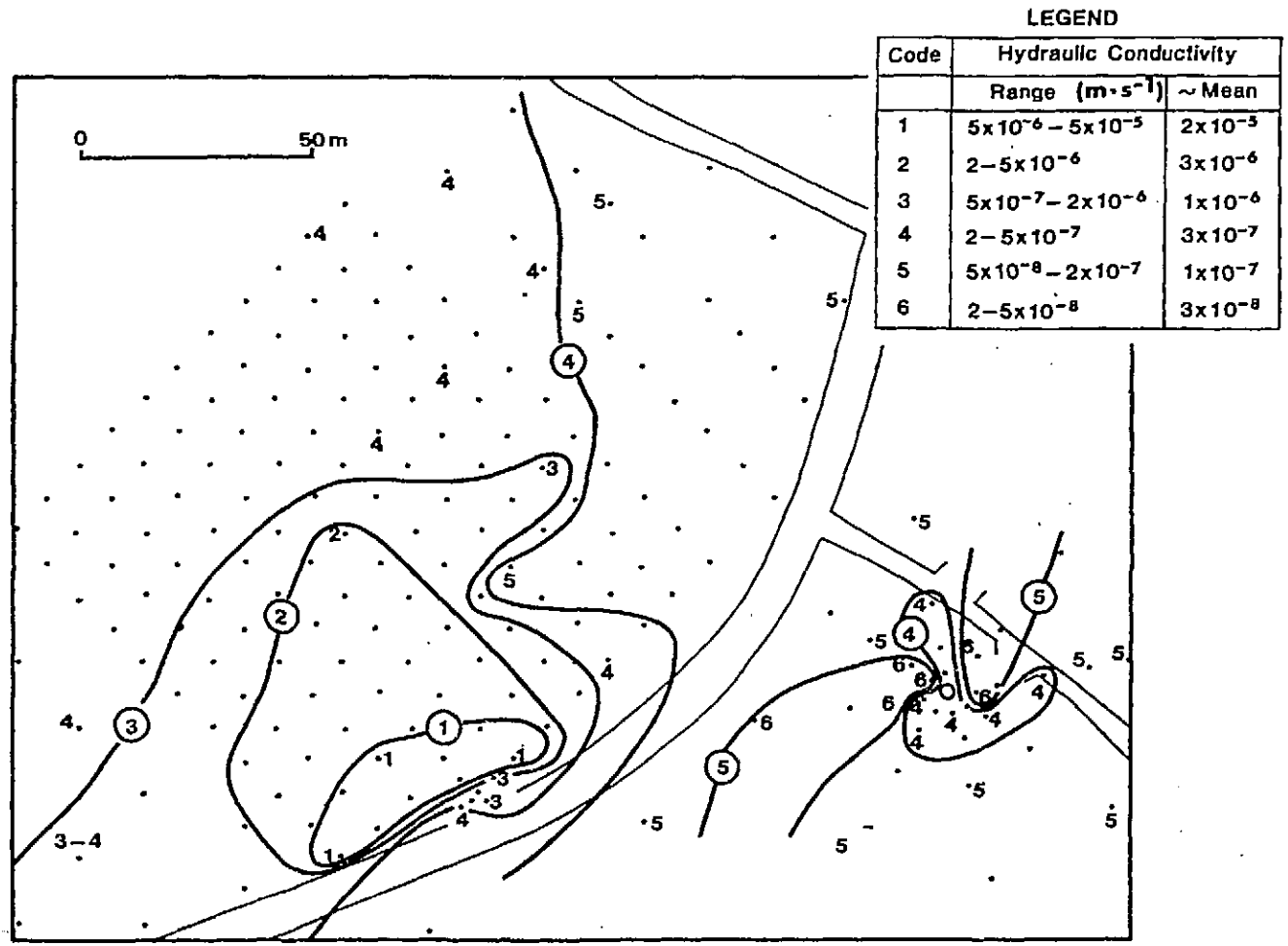

FIGURE 31: Modelled Values of Hydraulic Conductivity of Bedrock Pathways for He Gas Injected in Borehole B-34

APPENDIX A

THE APPLICATION OF VLF-EM AND REFRACTION SEISMIC SURVEY TECHNIQUES FOR DETERMINING OVERBURDEN THICKNESS AND DEPTH TO BEDROCK

CONTENTS

A.1 INTRODUCTION

An estimation of the overburden depth was requested for an area immediately north and adjacent to the URL lease area (Figure A-1). This information was to determine the topography of the bedrock surface beneath the overburden and from this to infer the location of fracture zones within the bedrock. Two reconnaissance geophysical methods were used for this estimation: refraction seismic surveys and Very Low Frequency Electromagnetic (VLF-EM) resistivity.

Refraction seismic surveys are one of the commonest methods to determine overburden depth and/or the bedrock relief beneath the overburden. If the overburden thickness is less than about 5 to 8 m, then a sledge hammer may be used with good results. When the overburden is thicker, however, a small explosive charge is required to place enough energy into the subsurface to be recorded over the length of the seismic spread.

VLF-EM resistivity was chosen as it is a rapid reconnaissance exploration survey method with good depth of search ability. There is a very good electrical resistivity contrast between the overburden (5 to 10 Ω·m) and the bedrock (1000 to 15 000 Ω·m). Unfortunately, VLF-EM signals cannot penetrate beyond about 10 m in overburden with this low an electrical resistivity. However, it was hoped that the technique might at least detect the bedrock/overburden interface in areas with shallow overburden.

A.2 INSTRUMENTS AND METHODS

The surveys were done using the following instruments and methods:

VLF-EM:

instrument - Geonics EM-16 serial no. 20080 with resistivity attachment serial no. 8301001

station spacing - 20 m

frequencies - 24.0 kHz (NAA Cutler, MA)
21.4 kHz (NSS Annapolis, MD)

coverage - 118 stations, 2.36 km

survey dates - 1989 October 12 and 13

Refraction Seismic:

instrument - Exploranium Geometrics 12 Channel Seismograph model ES1210F serial no. 19417

geophones - Mark Products Ltd. 20-200 Hz marsh geophones placed 30 to 40 cm below ground surface

separation - 5 and 10 m

energy source - 5-kg sledge hammer

coverage - 20 profiles

survey dates - 1989 October 13, 16, 17 and 18

Paper traces of the geophone response were collected using a time scale that permits the resolution of about 0.5 ms. The landowner was not willing to permit the use of explosives for these surveys, so about three to five hammer blows on a small base plate were used as the energy source. The signal enhancement capability of the ES210 seismograph was used to improve the signal-to-noise ratio of the relatively weak energy imparted at each blow of the hammer.

The survey grid was placed on the area of interest using short wooden laths that were painted, tapped into the ground using a light hammer, and labelled with felt-top ink marker. After the surveys had been completed, the laths were removed at the request of the landowner.

A.3 RESULTS

A.3.1 VLF-EM RESISTIVITY

The results of the VLF-EM resistivity survey are shown in Figures A-2, A-3, and Figure 9 in the report. Figure A-2 shows the apparent electrical resistivity of the earth as sensed by the VLF-EM field and Figure A-3 gives the phase angle between the electric and magnetic components of the VLF-EM field. The phase angle is also sensitive to the electrical nature of the subsurface.

The apparent electrical resistivity of the overburden in this area is a uniform 10 to 20 Ω·m except in a few restricted areas where the values increase from 20 to 100 Ω·m. At station 1+40N on line 2+00W, the apparent resistivity is 550 Ω·m.

There is also a large number of phase angle measurements on this grid with phase angles of 50° to 60°. Where the apparent resistivity is in the 10 to 20 Ω·m range the phase angle is almost always in the range from 50° to 60°. Where the phase angles are less than 40°, there is a good correlation with apparent resistivities above 30 to 50 Ω·m.

VLF-EM surveys are often affected by power and telephone lines and this may cause the 5 Ω·m apparent resistivity measurements recorded beneath most of the power lines.

A.3.2 REFRACTION SEISMIC RESULTS

The seismic refraction survey was conducted on three lines, L0+00N, L2+00W and L3+20W. The survey layout and locations of seismic spreads are shown in Figure A-4. The seismic refraction surveys were only partly successful

in defining the overburden depth because the energy levels from the hammer source were too low to give good refracted first arrivals wherever the overburden depths are greater than about 10 m. Eight of the 20 reversed profiles were successful in defining the overburden depth.

The overburden displays two distinct velocities: a top layer with low velocities (200-350 $m \cdot s^{-1}$) that is about 2 m in thickness and lies directly above a thicker layer with velocities of 1200 to 1500 $m \cdot s^{-1}$. The refraction seismic survey results for all 20 profiles are summarized in Table A-1.

A.4 INTERPRETATION

A.4.1 VLF-EM RESULTS

The interpreted depth to bedrock from this survey is shown in Figure 9. These depths were determined using a three-layer resistivity model for the area as shown in the inset in Figure 9. This model of the electrical data interpretation consists of a 2-m-thick top layer of 100 $\Omega \cdot m$, resistivity above a variable thickness of 5 $\Omega \cdot m$ material resting on a highly resistive rock with resistivities of 100 to 50000 $\Omega \cdot m$.

The following criteria were used to estimate the overburden depth:

- the VLF resistivity and phase variations are caused by variations in thickness of the electrically conductive layer immediately above the bedrock;
- the surface layer resistivity is 100 $\Omega \cdot m$ and this layer is assumed to be 2 m in thickness over the entire area;
- the bedrock resistivity is 5000 $\Omega \cdot m$;
- a three-layer, homogeneous earth model was used for interpretation; and
- since the phase angle is more sensitive to the depth of the overburden than the apparent resistivity, this angle was used for depth determinations.

The strongest argument for using the three-layer model in estimating the overburden depth originates in the 50 to 60° phase angle observed on the grid. The basic electrical resistivity layering almost anywhere on the Whiteshell Research Area is that of an electrically conductive overburden overlying an extremely resistive basement. If the standard two-layer interpretation curves are used for a conductor overlying a resistive bedrock, it is impossible to have VLF-EM phase angles greater than 45°. The high resistivities and low dip angles at the intersection of L1+50N and L2+00W are attributed to a shallow bedrock ridge.

A.4.2 REFRACTION SEISMIC INTERPRETATION

The results of the hammer refraction seismic surveys were interpreted using the standard forward and reversed method as described by Telford et al. (1975). The greatest uncertainty in the data came from the low energy level received back at surface from the refracted wave. Where the refracted signals were equal or even roughly equal, the overburden depth was estimated using the standard intercept time technique. The depths to bedrock could not be determined where the refracted arrivals were weak or non-existent. The interpreted depths along two lines, L2+00W and L3+00W, are shown in Figure 8, together with depths determined from the VLF-EM survey along these lines.

Three layers were also needed to explain the refraction seismic results. The top layer corresponds to an overburden that must be very dry because the compressional wave velocity is often lower than the speed of sound in air. The intermediate layer corresponds to an overburden that is saturated in water and exhibits a velocity of 4000 to 6000 $m \cdot s^{-1}$ and this corresponds very closely to the velocity of a weathered and undulating granite.

A.5 CONCLUSIONS

The depth of the overburden has been estimated on a reconnaissance survey grid in an area just adjacent to the URL (Figure 9). Both the VLF-EM and refraction seismic surveys encountered difficulties in estimating the overburden depth where the depths are greater than about 8 to 10 m. The depth of search of VLF-EM technique was limited by the electrically conductive overburden. The refraction seismic depth of search, however, was limited by the low signal-to-noise ratio from the hammer source. Parts of the subcrop, therefore, that were deeper than 15 m could not be mapped. The subcrop of a buried ridge 200 to 400 m NW of borehole B-34 has been confirmed by ground survey and drilling.

REFERENCE

Telford, W.M., Geldart, L.P., Sherift, R.E. and Keys, D.A. 1976. Applied Geophysics. Cambridge Univ. Press, London.

TABLE A-1

REFRACTION SEISMIC RESULTS AND CALCULATED OVERBURDEN THICKNESS FOR TRAVERSE PROFILES

Profile Number	Layer 1 Velocity ($m \cdot s^{-1}$)	Layer 2 Velocity ($m \cdot s^{-1}$)	Bedrock Velocity ($m \cdot s^{-1}$)	Overburden Thickness (m)	Comments
1	350	n/a	5000	2.5	
2	200	1500	?	?	too deep
3	300	1400	?	?	too deep
4	350	1250	4280	11-8	
5	350	1500	4000	9-14	
6	250	1500	4500	12-8	
7	250	1300?	?	>10?	poor energy
8	200	1600	?	>10?	poor energy
9	160	?	?	>10?	poor energy
10	200	1450	?	>10?	poor energy
11	300	?	?	?	poor energy
12	350	n/a	5000	2.5	
13	390	1550	5000	7-9	
14	300	1600	4000	3-8	
15	330	n/a	4500	2.5	
16	500	1800	?	?	poor energy
17	500	1500	?	?	poor energy
18	530	1500	?	?	poor energy
19	550	1425	?	?	poor energy
20	230	1400	?	?	poor energy

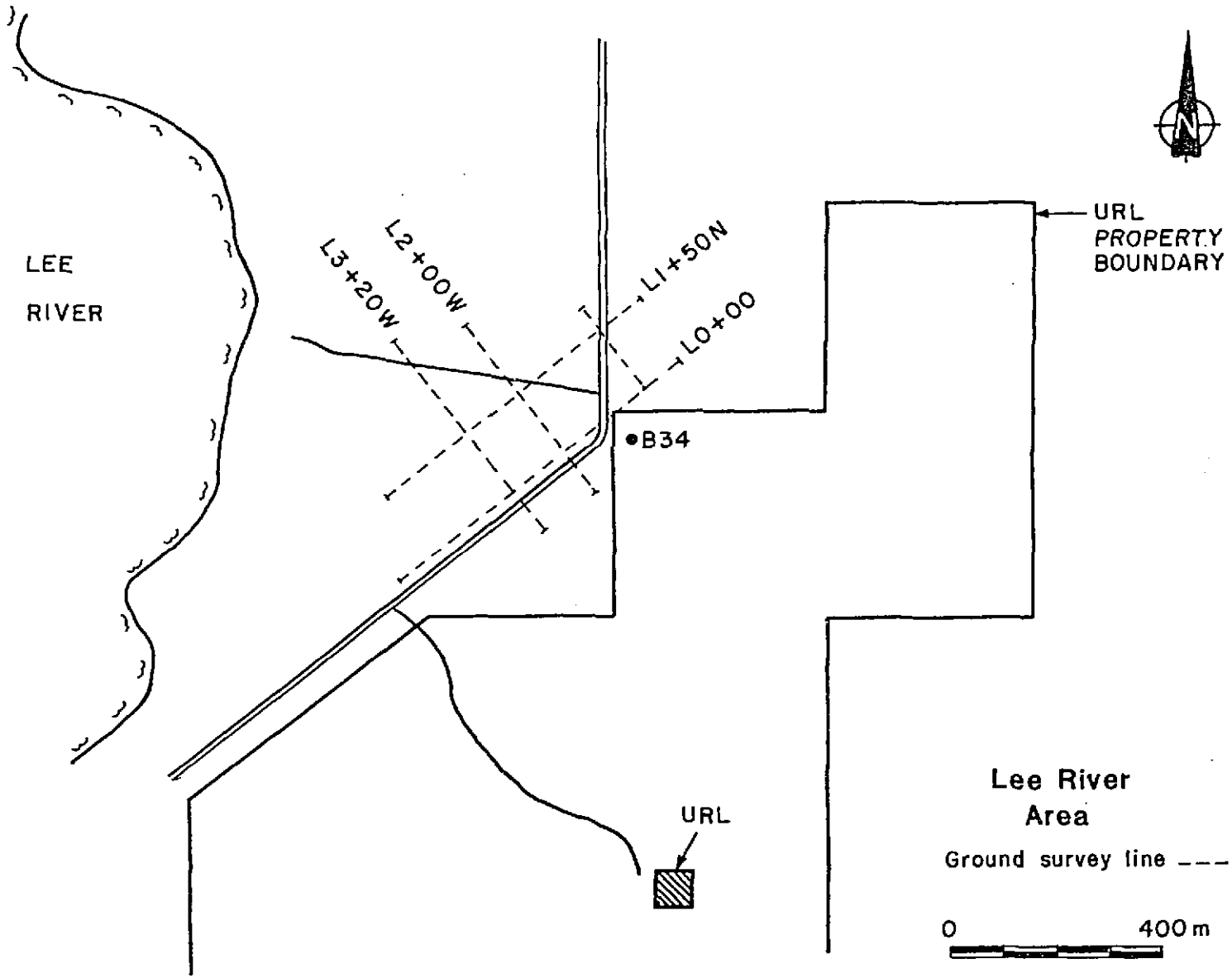

FIGURE A-1: Plan Map of the VLF-EM Survey Grid Northwest of Borehole B-34

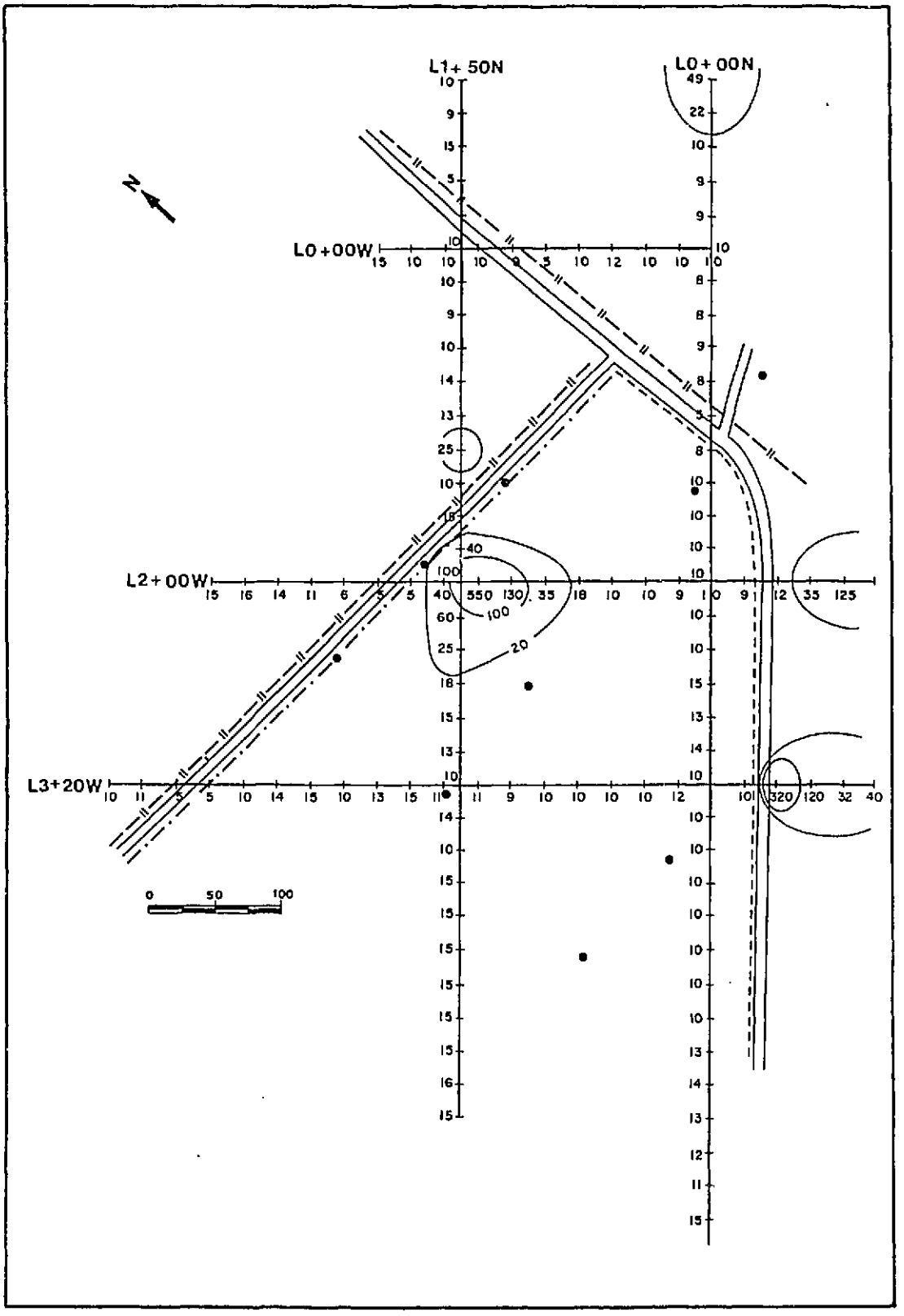

FIGURE A-2: VLF-EM Apparent Resistivity Results. Note the high resistivity of 20 to 100 Ω·m near the intersection of L1+50N and L2+00W.

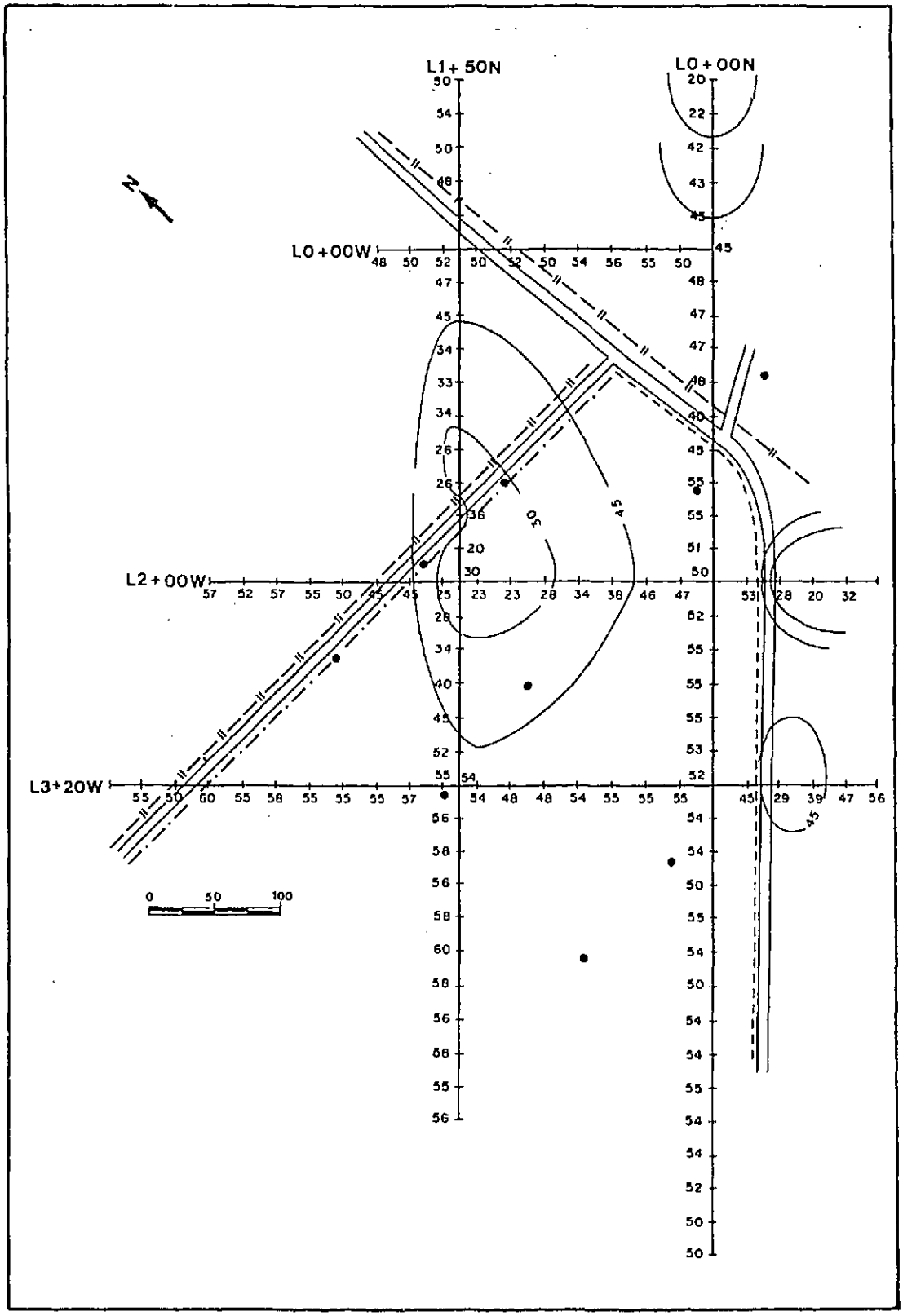

FIGURE A-3: VLF-EM Phase Angle Results. Note the reduced phase angles of 30 to 45° along line L1+50N and L2+00W. These low dip angles correspond to reduced overburden thickness associated with a buried bedrock ridge.

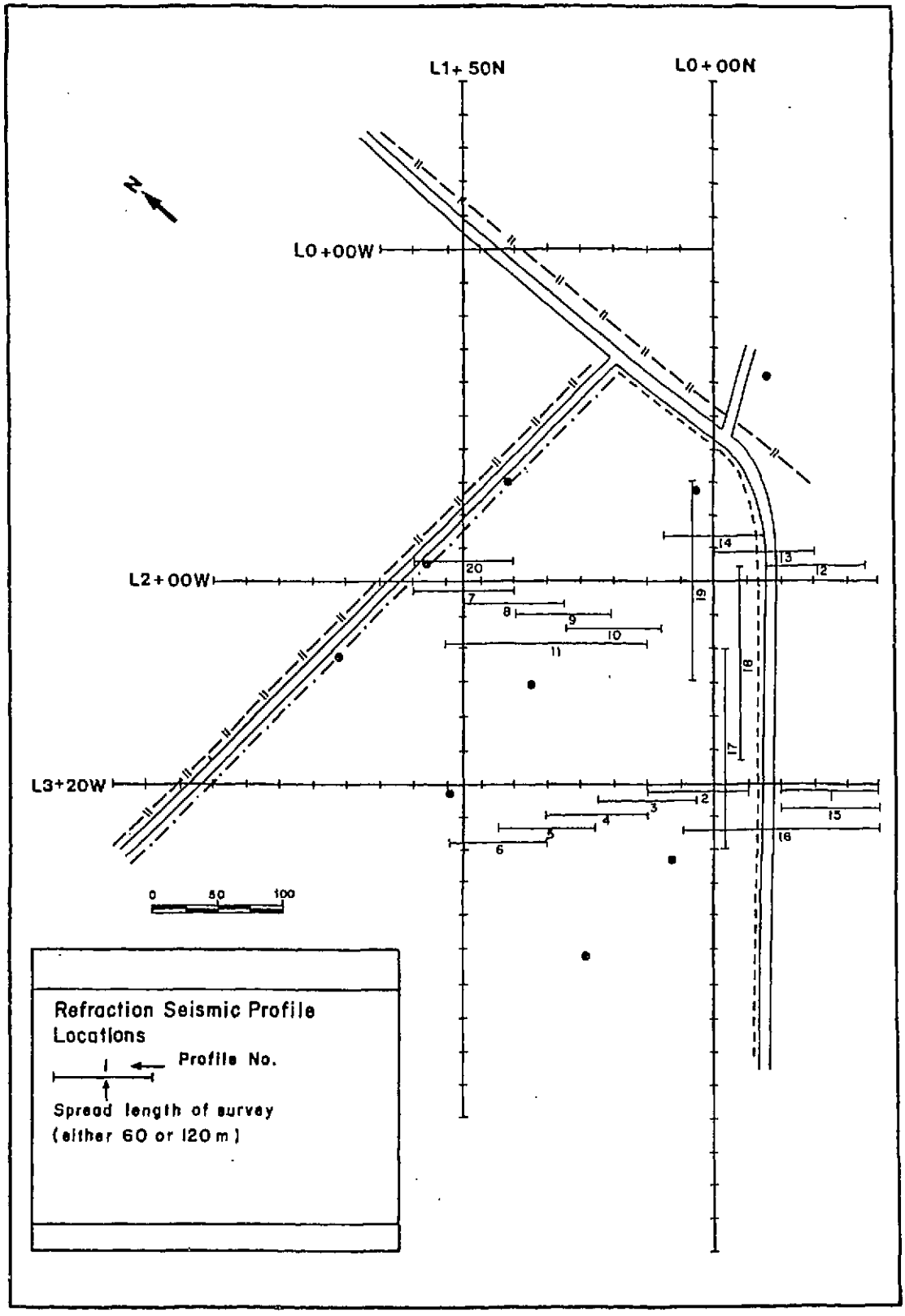

FIGURE A-4: Pattern of Seismic Refraction Survey Spreads 1 to 20 Along Lines L0+00W, L2+00W and L3+20W

APPENDIX B

HYDROGEOLOGICAL TESTING OF BOREHOLE B-34

CONTENTS

B.1 BOREHOLE CONFIGURATION

Borehole B-34 was drilled vertically in 1982 at 152-mm diameter to a depth of 61 m as part of a surface network of hydrogeological water-level monitoring boreholes. A one-metre-long packer was inflated at 32-m borehole depth, where no fracturing was noted in the borehole fracture log, effectively isolating Fracture Zone 2 (FZ2) in the bottom of the borehole from near-surface fracturing. The upper zone (Zone 1) extends from 13.5-m (thickness of cased overburden) to 32.0-m depth and the lower zone (Zone 2) extends from 33.0 to 61.0 m in depth. A 50-mm-ID, flexible PVC standpipe was attached to the packer from the surface and water-level measurements have been recorded over time in both Zone 1 and Zone 2 by quartz diaphragm electronic pressure transducers connected to a central data acquisition system. All hydrogeological tests were conducted within Zone 2 using the installed monitoring packer system.

The nearest observation borehole to borehole B-34 Zone 2 is borehole M5A, located approximately 228 m to the east. Borehole M5A has been installed with a packer system similar to the one installed within B-34. During testing at B-34, monitoring of the water levels within M5A was performed using a manual water level tape two to three times daily.

B.2 HYDRAULIC TESTING

Both slug test and constant-rate pumping tests were conducted to measure the transmissivity of FZ2 at the location of borehole B-34. During all testing, water-level measurements were collected from B-34 Zone 1 and during the constant-rate pumping tests from M5A as well. Water level data from B-34 Zone 2 were collected by a quartz diaphragm electronic pressure transducer and recorded on a computer hard disk for analysis.

B.3 PULSE TESTING

Six pulse tests were conducted using a displacement rod, 2 m in length and 25 mm in diameter, to induce a sudden increase or decrease in the hydraulic head acting upon FZ2 in the standpipe. The recovery to the undisturbed hydraulic head condition within FZ2 with time was recorded and plotted as normalized head versus log time. During these tests no response was noted within B-34 Zone 1.

The data were analysed using the Cooper (Cooper et al. 1967) and Ramey (Ramey et al. 1975) type curve matching techniques, with

$$T = B\frac{r_c^2}{t} \quad \text{and} \quad S = a\frac{r_c^2}{r_s^2}$$

where T = transmissivity,

S = storativity,

r_c = radius of the well casing (m),

r_s = radius of well (m),

t = match point time (s), and

B and a = curve matching parameters.

From the preliminary analysis of the pulse tests, the transmissivity ranges from 5 to 8 x 10^{-5} $m^2 \cdot s^{-1}$ and storativity ranges from 1 x 10^{-5} to 6 x 10^{-4}. It should be noted that, because of similarity of the type curves, the determination of the storage coefficient by this method has a large degree of uncertainty.

B.4 CONSTANT-RATE PUMPING TESTS

Two constant-rate pump tests were conducted within borehole B-34 Zone 2. The first test was conducted with a flow rate (Q) of 0.55 $L \cdot min^{-1}$ for 24 h. The second test was conducted with Q = 7.2 $L \cdot min^{-1}$ for approximately 72 h. During these tests the pumping well water level was drawn down 0.3 m and 5.78 m respectively, and the water level was being monitored within B-34 Zone 1 and M5A Zone 1. A response within B-34 Zone 1 was recorded during each pump test, indicating a hydraulic connection between B-34 Zone 1 and FZ2. The character of the drawdown within B-34 Zone 1, however, indicated that this connection was most likely due to a leak somewhere in the packer-standpipe system and not through the fractured granite. Borehole M5A Zone 1 did not respond to the low Q test, although a 0.15-m drawdown within this zone was recorded during the 7.2 $L \cdot min^{-1}$ pump test corresponding to the time of pumping.

The water level within all monitored wells was recorded and drawdown was plotted versus log time since pumping began. The drawdown time plot should plot as a straight line unless a boundary condition is within the influence of the test, at which point the slope of the drawdown time plot line will change.

The pump tests were analysed using the Jacob analysis (Dricoll 1986), with

$$T = \frac{2.3Q}{4\pi\Delta S} \text{ and } S = \frac{2.25Tt_o}{r^2}$$

where T = transmissivity ($m^2 \cdot s^{-1}$),

S = storativity,

Q = pumping rate ($m^3 \cdot s^{-1}$),

r = distance to observation well (m),

ΔS = drawdown over one log cycle (m), and

t_o = intercept of straight line extrapolated to zero m drawdown (s).

At the pumping well the transmissivity was calculated from both pumping tests to be approximately 3 x 10^{-5} $m^2 \cdot s^{-1}$ from Jacob analysis. The storage coefficient at the pumping well cannot be derived using the Jacob analysis. The drawdown data recorded manually within M5A Zone 1 at a distance of 228 m from the pumping well and analysed using the Jacob analysis indicate a transmissivity of 5 x 10^{-5} $m^2 \cdot s^{-1}$ and a storativity of 3 x 10^{-4}. The drawdown time plot also indicates that a change in slope of the straight line occurs after approximately 300 s of pumping, which suggests that an impermeable boundary condition exists within the influence of the test.

B.5 CONCLUSIONS

Preliminary analysis of the data collected during the hydrogeological testing carried out within borehole B-34 during 1990 August 8 and September 1 indicates that

1) the transmissivity within FZ2 in the region intersected by borehole B-34 is approximately 5 x 10^{-5} $m^2 \cdot s^{-1}$;

2) the storativity of FZ2 in the region of borehole B-34 is in the order of 5 x 10^{-4};

3) an impermeable boundary was detected at 300 s of pumping during both the high and low flow rate pump tests; and

4) a small leak in the existing borehole packer system was discovered and verified upon the removal of the system. The leak was repaired and the packer-standpipe system was replaced and allowed to stabilize prior to the injection of the gas.

REFERENCES

Cooper, H.H., Bredehoeft, J.D. and Papadopulus, I.S. 1967. Response of a finite-diameter well to an instantaneous charge of water. Water Resources Research 3, 263-269.

Driscoll, G., Phd. 1986. Groundwater and Wells, 2nd Edition. Johnson Division, St. Paul, MN, 205-267.

Ramey, H.J., Argarwal, R.G. and Martin, I. Analysis of slug test or DST flow period data. Journal of Canadian Petroleum Technology 14, 37-42.

APPENDIX C

SAMPLING AND ANALYTICAL TECHNIQUES

CONTENTS

The sampling and analytical techniques used generally follow those of Gregory and Durrance (1987) and Gregory (1987) but differ in some respects, as indicated below.

C.1 SOIL GAS SAMPLING

The collection of soil gas involved pumping of soil gas from a hollow probe driven 0.5 m into the ground. Two types of probe were used depending on whether single or repeated sampling at a site was required. Single sampling used the removable equipment described by Gascoyne and Wuschke (1990). If a site was to be repeatedly sampled, a 5/8-in.-OD (nominal) stainless steel tube was emplaced in the ground permanently using the hammer device of the single mobile sampler. The orifice of the tube was capped by a rubber stopper between gas samplings.

The following procedure describes sampling of soil gases from either type of probe. The hollow soil probe has a length of about 75 cm and an internal diameter of about 10 mm. A pounding hammer (consisting of a steel rod that slides in a steel hammer head) is inserted into the probe with the end of the steel rod projecting out of the probe. This prevents the probe from blocking as it is hammered into the ground and also creates a gas space at the base of the probe.

To sample soil gases, the hammer is removed and a brass manifold inserted into the collar of the probe. The manifold is fitted with a Whitey toggle valve, a silicon rubber septum for gas sampling with a syringe and a 6-mm-diameter outlet for connecting the manifold to the pump. About 20 strokes of the hand pump are made to remove introduced air from the system. Two or three 10-mL plastic syringes are then filled with soil gases through the septum. After sampling, an extraction tool, which is simply a steel wrench-like instrument, slots into grooves at the collar of the removable soil probe and is used to pull the probe from the ground.

C.2 ANALYSIS OF HELIUM

To analyse helium in soil gases, a helium-leak detector was fitted with an external inlet system that allowed the introduction of the gaseous sample into the spectrometer under constant pressure. The electrical output of the leak detector was a leak indicator meter connected in parallel to a chart recorder. An external vacuum pump was also connected to the inlet system enabling rapid evacuation of the system.

The helium analyser for this project was the Veeco MS18AB mass spectrometer leak detector. It is solely designed for the detection of ions of mass-to-charge ratio of 4^+. The principles of operation of the Veeco will not be described here. The inlet system and method of analysis of the soil gas samples is described below (from Gascoyne and Wuschke (1990) with amendments).

The external inlet system allows introduction of sample in small controlled quantities under constant pressure and for pre-concentration of helium. There are basically four sections to the inlet system: 1) evacuation valve and external vacuum pump; 2) injection port and sample clear valve; 3) the variable leak valve; and 4) U-trap.

Figure C-1 is a schematic diagram of the inlet system. Samples are introduced into the system through a silicon rubber septum and held in place by a nut on one port of a four-port union. The gas partly inflates a rubber storage balloon connected to a second port of the union. Another port allows gas to flow to the variable leak valve and the remaining port is connected to the sample clear valve and external vacuum pump. The storage balloon acts as an expansion bladder and maintains a constant pressure supply to the variable leak valve.

Between the inlet to the mass spectrometer and the leak valve there is a U-trap made out of a 3/8-in. (nominal) stainless steel tubing packed with activated charcoal. During analysis, the U-trap is immersed in a Dewar filled with liquid nitrogen. The use of the U-trap has two beneficial effects:

1) gases that can contaminate the spectrometer or degrade the filament, thereby reducing sensitivity, are removed (e.g., oxygen, water vapour, and carbon dioxide); and

2) since the number of gas molecules entering the spectrometer has been reduced, the leak valve can be open to increase the throughput, thereby increasing the partial pressure of ^4He entering the spectrometer while maintaining a low pressure at the spectrometer head. The result is a dramatic increase in sensitivity.

When evacuating the inlet system, the U-trap by-pass valve is opened to prevent gases from being constantly pumped through the U-trap. In this way, the life of the activated charcoal within the trap is prolonged and overloading of the U-trap avoided. The pumpdown of the inlet system continues for approximately 15 min after completion of analysis. This allows any gases adsorbed onto the charcoal to degas and be pumped out of the system.

Laboratory air, presumed to be 5240-ppb* He, along with 20-ppm** and 10-ppm He standards in nitrogen were used as calibration gases. Duplicate samples from each site were analysed with laboratory air samples bracketing each soil gas sample. Ten millilitres of gas was injected at a time, providing approximately 90% of output signal. Since the quantity of He in the soil gas can be either greater or less than that in air, the results were reported as He anomalies (Δ) rather than in absolute amounts. The He anomaly is calculated simply by subtracting 5240 ppb from determined quantities of He in the sample and expressing the result as a negative or positive value in ppb. High levels of He in some samples were determined either by changing the scale adjuster on the meter readout or diluting the sample by injecting it into an air-filled 750-mL glass bottle fitted with stopper and septum, and analysing the diluted sample.

---

* 1 ppb = 1 nL/L
** 1 ppm = 1 μL/L

Figure C-2a shows an ideal He output signal on the chart recorder of the leak detector and a typical signal. An ideal output signal is rarely achieved because of factors such as pressure changes, electronic noise and amplifier drift. In many cases, there is an initial overshoot of the signal followed by a flat plateau region (Figure C-2b). The overshoot is due to the dynamic property of the constant-pressure inlet system and the adsorptive properties of the U-trap. Problems of signal response were also incurred if the mass spectrometer was exposed to full vacuum between injections of standard or sample gases. Pump-out time was therefore limited to only one or two seconds to minimize this effect.

The linearity of the response of the mass spectrometer to helium was determined by separately injecting laboratory air, 10-ppm and 20-ppm He as standards. Within experimental error, the relationship between the response of the mass spectrometer to concentration of helium was found to be linear.

In previous tests (Gascoyne and Wuschke 1990) it was found that there was a diffusive loss of 0.33% per hour of He from the 10-mL plastic syringes. In an attempt to minimize this problem, all helium samples were analysed as quickly as possible, usually within 24 h of sampling. Losses were therefore kept to within 10%.

REFERENCES

Gregory, R.G. and Durrance, E.M. 1987. Helium, radon and hydrothermal circulation associated with the Carnmenellis radiothermal granite of southwest England. Journal of Geophysical Research 92 (B12), 12567-12586.

Gregory, R.G. 1987. Soil gas emanometry and hydrothermal mineralization in southwest England. Unpublished. Ph.D Thesis, University of Exeter, Exeter, U.K.

Gascoyne, M. and Wuschke, D.M. 1990. Fracture detection and groundwater flow characterization in poorly exposed ground using helium and radon in soil gases. U.K. Department of the Environment Report DOE/RW/90/079.

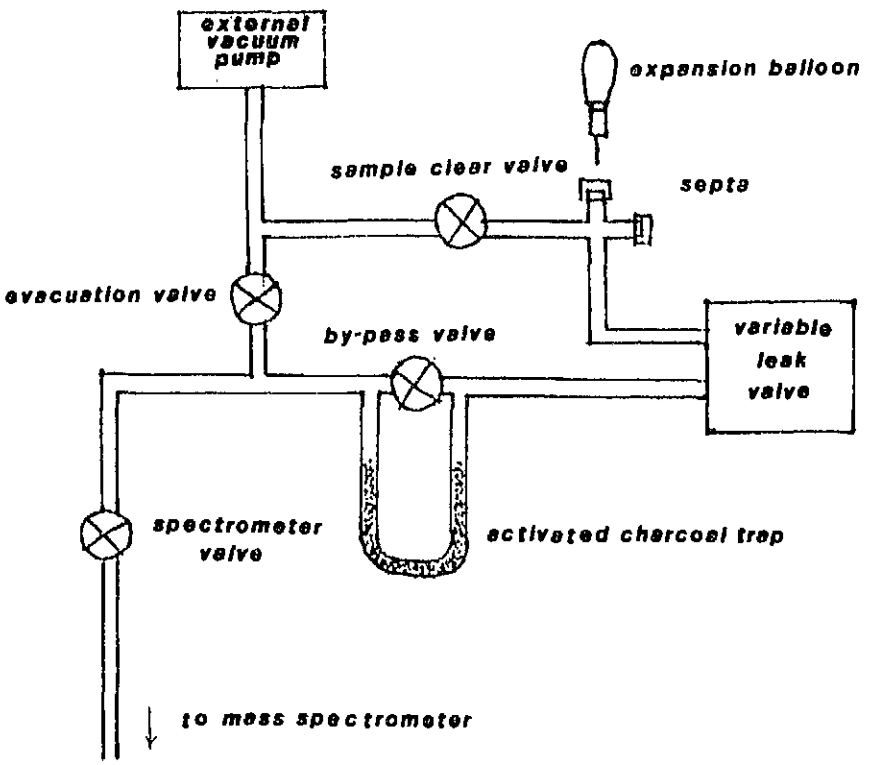

FIGURE C-1: Sample Inlet System for the Helium Mass Spectrometer

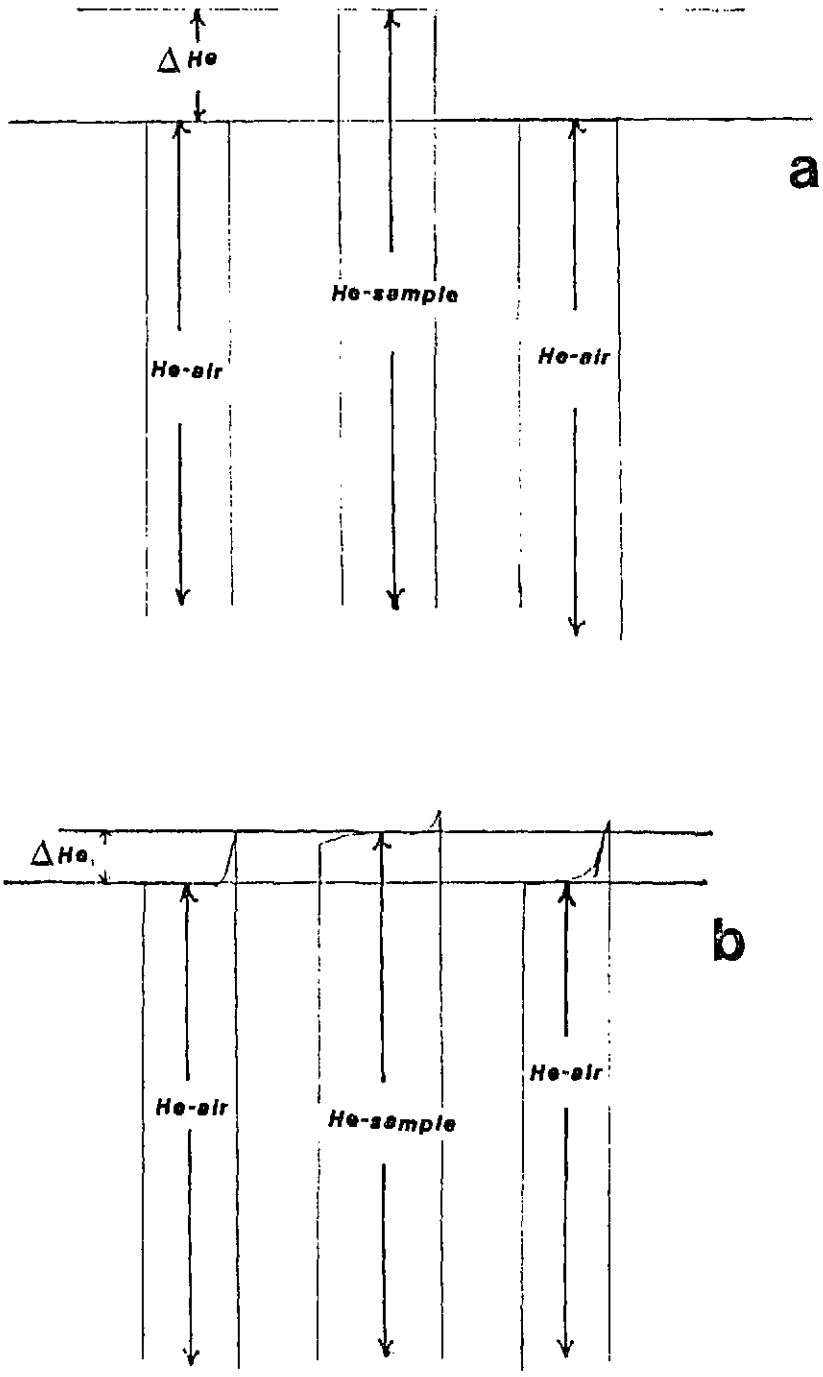

FIGURE C-2: Examples of Helium Signals on the Mass Spectrometer: a) idealized, b) typical showing initial spikes

ISSN 0067-0367

To identify individual documents in the series, we have assigned an AECL- number to each.

Please refer to the AECL- number when requesting additional copies of this document

from

Scientific Document Distribution Office
AECL Research
Chalk River, Ontario, Canada
K0J 1J0

Price: B

ISSN 0067-0367

Pour identifier les rapports individuels faisant partie de cette série, nous avons affecté un numéro AECL- à chacun d'eux.

Veuillez indiquer le numéro AECL- lorsque vous demandez d'autres exemplaires de ce rapport

au

Service de Distribution des Documents Scientifiques
EACL Recherche
Chalk River, Ontario, Canada
K0J 1J0

Prix: B